Probing Challenges of Asphaltenes in Petroleum Production through Extended−SARA (E−SARA) Analysis

by

Peiqi Qiao

A thesis submitted in partial fulfillment of the requirements for the degree of

Doctor of Philosophy

in

Chemical Engineering

Department of Chemical and Materials Engineering
University of Alberta

ABSTRACT

Asphaltenes are polyaromatic compounds present in crude oils, which are defined as being soluble in aromatic solvents and insoluble in *n*−alkanes. The partition of self−associated asphaltene aggregates at oil−solid and oil−water interfaces is the root cause of a number of major problems encountered in oil production and processing. However, it has been noted that not all asphaltene molecules contribute equally to these problems. This thesis focuses on probing properties of the crucial "problematic" asphaltene subfractions using extended−saturates, aromatics, resins, and asphaltenes (E−SARA) analysis.

Unlike most studies on asphaltene fractionation based on solubility or density differences, E−SARA analysis provides a unique way to fractionate asphaltenes according to their interfacial behaviors and adsorption characteristics at either oil−solid or oil−water interfaces that is directly linked with problems encountered in petroleum production and processing. Through the E−SARA fractionation based on asphaltene adsorption onto calcium carbonate, the adsorbed asphaltene subfractions were found to contain a higher amount of carbonyl, carboxylic acid or derivative groups than the remaining asphaltenes. Using the E−SARA fractionation based on asphaltene adsorption at oil−water interfaces, the "interfacially active asphaltenes" (IAA) were extracted as asphaltenes irreversibly adsorbed onto emulsified water droplets, while the asphaltenes remaining in the oil phase were considered as "remaining asphaltenes" (RA). Despite the small percentage of IAA (< 2 wt%) in whole asphaltenes (WA), IAA subfractions were found to play an essential role in stabilizing W/O emulsions by forming thick and rigid films at oil−water interfaces with severe aging effects, as opposed to RA which showed no stabilization potential for W/O emulsions.

In this thesis research, the effect of solvent aromaticity on the compositions of IAA and RA was studied using toluene and heptol 50/50 as the extraction solvent, respectively. Heptol 50/50, a mixture of *n*−heptane and toluene at a 1:1 volume ratio, is a less aromatic solvent than toluene. A lower fractional yield (1.1 ± 0.3 wt%) of toluene−extracted IAA (T−IAA) than that (4.2 ± 0.3 wt%) of heptol 50/50−extracted IAA (HT−IAA) was obtained. However, T−IAA exhibited a greater interfacial activity and a higher W/O emulsion stabilization potential than HT−IAA, as shown by the measurements of interfacial tension, interfacial shear rheology, crumpling ratio, and bottle test of W/O emulsion stability. Such differences are attributed to the higher oxygen and sulfur content of T−IAA than HT−IAA, highlighted in the presence of sulfoxide groups as verified by elemental analysis, Fourier transform infrared (FTIR) spectroscopy, and X-ray photoelectron spectroscopy (XPS). In contrast to two IAAs, the compositions of two RAs (T−RA and HT−RA) were found to be essentially the same regardless of solvent type used in fractionation. Both RAs had a lower sulfur and oxygen (in particular) content than IAAs, giving rise to their considerable less interfacial activities.

Asphaltenes were found to adsorb at oil−water interfaces in the form of asphaltene aggregates. The aggregation kinetics of IAAs and RAs were investigated using dynamic light scattering (DLS), indicating the enhanced asphaltene aggregation by reducing solvent aromaticity. In a given solvent, T−IAA exhibited the strongest aggregation tendency, followed by HT−IAA, then T−RA and HT−RA, following the same trend with their interfacial activities and emulsion stabilization potentials. The interaction forces between immobilized fractionated asphaltenes were measured using an atomic force microscope (AFM). The decreasing solvent aromaticity was found to reduce steric repulsion and increase the adhesion between asphaltenes with asphaltenes adopting a more compressed conformation. IAAs, in particular T−IAA, exhibited stronger adhesion forces than RAs, showing good agreement with the results from DLS measurements. In spite of the small sulfoxide content in asphaltenes, the sulfoxide groups are believed to play a critical role in enhancing asphaltene aggregation in the bulk oil phase.

Using E−SARA analysis, the complexity of asphaltenes can be reduced by targeting specific asphaltene subfractions that have critical influences in the relevant systems of interests. The key chemical functionalities that govern asphaltene adsorption and aggregation are identified through the characterizations of fractionated asphaltenes, leading to a better understanding of the related molecular mechanisms. The fundamental findings from this thesis is essential to providing the optimal solutions of asphaltene−related problems in petroleum industry.

PREFACE

This thesis is composed of a series of published papers. The following is a statement of contributions made to the jointly authored papers contained in this thesis:

- Chapter 1 Introduction. Original work by Peiqi Qiao.
- Chapter 2 Literature review. Original work by Peiqi Qiao.
- Chapter 3 A version of this chapter has been published as: Qiao, P.; Harbottle, D.; Tchoukov, P.; Masliyah, J. H.; Sjöblom, J.; Liu, Q.; Xu, Z., "Fractionation of Asphaltenes in Understanding Their Role in Petroleum Emulsion Stability and Fouling", *Energy Fuels* **2017**, *31*, 3330−3337. Qiao was responsible for concept development and manuscript preparation. Xu supervised the project. Harbottle and Tchoukov were greatly involved in manuscript corrections. Harbottle, Tchoukov, Masliyah, Sjöblom, Liu and Xu proofread the manuscript prior to submission.
- Chapter 4 A version of this chapter has been published as: Qiao, P.; Harbottle, D.; Tchoukov, P.; Wang, X.; Xu, Z., "Asphaltene Subfractions Responsible for Stabilizing Water−in−Crude Oil Emulsions. Part 3. Effect of Solvent Aromaticity", *Energy Fuels* **2017**, *31*, 9179−9187. Qiao was responsible for experimental work, data analysis, and manuscript preparation. Xu supervised the project. Harbottle, Tchoukov and Wang were greatly involved in data interpretation and manuscript corrections. Harbottle, Tchoukov, Wang and Xu proofread the manuscript prior to submission.
- Chapter 5 A version of this chapter has been published as: Qiao, P.; Harbottle, D.; Li, Z.; Tang, Y.; Xu, Z., "Interactions of Asphaltene Subfractions in Organic Media of Varying Aromaticity", *Energy Fuels* **2018**, *32*, 10478−10485. Qiao was responsible for experimental work, data analysis, and manuscript preparation. Xu supervised the project. Harbottle and Li were greatly involved in data interpretation and manuscript corrections. Tang helped with AFM sample preparation. Harbottle, Li and Xu proofread the manuscript prior to submission.
- Chapter 6 Conclusion. Original work by Peiqi Qiao.

Other co−authored publications not listed as Thesis Chapters include:

- Wang, X.; Zhang, R.; Liu, L.; Qiao, P.; Simon, S.; Sjöblom, J.; Xu, Z.; Jiang, B., "Interactions of Polyaromatic Compounds. Part 2. Flocculation Probed by Dynamic Light Scattering and Molecular Dynamics Simulation", *Energy Fuels* **2017**, *31*, 9201−9212. Qiao was involved in data interpretation.
- Yang, F.; Tchoukov, P.; Qiao, P.; Ma, X.; Pensini, E.; Dabros, T.; Czarnecki, J.; Xu, Z., "Studying demulsification mechanisms of water−in−crude oil emulsions using a modified thin liquid film technique", *Colloids Surf., A.* **2018**, *31*, 215−223. Qiao was responsible for a part of experiments using thin liquid film technique.
- Li, Z.; Manica, R.; Zhang, X.; Qiao, P.; Liu, Q.; Xu, Z., "Hydrodynamic interaction between oil drops and a hydrophilic surface in aqueous solution", *to be submitted*. Qiao was responsible for a part of experiments using thin liquid film force apparatus.
- Ballard, D.; Qiao, P.; Charpentier, T.; Xu, Z.; Roberts, K.; Prevost, S.; Grillo, I.; Cattoz, B.; Dowding, P.; Harbottle, D. "Aggregation Behavior of E−SARA Asphaltene Subfractions in Solvents of Varying Aromaticity by Small−Angle Neutron Scattering", *to be submitted*. Qiao was responsible for a part of experiments using small−angle neutron scattering.

ACKNOWLEDGEMENTS

I would like to take this opportunity to thank my supervisors, Dr. Zhenghe Xu and Dr. Tony Yeung for their guidance, support, encouragement throughout my graduate studies. Without their help, I would have never been able to reach this far.

Special thanks are given to Dr. David Harbottle and Dr. Plamen Tchoukov. They are both excellent scientists and also great friends for me. They spent a lot of time helping me become an independent researcher, and it was their encouragement and support that kept me going.

I would like to thank Ms. Jie Ru, Mr. James Skwarok and Ms. Lisa Carreiro for their kind assistance with my projects. I would also like to thank all members in the Oil Sands Research Group, in particular Ms. Yin Liang, Ms. Jiebin Bi, Ms. Xi Wang, Mr. Rui Li, Dr. Fan Yang and Dr. Zuoli Li for their great help and insightful suggestions on my work.

I am grateful for the financial support from NSERC and Alberta Innovates−Energy & Environmental Solutions under NSERC−Industry Research Chair Program in Oil Sands Engineering.

Finally, my deepest gratitude goes to my family, in particular my grandparents, mother, father and fiancée, for their solid support and invaluable encouragement throughout my life. It is to you that I dedicate this work.

TABLE OF CONTENTS

LIST OF TABLES

LIST OF FIGURES

CHAPTER 1 INTRODUCTION

1.1 BACKGROUND

The global oil demand has been continuously increasing for decades due to the rapid population growth, technology development, and global trade expansion. As we are depleting our conventional oil resources, a large proportion of this demand is expected to be addressed through the active production of unconventional oils, such as oil sands, oil shale, tight oil, extra−heavy oil, and ultra−deepwater oil. However, unconventional oils are technologically and/or economically difficult to extract in comparison with their conventional counterparts. A range of specialized technology and equipment are required to deal with the composition and location of unconventional oils, making it hard to make up for the decline of conventional oil production rate. It is therefore critical to optimize current oil extraction and production process in order to meet the world's ever−growing desire for oil.

As a complex mixture of diverse organic compounds, crude oil is often divided for convenience into four main fractions in the order of increasing polarity: saturates, aromatics, resins and asphaltenes (SARA).[1–3] Among these four fractions, asphaltenes are considered the main contributor to many crude oil production problems from extraction, transportation to refining.[4–6] According to the definition, the asphaltene fraction is a solubility class of oil being precipitated out of crude by adding paraffinic solvents, usually *n*−pentane or *n*−heptane. The amount of asphaltenes in crude oil varies considerably in oils of different geochemical origins. High asphaltenic crudes are produced worldwide in regions including Alberta, Texas, Alaska, Mexico and Saudi Arabia.[7]

Asphaltenes are known to self−associate into different types of aggregates.[8] The destabilized asphaltene aggregates cause clogging and fouling within wellbores, flowlines, separators, and other surface handling equipment through precipitation and deposition as a result of temperature, pressure, and oil−phase composition changes.[6,9,10] In addition, asphaltenes play a significant role in the stabilization of undesirable water−in−oil (W/O) emulsions by adsorbing at water−oil interfaces.[11–13] The adsorbed asphaltenes form rigid interfacial networks that prevent the coalescence of emulsified water droplets. The salts and fine solids carried by water droplets pose serious corrosion problems to pipelines and downstream refining facilities. These asphaltene–related issues have become more concerning in recent years as a result of growing production of high asphaltenic heavy oils and increasing carbon dioxide injection for enhanced oil recovery which induces asphaltene instability in the reservoirs.[14]

Tremendous effort has been devoted to investigating complex asphaltenes behaviors in past decades in order to remediate or prevent asphaltene–related problems in petroleum industry. However, the detailed asphaltene aggregation and phase separation mechanisms remain elusive since asphaltenes are often characterized by bulk properties and exact molecular compositions of asphaltenes are unknown. Individual molecules in the asphaltene fraction differ in molecular weight, composition, functionality, polarity and just about any other property except their insolubility in *n*–alkanes. In fact, not all asphaltene molecules contribute equally to asphaltene aggregation.[15–17] Fractionation has been used as a common method to reduce the asphaltene polydispersity and improve the understanding of asphaltene properties. Asphaltenes can be fractionated into different subfractions based on solubility, density and chromatography.[18–20] Fractionation studies have provided a significant insight into the distribution of asphaltene properties. However, limited knowledge is available on the most interfacially active asphaltenes, which are the root cause of asphaltene–related problems by preferentially depositing and partitioning at oil–water interfaces or solid surfaces.

1.2 OBJECTIVES AND THESIS SCOPE

This work is aimed to establish an effective methodology for studying interfacially active asphaltenes in order to provide new knowledge to overcome challenges caused by asphaltene adsorption in oil industry, leading to our three main objectives as follows:

1) To develop an asphaltene fractionation concept which allows us to appropriately isolate and study the specific asphaltene subfractions with high affinity to oil–water interfaces or solid surfaces.
2) To investigate the mechanism of asphaltene adsorption at oil–water interfaces by isolating the most oil–water interfacially active asphaltenes from whole asphaltenes

dissolved in solvents of different aromaticity, characterizing the resulting asphaltene subfractions in terms of functional groups, and then comparing the interfacially active asphaltenes to the remaining asphaltenes in terms of oil−water interfacial activity and W/O emulsion stabilization potential.

3) To reveal the key chemical functionalities that govern asphaltene aggregation in organic media of varying aromaticity by studying the aggregation kinetics of the oil−water interfacially asphaltenes and the remaining asphaltenes, as well as measuring the molecular interaction forces between fractionated asphaltene molecules.

In the first part of the thesis, the extended−SARA (E−SARA) analysis is proposed as a novel concept of asphaltene fractionation according to their adsorption characteristics. Two examples of E−SARA analysis were discussed in detail to illustrate its advantages of distinguishing asphaltene subfractions with high affinity to water or solid surfaces. Combined with chemical characterizations and molecular simulations, this original asphaltene fractionation provides a unique way of studying the role of specific chemical functionality in asphaltene aggregation, precipitation, and adsorption.

The second part of the thesis systematically studies the effect of solvent aromaticity on the physicochemical properties of asphaltene subfractions obtained using E−SARA fractionation based on asphaltene adsorption at oil−water interfaces. Toluene and heptol 50/50 (a mixture of *n*−heptane and toluene at a 1:1 volume ratio) were used as the organic solvent for asphaltenes, respectively. This work identified and confirmed the role of certain functional groups in enhancing oil−water interfacial activity of asphaltenes.

In the last part of the thesis, the focus of E−SARA studies extends from interfacial activity of asphaltene subfractions to their aggregation behaviors in bulk oil phase. The dynamic light scattering (DLS) technique was used to measure the aggregation kinetics of fractionated asphaltenes in varying solvent aromaticity. The DLS results agreed well with the interaction force measurements using an atomic force microscope (AFM) between fractionated asphaltenes in different organic solvents. The study linked the experimental data with theoretical predictions, providing a molecular level understanding of asphaltene interactions in organic phase.

The major contributions of this thesis research to science is developing the E−SARA analysis, which is the fractionation of whole asphaltenes according to their interfacial activities and adsorption characteristics. E−SARA analysis optimizes the comprehensive investigations of complex asphaltenes by targeting specific asphaltene subfractions that have critical influences in the relevant systems of interest. Through the aid of chemical characterization and computational modeling, certain asphaltene characteristics were attributed to the presence of key chemical functional groups in asphaltenes. E−SARA analysis provided necessary information to improve our understanding of the governing mechanisms of asphaltene adsorption and aggregation. Incorporating such knowledge with industrial practices allows the design of smarter strategies to mitigate or prevent asphaltene−induced problems (emulsion stabilization, solid surface deposition, etc.) in petroleum industry.

1.3 THESIS STRUCTURE

This thesis has been structured as a compilation of papers. Chapters 3−5 are research papers published in scientific journals. The key content of each chapter is given below as an outline of the thesis.

Chapter 1 presents the overall introduction to the thesis, including the background, objectives, and thesis scope.

Chapter 2 provides a comprehensive literature review on current experimental and theoretical investigation of asphaltenes.

Chapter 3 introduces the concept of E−SARA analysis as the fractionation of whole asphaltenes according to their adsorption at oil−water interfaces or solid surfaces. The detailed procedures of E−SARA analysis were described, and characterizations of resulting asphaltene subfractions were thoroughly discussed. A version of this chapter has been published in:

Peiqi Qiao, David Harbottle, Plamen Tchoukov, Jacob Masliyah, Johan Sjoblom, Qingxia Liu, and Zhenghe Xu, Fractionation of Asphaltenes in Understanding Their Role in Petroleum Emulsion Stability and Fouling, *Energy Fuels* **2017**, *31*, 3330−3337.

Chapter 4 illustrates the effect of solvent aromaticity on the composition of asphaltene subfractions which stabilize W/O emulsions. Asphaltene subfractions were extracted by E−SARA analysis according to their adsorption at oil−water interfaces from either toluene or heptol 50/50 solutions. The combination of the experimental results with theoretical prediction revealed the key functional groups that are critical to the asphaltene−induced stabilization of W/O emulsions. A version of this chapter has been published in:

Peiqi Qiao, David Harbottle, Plamen Tchoukov, Xi Wang, and Zhenghe Xu, Asphaltene Subfractions Responsible for Stabilizing Water−in−Crude Oil Emulsions. Part 3. Effect of Solvent Aromaticity, *Energy Fuels* **2017**, *31*, 9179−9187.

Chapter 5 discusses the molecular interactions of asphaltene subfractions in organic media of varying aromaticity. Whole asphaltenes were fractionated based on their affinity to oil−water interfaces using E−SARA analysis. The aggregation kinetics of fractionated asphaltenes was studied by DLS. The AFM technique was applied to measure the interaction forces between immobilized fractionated asphaltenes. The good agreement between DLS and AFM results indicated the essential role of key functional groups in governing asphaltene aggregation in the bulk oil phase. A version of this chapter has been published in:

Peiqi Qiao, David Harbottle, Zuoli Li, Yuechao Tang, and Zhenghe Xu, Interactions of Asphaltene Subfractions in Organic Media of Varying Aromaticity, *Energy Fuels* **2018**, *32*, 10478−10485.

Chapter 6 presents the conclusions of this thesis and recommendations for future research.

1.4 REFERENCES

(1) Jewell, D. M.; Weber, J. H.; Bunger, J. W.; Plancher, H.; Latham, D. R. *Anal. Chem.* **1972**, *44*, 1391–1395.

(2) Jewell, D. M.; Albaugh, E. W.; Davis, B. E.; Ruberto, R. G. *Ind. Eng. Chem. Fundam.* **1974**, *13*, 278–282.

(3) Chen, T.; Lin, F.; Primkulov, B.; He, L.; Xu, Z. *Can. J. Chem. Eng.* **2017**, *95*, 281–

289.

(4) Akbarzadeh, K.; Hammami, A.; Kharrat, A.; Zhang, D.; Allenson, S.; Creek, J.; Kabir, S.; Jamaluddin, A. J.; Marshall, A. G.; Rodgers, R. P.; Mullins, O. C.; Solbakken, T. *Oilfield. Rev.* **2007**, *19*, 22–43.

(5) Kilpatrick, P. K. *Energy Fuels* **2012**, *26*, 4017–4026.

(6) Adams, J. J. *Energy Fuels* **2014**, *28*, 2831–2856.

(7) Eskin, D.; Mohammadzadeh, O.; Akbarzadeh, K.; Taylor, S. D.; Ratulowski, J. *Can. J. Chem. Eng.* **2016**, *94*, 1202–1217.

(8) Mullins, O. C. *Annu. Rev. Anal. Chem.* **2011**, *4*, 393–418.

(9) Drummond, C.; Israelachvili, J. *J. Pet. Sci. Eng.* **2004**, *45*, 61–81.

(10) Torres, C.; Treint, F.; Alonso, C.; Milne, A.; Lecomte, A. *Proceedings of the SPE/ICoTA Coiled Tubing Conference and Exhibition*; The Woodlands, TX, April 12−13, 2005; SPE−93272−MS, DOI: 10.2118/93272−MS.

(11) Yarranton, H. W.; Hussein, H.; Masliyah, J. H. *J. Colloid Interface Sci.* **2000**, *228*, 52–63.

(12) Tchoukov, P.; Yang, F.; Xu, Z.; Dabros, T.; Czarnecki, J.; Sjöblom, J. *Langmuir* **2014**, *30*, 3024–3033.

(13) Harbottle, D.; Chen, Q.; Moorthy, K.; Wang, L.; Xu, S.; Liu, Q.; Sjoblom, J.; Xu, Z. *Langmuir* **2014**, *30*, 6730–6738.

(14) Gonzalez, D. L.; Ting, P. D.; Hirasaki, G. J.; Chapman, W. G. *Energy Fuels* **2005**, *19*, 1230–1234.

(15) Czarnecki, J.; Tchoukov, P.; Dabros, T. *Energy Fuels* **2012**, *26*, 5782–5786.

(16) Czarnecki, J.; Tchoukov, P.; Dabros, T.; Xu, Z. *Can. J. Chem. Eng.* **2013**, *91*, 1365–1371.

(17) Qiao, P.; Harbottle, D.; Tchoukov, P.; Masliyah, J. H.; Sjoblom, J.; Liu, Q.; Xu, Z. *Energy Fuels* **2017**, *31*, 3330−3337.

(18) Fossen, M.; Kallevik, H.; Knudsen, K. D.; Sjöblom, J. *Energy Fuels* **2007**, *21*, 1030–1037.

(19) Kharrat, A. M. *Energy Fuels* **2009**, *23*, 828–834.

(20) Jarvis, J. M.; Robbins, W. K.; Corilo, Y. E.; Rodgers, R. P. *Energy Fuels* **2015**, *29*, 7058–7064.

CHAPTER 2 LITERATURE REVIEW

2.1 ASPHALTENE PROPERTIES

2.1.1 Asphaltene Composition

As asphaltenes represent a solubility class of petroleum being soluble in aromatic solvents but insoluble in *n*−alkanes, they encompass a wide variety of molecular structures and functional groups. Typical asphaltene molecules are large polynuclear hydrocarbons consisting of condensed aromatic rings, aliphatic side chains, and various heteroatom (nitrogen, oxygen and sulfur) groups. Asphaltenes contain both acidic and basic functionalities, as suggested by non−aqueous potentiometric titration studies.[1] The common elemental composition of Athabasca asphaltenes is listed in Table 2.1.[2] The atomic H/C ratio of asphaltenes is between 1.0 and 1.2, suggesting the backbone of fused aromatic hydrocarbons.[3] Nitrogen in asphaltenes is mostly present in pyrrolic, pyridine and quinoline groups, while oxygen is mainly present in hydroxyl, carbonyl, and carboxyl groups.[4] Asphaltenes are rich in sulfur, and the major sulfur−containing functional groups are thiophene, sulfide and sulfoxide.[4] Asphaltenes also contain trace amounts of metals such as nickel, vanadium and iron, indicating the presence of porphyrin and porphyrin−like groups.[4]

Table 2.1 Elemental Composition (wt%) of Athabasca asphaltenes.

C	H	N	O	S
80.5 ± 3.5	8.1 ± 0.4	1.1 ± 0.3	2.5 ± 1.2	7.9 ± 1.1

The average molecular composition of asphaltenes can be mimicked by proper model compounds that resemble the properties and behaviors of real asphaltenes. A great deal of research effort has been placed on the synthesis of different asphaltene model compounds with well−defined structures in order to understand the molecular mechanisms behind asphaltene properties. Akbarzadeh et al, for example, launched a series of pyrene−based asphaltene model molecules (Figure 2.1a) to investigate their self−association properties.[5] Nordgåd, Sjöblom and their colleagues synthesized a series of perylene−based model compounds (Figure 2.1b) to study their interfacial behaviors at oil−water interfaces.[6–8] Alshareef et al. designed several cholestane−derived model compounds (Figure 2.1c) to study their thermal cracking reactions.[9] In this type of model compounds, the steroid A−ring of cholestane is covalently fused to a range of benzoquinoline groups substituted with different chemical functionalities.

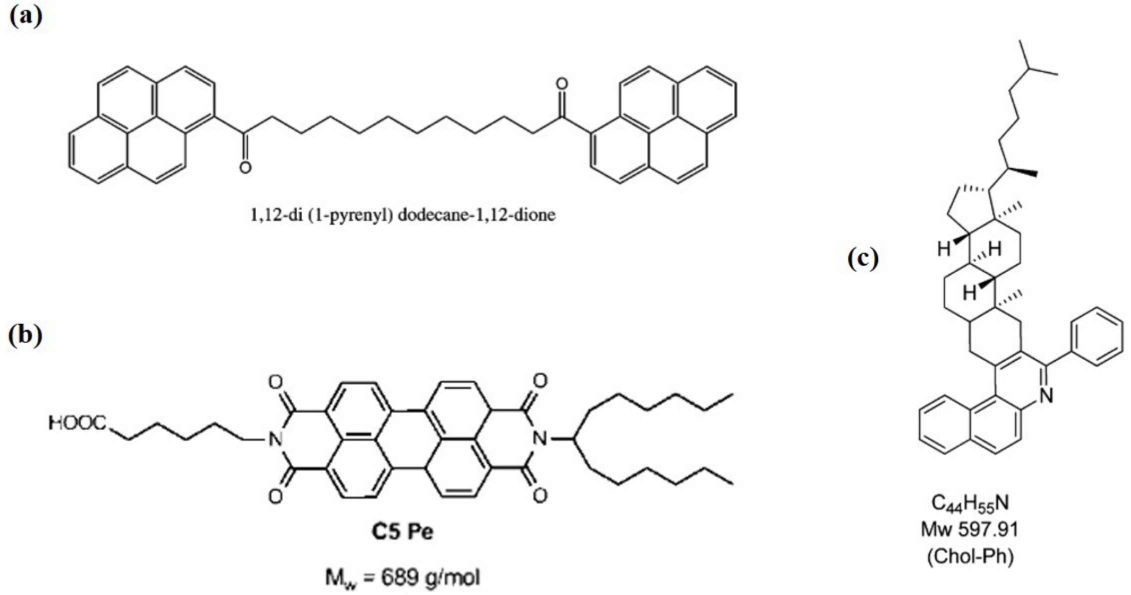

Figure 2.1 Asphaltene model compounds. (a) Pyrene−based model compound, reprinted with permission from ref 5. Copyright 2005 American Chemical Society. (b) Perylene−based model compound, reprinted with permission from ref 7. Copyright 2008 American Chemical Society. (c) Cholestane−based model compound, reprinted with permission from ref 9. Copyright 2012 American Chemical Society.

2.1.2 Asphaltene Molecular Weight

The molecular weight (MW) of asphaltenes has been a source of controversy for decades. Previous studies based on vapor pressure osmometry (VPO)[10,11] and gel permeation chromatography (GPC)[12] estimated that the average molecular weight of asphaltenes varied significantly from 3000 to 10000 daltons (Da). The VPO method provides the average molecular weight of asphaltenes based on the equilibrium solvent vapor pressure when asphaltenes are dissolved in a good solvent such as benzene and toluene, whereas GPC gives the molecular weight distribution according to the elution time of asphaltene solution from a porous gel column. Both results suffer from several uncertainties, among which strong asphaltene aggregation being considered the dominant impedance. Asphaltenes begin to aggregate at very low concentrations at parts per billion (ppb) level,[13,14] and the measured large molecular weight owes to the presence of asphaltene aggregates instead of individual molecules. Therefore, the results for concentrated asphaltene solutions need to be extrapolated to infinite dilution, which is outside the experimental range, inducing substantial experimental errors.

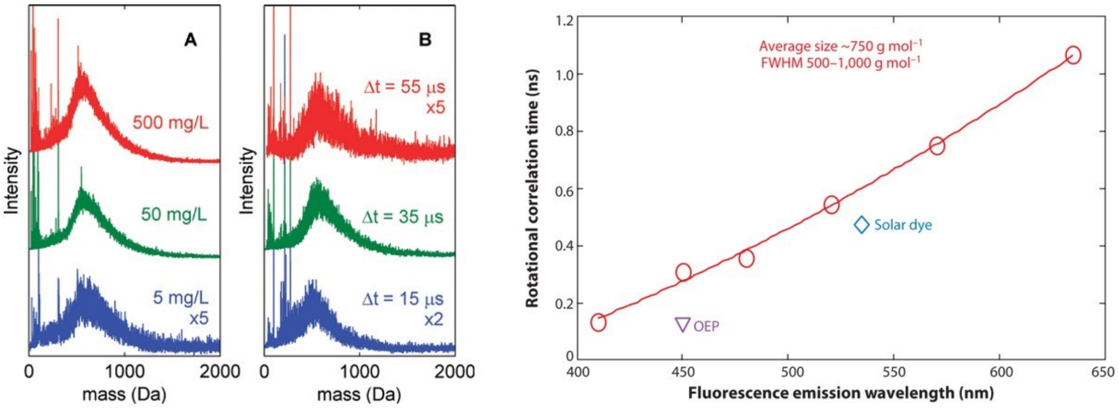

(i) **(ii)**

Figure 2.2 (i) L^{2}MS mass spectra of asphaltenes (a broad maximum near 600 Da) with negligible differences observed at different (A) sample concentrations and (B) desorption−ionization time delays, reprinted with permission from ref 19. Copyright 2008 American Chemical Society. (ii) TRFD gives the rotational correlation times of asphaltenes and model compounds, reprinted with permission from ref 23. Copyright 2011 Annual Reviews.

The mass spectrometry (MS) and fluorescence depolarization techniques have been utilized to resolve the discrepancy on average molecular weight of asphaltenes. In MS, the mass−to−charge ratio is directly measured by ionizing asphaltene species in a number of methods such as electrospray ionization (ESI),[15,16] field ionization (FI), atmospheric pressure photoionization (APPI),[17] atmospheric pressure chemical ionization (APCI),[18] and laser ionization laser desorption (L^2).[19,20] In general, MS technique is a powerful tool for analysis of complex asphaltenes. However, the MS−based measurements do not lead to asphaltene composition as a result of ionization efficiency differences among individual asphaltene molecules. Time−resolved fluorescence depolarization (TRFD) is another technique being used to determine the average molecular weight of asphaltenes.[21–23] TRFD provides the information concerning molecular size of asphaltenes by measuring the depolarization of the fluorescence emission. Such information is interpreted to infer asphaltene molecular weight by comparison with model compounds. TRFD has the capability of working with highly diluted asphaltene solution, thereby minimizing the effect of asphaltene aggregation. The molecular mass of asphaltenes obtained using MS and TRFD techniques are converged in the range of 400 to 1500 Da, with an average value of about 750 Da (Figure 2.2).

2.1.3 Asphaltene Molecular Structure

The discussions on asphaltene molecular weight are closely related to their molecular structures. The exact molecular structure of asphaltenes is a matter of considerable speculation due to the complexity and polydispersity of asphaltene molecules. There had been a long−standing debate as to whether asphaltenes were composed of several polycyclic aromatic hydrocarbon (PAH) cores linked with aliphatic chains, known as the archipelago model, or if they comprised a single PAH core with peripheral alkyl chains, known as the island model (Figure 2.3)[24]. The main difference between island model and archipelago model is the number of aromatic moiety per asphaltene molecule. The typical asphaltene molecular weight is more than 2000 Da in archipelago model, whereas the island type asphaltene molecule has a molecular weight of 500 to 1000 Da.[4] The molecular weight of island−like asphaltene molecules thus fits comfortably within the range determined by MS and TRFD techniques.

It is now generally regarded that asphaltenes are primarily present in the form of island structure with a PAH core of 6−7 fused rings on average.[25–28] In comparison with archipelago structure, island structure matched better with asphaltene ultraviolet (UV) fluorescence emission and absorption spectra.[24] The TRFD[21,22,29,30] and fluorescence correlation spectroscopy (FCS) studies[31] by Mullins et al. indicated that asphaltene molecules are not cross−linked PAHs according to their rotational and translational diffusion, respectively. In good agreement with nondestructive TRFD and FCS studies, L^2MS studies revealed that asphaltenes exhibited identical fragmentation behaviors with island model compounds.[32] Both asphaltenes and island model compounds were stable under harsh fragmentation conditions; on the contrary, archipelago model compounds exhibited energy−dependent fragmentation, also confirmed by laser−induced acoustic desorption (LIAD)/electron ionization (EI) MS analysis.[33] By combining atomic force microscopy (AFM) and scanning tunneling microscopy (STM), Schuler et al. highlighted the dominant detection of island structure in molecular imaging with atomic resolution of more than 100 asphaltene molecules.[34] These observations add credibility to the dominance of island structural motifs in asphaltenes. However, it is important to note that the island model is not the sole asphaltene structure, as suggested by the characterization of asphaltene thermal cracking products.[35] Several archipelago type structures were also reported in the work of Schuler et al.[34,36] Acevedo et al. proposed that the molecular structure difference results in the solubility variation of fractionated asphaltenes in toluene.[37] Asphaltene structures vary significantly based on the different geochemical source of origins and precipitation conditions for asphaltenes.[38]

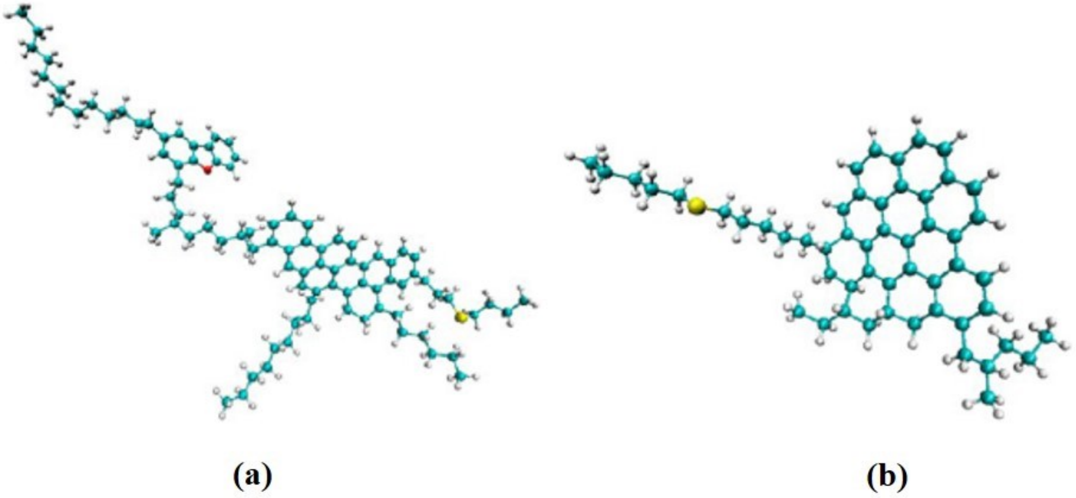

Figure 2.3 Asphaltene molecule in (a) archipelago model (MW: 1248 Da) and (b) island model (MW: 726 Da), reprinted with permission from ref 24. Copyright 2013 American Chemical Society.

2.2 ASPHALTENE AGGREGATION

The controversy around asphaltene molecular weight and structure is a direct consequence of the strong aggregation tendency of asphaltenes. The exceptionally high molecular mass of asphaltenes obtained from VPO and GPC represents the asphaltene aggregates rather than individual asphaltene molecules. Asphaltene molecules self−associate with each other forming stable aggregates even in a very dilute solution of a good solvent like toluene.[39] Therefore, most of asphaltene aggregation studies to date were performed in toluene to avoid the complexity and polydispersity brought by natural petroleum fluids. Asphaltenes aggregates were previously referred to as asphaltene micelles as asphaltenes were considered similar to standard surfactants.[40] Asphaltene aggregates were assumed similar to inverted micelles of surfactants formed in oil solutions. Reins were believed as the key contributor to asphaltene aggregation by surrounding asphaltene micelles to keep them suspended in the oil phase. However, it has been shown that asphaltenes aggregates can be formed in the absence of resins.[41] Moreover, unlike surfactants, asphaltenes lack the amphiphilic characters.[42] There are normally no identifiable hydrophilic heads in asphaltene structures; thus, the driving force for asphaltene aggregation cannot be head−head interactions. Yarranton reported that the primary asphaltene aggregate consisted of only two to six asphaltene monomers on average,[43] making the critical micelle concentration (CMC) inapplicable for asphaltenes due to such low aggregation number. In addition, asphaltenes adsorb irreversibly at the oil−water interface,[44] which is another evident dissimilarity between asphaltenes and surfactants.

There has been a growing consensus in recent years that asphaltenes aggregate in a hierarchical model, named as Yen−Mullins model which was first proposed by Yen[45] and later modified by Mullins.[46,47] The Yen−Mullins model describes a stepwise asphaltene aggregation process, as illustrated by Figure 2.4.[47] The asphaltenes are dominated by the island geometry with a single PAH core surrounded by alkyl chains. The average molecular weight of asphaltenes is about 750 Da, and the average number of fused rings is seven, as indicated by molecular imaging,[25] molecular orbital (MO) calculations[26] and Raman spectroscopy studies.[27] As asphaltene concentration exceeds the critical nanoaggregate concentration (CNAC), a small number (5 to 10) of asphaltene molecules start to form a nanoaggregate structure in primary aggregation. The high−quality ultrasonic spectroscopy[13] and direct−current (DC) electrical conductivity[14] measurements determined the CNAC of asphaltenes in toluene in the range of 50 to 150 mg/L as it varied based on the asphaltene source and thermodynamic conditions. The formation of asphaltene nanoaggregates above the CNAC was also corroborated by centrifugation studies.[48] In addition, the same CNAC was identified by nuclear magnetic resonance (NMR) diffusion measurements.[49] Lisitza et al. showed that the average self−diffusion coefficient reduces greatly above the CNAC.[49] The substantial change in spin−echo signal of asphaltenes at the onset of aggregation indicated the restricted environment of peripheral alkyl chains upon aggregation. The authors suggested that individual asphaltene molecules associated with each other to form nanoaggregates primarily through skewed π−π stacking interactions, giving a negative enthalpy. The entropy was found positive due to the entropy gain of solvent upon aggregation, suggesting the entropically driven formation of asphaltene nanoaggregates. The disordered core−shell disk structure of asphaltene nanoaggregates was recognized by coupled small−angle neutron scattering (SANS) and small−angle X-ray scattering (SAXS),[50] showing excellent agreement with Yen−Mullins model. The asphaltene structural details were observed by incorporating SANS and SAXS sensitivity to nuclear and electron density, respectively. The nanoaggregate core consists of densely packed aromatic structures, and its shell is highly concentrated in aliphatic carbons. The formation of nanoaggregates is mainly attributed to the attractive π−π stacking interactions between PAH cores of asphaltene monomers. In contrast, the steric hindrance caused by peripheral alkane substituents limits the aggregation number by preventing the close approach of new PAH cores to the interior PAHs of nanoaggregates. Therefore, additional asphaltene monomers continue to form new nanoaggregates of a small aggregation number.

Asphaltene nanoaggregates begin to form clusters in secondary aggregation at the critical clustering concentration (CCC), which is a significantly higher concentration than the CNAC. As with the CNAC, DC electrical conductivity measurements obtained a break in the curve at the CCC (about 2 g/L).[46] The small slope change in the curve indicated the small aggregation number (less than 10), suggesting the entropically driven formation of clusters. For asphaltene−in−toluene solutions subject to *n*−heptane addition, Anisimov et al. suggested that the asphaltene aggregation kinetics is substantially changed from diffusion−limited aggregation (DLA) to reaction−limited aggregation (RLA) as asphaltenes concentration increased from the CNAC to the CCC.[51,52] The authors indicated that asphaltenes are dispersed primarily as nanoaggregates when asphaltene concentration is below the CCC but above the CNAC. The nanoaggregates likely adhere upon collision; thus, DLA is the governing aggregation mechanism. However, above the CCC, the clusters of nanoaggregates become dominant as the secondary aggregation occurs. The chance for two clusters sticking when they collide is low due to their fractal nature.[53] A surface morphological change of clusters is required for the flocculation of clusters, hence appearing in RLA kinetics. The clusters are formed as a result of alkyl−alkyl and alkyl−aromatic interactions between the asphaltene nanoaggregates.[54] In addition, Dutta Majumdar and co−workers indicated the small role of T−shaped interactions in cluster formation (Figure 2.5).[54] The complete Yen−Mullins aggregation hierarchy for asphaltenes has been observed by molecular dynamics (MD) simulation studies accelerated by high−performance graphics processing unit (GPU) hardware.[55,56]

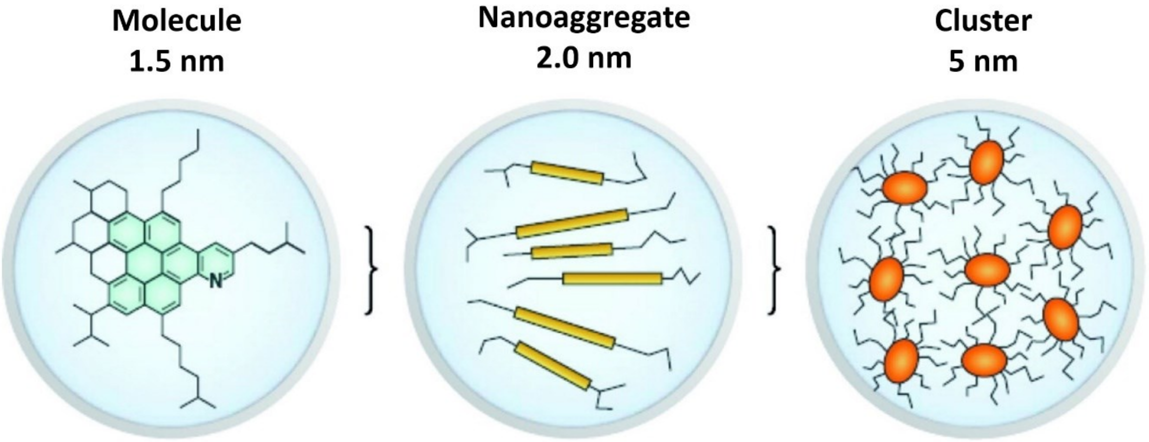

Figure 2.4 Yen−Mullins model. All three structures that constitute Yen−Mullins model: individual asphaltene molecule, nanoaggregate, and cluster of nanoaggregates, reprinted with permission from ref 47. Copyright 2012 American Chemical Society.

The supramolecular assembly model proposed by Gray et al. describes asphaltene aggregates as three−dimensional porous organic networks with accessible volume,[57] containing a significant level of solvent as supported by SANS[58] and MD simulation studies.[59] In agreement with the polymerization model suggested by Yarranton et al.,[60] the authors believed that most asphaltene molecules contain multiple active sites (functional groups) which are capable of associating with other asphaltenes. The formation of this supramolecular network is a result of multiple cooperative interactions, including aromatic π–π stacking, hydrogen bonding, acid–base interactions, metal coordination, and hydrophobic pockets. The exposed functional groups on the network surface can strongly interact with other active sites, giving rise to asphaltene adsorption onto a wide range of surfaces, such as silica,[61] alumina[62] and metal.[63] As a flexible network, the asphaltene aggregate can respond to external forces[64] and solvent strength.[65,66]

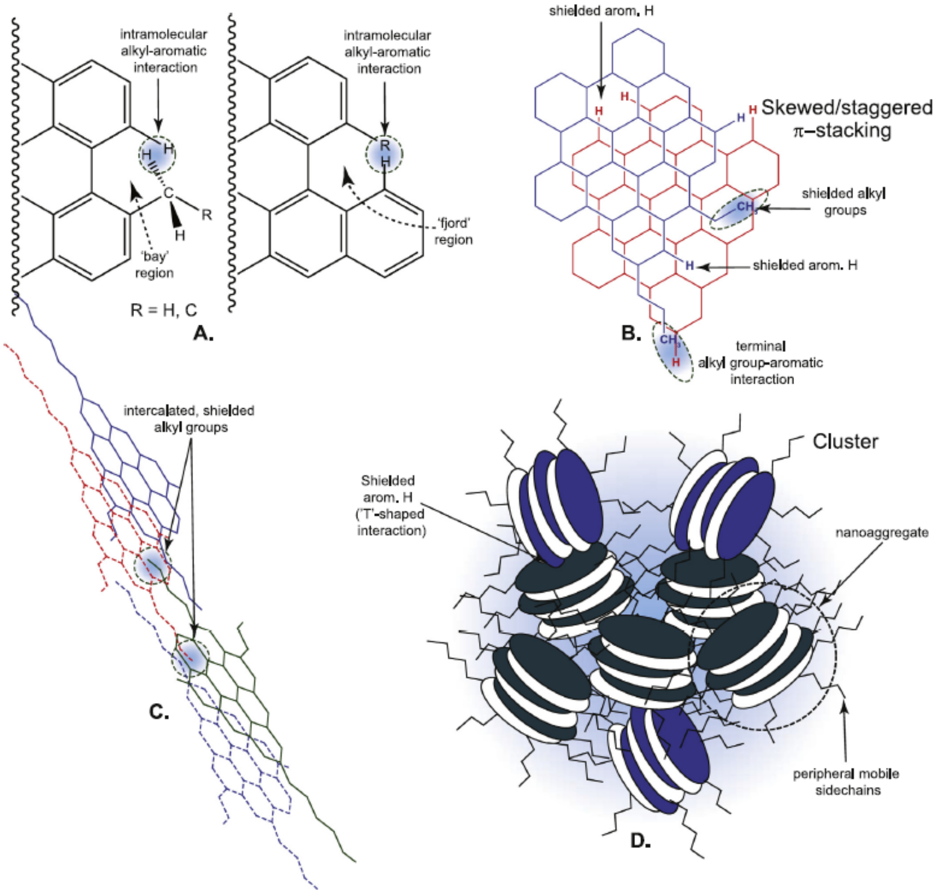

Figure 2.5 Possible molecular interactions in asphaltene aggregation. (A) Alkyl–aromatic interactions, (B) and (C) aromatic–aromatic interactions, and (D) cluster formation from nanoaggregates, reprinted with permission from ref 54. Copyright 2017 Elsevier.

The solvent aromaticity has a considerable effect on asphaltene aggregation. Asphaltenes have a stronger tendency to aggregate in an aliphatic solvent such as *n*−heptane than in an aromatic solvent such as toluene.[41] Sedghi et al indicated that the aromatic interactions between toluene and PAH cores of asphaltenes greatly contribute to the lower association free energy of asphaltenes (in absolute value) in toluene than in *n*−heptane.[67] The size of fractal asphaltene clusters increases by the addition of *n*−heptane.[68] AFM studies by Wang et al.[65] and SFA studies by Natarajan et al.[69] and Zhang et al.[70] showed that the addition of *n*−heptane changes the colloidal interactions between asphaltenes in their toluene solution. As the volume fraction of *n*−heptane increases, the long−range steric repulsion between asphaltene surfaces in toluene is reduced and the weak adhesion is generated. The asphaltene films adsorbed on the silica or mica surfaces swell in toluene, but undergo a conformational change to more collapsed structures by adding *n*−heptane. In addition to dependency on solvency, the aggregation of asphaltenes also relies on temperature. Torkaman et al. reported that the average size of asphaltene clusters is reduced with rising temperature since the decreasing viscosity is outweighed by the increasing solubility of asphaltene aggregates.[71]

2.3 ASPHALTENE PRECIPITATION

Asphaltenes can precipitate out from petroleum oils due to the composition, temperature or pressure change. According to the solubility definition of asphaltenes, *n*−pentane and *n*−heptane are two precipitants commonly used to extract asphaltenes from crude oils. The asphaltenes extracted by *n*−pentane are different in chemical composition from those extracted by *n*−heptane as a result of solubility parameter difference between these two solvents.[72] The *n*−heptane can dissolve some asphaltene molecules which are not compatible with *n*−pentane. The precipitated asphaltene aggregates can also occlude some materials which are miscible with precipitants. The dissolution and reprecipitation of asphaltenes gives mass loss as the amount of occluded material decreases with each cycle.[73]

Asphaltene precipitation leads to a series of problems including but not limited to formation damage,[74,75] pipeline plugging,[76] equipment fouling[77] and formation of stable water−in−oil (W/O) emulsions.[78–80] The prediction of asphaltene precipitation is of considerable interest to oil industry in order to minimize asphaltene remediation costs. The onset of asphaltene precipitation from crude oils was previously investigated using a number of techniques upon titration with a precipitant (usually *n*−heptane). Wattana et al. determined the onset of asphaltene precipitation by detecting the deviation of oil refractive index from its linear relationship with precipitant volume.[81] The authors reported that the refractive index (RI) of oil no longer follows the linear mixing rule as asphaltenes begin to precipitate out from the oil. Similarly, UV−visible (Vis) spectroscopy[82,83] and near−infrared (NIR) spectroscopy[84] were applied to identify the precipitation onset of asphaltenes by monitoring the point of minimum light absorbance or optical density, as it stops from decreasing once the asphaltene precipitation occurs. However, these experiments were performed with a short time span assuming the immediate equilibration upon precipitant addition. The oils were considered stable if there were no measured deviations shortly detected after the addition of precipitants; thus, the time effect on asphaltene precipitation was neglected.

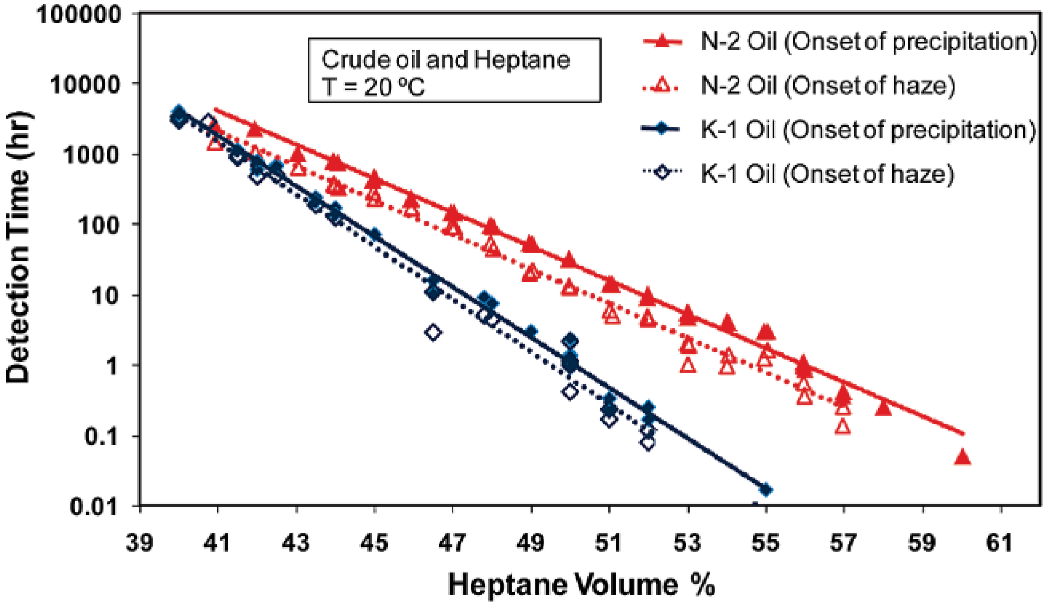

Figure 2.6 The relationship between detection time and heptane volume for asphaltene precipitation (particles are 0.5 μm in diameter) onset and haze (particles are 0.2−0.3 μm in diameter) onset, determined by optical microscopy, reprinted with permission from ref 86. Copyright 2009 American Chemical Society.

Asphaltene precipitation is a time−dependent process. Angle et al. reported asphaltene precipitation below the critical precipitant concentration when enough time was allowed.[85]

Using optical microscopy and centrifugation−based separation, Maqbool et al. demonstrated that the detection time for asphaltene precipitation increases exponentially with decreasing precipitant concentration, as shown by Figure 2.6.[86] The detection time for asphaltene precipitation varies from several minutes to months depending on the precipitant concentration. It clearly indicates the significance of time effect in understanding asphaltene precipitation process.

Different models have been proposed for predicting asphaltene precipitation. One example is the two−component asphaltene solubility model (ASM) developed by Wang and Buckley[87] based on Flory–Huggins polymer theory.[88,89] The ASM model treats the crude oil as a mixture of two pseudo components (asphaltenes and mixed solvent). It simply characterizes the components using a correlation between solubility parameters and RI rather than making any arbitrary composition assumptions upon phase separation. The ASM model defines the precipitation onset using Gibbs free energy curve, showing good agreement with experimental observations. However, its drawback is that it is less accurate in predicting the amount of asphaltene precipitated by different *n*−alkane solvents since the same solubility parameter can be used under different solvent conditions. In addition to regular solution theory, the equation of state (EoS) is another approach for asphaltene precipitation modeling.[90] The most widely used EoS model for predicting asphaltene precipitation is the statistical associating fluid theory (SAFT), which was developed by Chapman et al.[91,92] who extended Wertheim's thermodynamic perturbation theory[93–96] to characterize the mixture. In the SAFT EoS, molecules are represented in the form of chains with bonded spherical segments. The residual free energy is the free energy sum of segments, bonding, and directional interactions (such as hydrogen bonding). One of the SAFT variations is the perturbed chain−SAFT (PC−SAFT) proposed by Gross and Sadowski.[97] Ting et al.[98] and Gonzalez et al.[99] showed that the PC−SAFT is adequately capable of predicting the asphaltene precipitation onset and the unstable region with high accuracy. The petroleum molecules can be fractionated into multiple components in the PC−SAFT, giving more flexibility in binary interaction parameter and hence providing better estimation results.

Asphaltene precipitation can be postponed or prevented by adding chemical additives serving as inhibitors. SANS[100] and dynamic light scattering (DLS)[101] measurements indicated that the size of asphaltene aggregates decreases in the presence of resins. Resins can be classified as an oil fraction being insoluble in liquid propane but soluble in *n*−pentane. The addition of resins reduces the aggregation rate of asphaltenes by disrupting the aromatic π−π stacking and polar interactions between asphaltene monomers. The polymerization model proposed by Yarranton et al. describes the resins as terminators in the polymerization−like association of asphaltenes. Some amphiphilic molecules, such as alkylphenols[102,103] and dodecyl benzene sulfonic acid (DBSA),[104] have been used as efficient asphaltene aggregation inhibitors. They generally consist of a head group of polarity or acidity allowing them interact with asphaltenes, and an alkyl tail which improves their solubility in *n*−alkanes and blocks other asphaltene molecules. Recently, metal oxides nanoparticles have also been used as inhibitors with advantages of high interaction potential, high mobility in porous media and thermal catalytic capability.[105−108]

2.4 ASPHALTENE ADSORPTION AT SOLID SURFACES

Asphaltenes can adsorb from oils onto a wide arrange of solid surfaces such as clay minerals, silica, alumina, metal, and glass, etc. On the one hand, asphaltene adsorption at solid surfaces is a ubiquitous phenomenon throughout the entire oil production and processing, causing pipeline plugging, equipment fouling, and catalyst poisoning, to name a few.[109] Extensive research efforts have been devoted to understanding the underlying adsorption mechanisms and providing solutions to resolve asphaltene adsorption−related issues. On the other hand, the removal of asphaltenes from crude oils can be achieved by taking advantage of their strong adsorption at solid surfaces. It has been demonstrated as a promising way to upgrade oil at the earliest stages through in−situ adsorption of asphaltenes onto the nanoparticulated materials within the reservoir.[107]Asphaltenes adsorbed onto nanoparticles are suitable for catalytic steam gasification/cracking.[105] The asphaltenes desorbed from sorbents can then be utilized for coking, paving and coating. The asphaltene adsorption process often follows a Langmuir−type isotherm. The formation of mono− or multilayer asphaltene films can be related to a number of factors such as sorbent, solvent, asphaltene composition, asphaltene concentration, flow condition, temperature, and moisture content.[110]

2.4.1 Clay Minerals

Clay minerals are a major contributor to the fines content of crude oils. They are hydrous aluminum phyllosilicates composed of tetrahedral silicate sheets and octahedral hydroxide sheets in different ratios. A typical 1:1 clay, like kaolinite, consists of one tetrahedral sheet and one octahedral sheet; while a 2:1 clay, such as illite or montmorillonite, consists of an octahedral sheet sandwiched between two tetrahedral sheets. Using UV−Vis spectroscopy, Pernyeszi et al.[111] showed that kaolinite exhibits a higher adsorption capacity for asphaltenes than illite. Saada et al.[112] and Jada et al.[113] attributed this adsorption capacity difference to the presence of water, and specific hydrophilicity/hydrophobicity difference between kaolinite and illite. The authors indicated that water cannot totally inhibit the adsorption of asphaltenes onto kaolinite and illite. However, kaolinite is more hydrophobic than illite thus retaining less water on surface and showing greater affinity to asphaltenes. It should be noted that the adsorption capacity of clay minerals can significantly change according to their source of origins.[110] Dudášová et al. suggested that the asphaltene adsorption is due to the polar interactions between clay surfaces and asphaltenes.[114] Clay minerals are naturally hydrophilic, but their oil wettability greatly increases upon asphaltene adsorption, allowing them to partition at oil−water interfaces to effectively stabilize W/O emulsions.[115]

2.4.2 Silica and Alumina

The hydrophilicity/hydrophobicity of silica can be tuned by controlling the number of surface hydroxyl groups through silylation, calcination, hydration or acid treatments. Dudášová et al. showed that hydrophilic silica has a greater asphaltene adsorption capacity (e.g. 3.78 mg/m^2) than hydrophobic silica (e.g. 0.69 mg/m^2).[114] The similar observation was also made by Hannisdal et al.[115] Using near edge X-ray absorption fine structure (NEXAFS) spectroscopy and spectroscopic ellipsometry, Turgman−Cohen and his colleagues studied the asphaltene adsorption onto silica substrate modified with mixed self−assembled monolayers (SAMs) of aliphatic and aromatic trichlorosilanes.[116] The polar interactions between asphaltenes and silica are recognized as the dominant interaction governing asphaltene adsorption. SAM coating can adjust the interaction strength by shielding polar hydroxyl groups from asphaltenes, as shown by the reduced asphaltene adsorption with increasing SAM thickness. Similarly, Fritschy and Papirer reported the decreasing amount of adsorbed asphaltenes due to the reduction of silica hydroxyl groups by calcination.[117]

Alumina is widely used as a catalyst or catalyst support for oil upgrading and refining.[118] Nassar et al. showed that the asphaltene adsorption capacity of alumina is relative to its surface acidity (Figure 2.7).[119] The acidic alumina exhibits higher adsorption capacity than basic and neutral alumina. Likewise, Araújo et al. indicated the enhanced adsorption of PAHs with increasing acidity of silica−alumina.[120] On the other hand, the alumina surface basicity is proportional to its catalytic activity toward asphaltene oxidation, with the basic alumina showing the highest catalytic effect followed by neutral and then acidic alumina.[119] Alumina nanoparticles can be utilized as effective asphaltene sorbents due to their high surface area/volume ratio and high dispersed nature.[121]

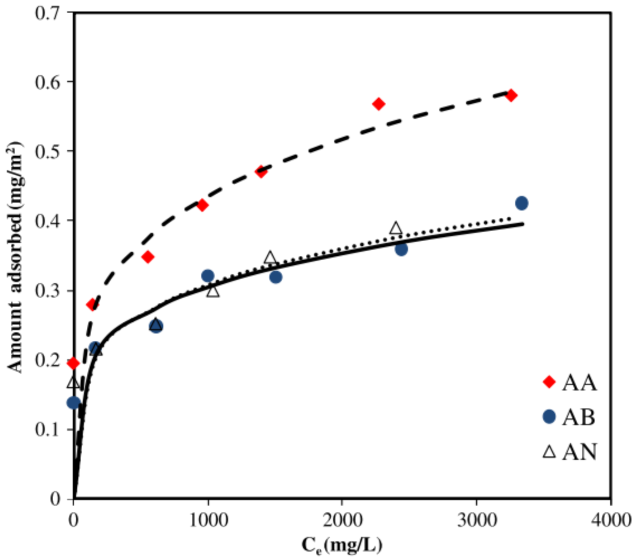

Figure 2.7 Adsorption isotherms of asphaltenes onto acidic alumina (AA), basic alumina (AB) and neutral alumina (AN), reprinted with permission from ref 119. Copyright 2011 Elsevier.

2.4.3 Metal

Asphaltene adsorption on metal has been investigated by a number of research groups using quartz crystal microbalance (QCM). QCM is a sensitive technique that measures the adsorbed mass on different surfaces coated on a piezoelectric quartz crystal through monitoring the resonant frequency and dissipation (or resistance) change of the crystal during the adsorption process. Ekholm et al. showed that asphaltenes form a rigid layer on the hydrophilic gold surface at small concentrations, with the possible formation of multilayers as asphaltene concentration increases.[122] The resins are not able to desorb the adsorbed asphaltenes from the gold surface, indicating the irreversible asphaltene adsorption. Goual and co−workers suggested that there is a critical asphaltene/resin ratio for adsorption of asphaltene−resin mixture on gold surfaces.[123] Below the ratio, asphaltenes continuously adsorb onto gold surfaces as they are not stabilized by resins; however, above the ratio, the well−stabilized asphaltenes prevent the further asphaltene adsorption. Combining QCM and X-ray photoelectron spectroscopy (XPS), Rudrake et al. estimated the thickness of adsorbed asphaltene films on gold surfaces in the range of 6–8 nm.[124] XPS results indicated that the bulk asphaltenes are generally deficient in oxygen−containing species in comparison with asphaltenes adsorbed onto gold. Zahabi and Gray showed that asphaltene adsorption on gold is detectable below the asphaltene precipitation onset, and the amount of adsorbed asphaltenes increases significantly beyond the precipitation onset.[61]

Alboudwarej et al. investigated the asphaltene adsorption onto stainless steel (304L), iron, and aluminum powders using UV−Vis spectroscopy.[63] Stainless steel (304L) exhibits the highest adsorption capacity probably due to the surface morphology difference and the presence of other elements in stainless steel, such as chromium, nickel and sulfur. The same metal with different morphologies can give varied asphaltene adsorption capacity values.[125] Asphaltene adsorption is also driven by solvent aromaticity. Alboudwarej et al. showed that, as the solvent aromaticity increases, asphaltene aggregation is hindered resulting in decreasing adsorption.[63] In addition, asphaltene adsorption decreases with increasing temperature for the same reason.

2.4.4 Glass

Asphaltene adsorption on glass is a phenomenon commonly observed in laboratories. Castillo et al.[126] and Acevedo et al.[127] developed photothermal surface deformation (PSD) spectroscopy to study asphaltene adsorption on the glass surface. In general, PSD spectroscopy directs a laser beam onto sample surface and detects the induced surface deformation by measuring reflected beam signal. The signal can then be related to the amount of materials adsorbed onto the sample surface through calibration. The authors observed the multilayer adsorption of three examined asphaltenes on glass. The formation of asphaltene multilayers was also confirmed by Labrador and co−workers.[128] The authors reported the thickness of asphaltene films on glass surfaces in a large range (20−298 nm) by studying five different asphaltenes using ellipsometry. It clearly shows that the asphaltene film thickness is greatly affected by the source origins of asphaltene samples.

2.5 ASPHALTENE ADSORPTION AT OIL−WATER INTERFACES

Asphaltenes can effectively stabilize W/O emulsions by irreversibly adsorbing at oil−water interfaces in the form of rigid films that prevent water droplet coalescence. A water droplet aged in an asphaltene solution would crumple upon volume reduction, indicating the presence of a crinkled skin, which is an interfacial asphaltene film formed around the water droplet (Figure 2.8).[70] Zhang et al. conducted Langmuir trough compression experiments to investigate the properties of asphaltene films formed at toluene−water interfaces.[129] Interfacial pressure−area (π−A) isotherms were obtained by compressing the interfacial asphaltene film at a specific compression rate. After the first two compressions were completed, the initial top toluene phase was replaced by fresh toluene followed by another compression. The π−A isotherm obtained from the third compression is identical to those from first two compressions, showing the irreversible nature of asphaltene films.

By studying the stability of interfacial asphaltene film using thin liquid film (TLF) technique, Tchoukov et al. found that asphaltene films become more stable with increasing aging time. The 1 h−aged asphaltene films are thicker than 15 min−aged asphaltene films. Larger asphaltene aggregates are observed in 1 h−aged films. In comparison with 15 min−aged asphaltene films, the drainage of 1 h−aged films is much slower, indicating the higher film stability. The aging effect is corroborated by interfacial rheology studies. Bouriat et al., for example, conducted interfacial dilatation rheology experiments on asphaltene films formed at cyclohexane−water interfaces.[130] The authors found that the dilatational elastic modulus (E′) of an asphaltene film increases with aging time. Harbottle et al. suggested that the asphaltene film stability is more sensitive to the shear rheological properties rather than dilatation rheological properties.[80] During shear deformation, the interfacial area remains constant while the interface shape is changed, as opposed to the variable interfacial area and the intact interface shape during dilatational deformation. The authors demonstrated a progressive transition of asphaltene film from viscous dominant to elastic dominant, corresponding well with the droplet coalescence test. Initially, only the shear viscous modulus (G″) is measurable. After certain aging time, the shear elastic modulus (G′) is detected. The kinetic growth of G′ is much faster than that of G″, and G′ exceeds G″ eventually. This transition time depends on asphaltene concentration and solvent aromaticity. It becomes shorter with increasing asphaltene concentration and/or decreasing solvent aromaticity as a result of enhanced asphaltene aggregation. It is now generally regarded that the asphaltene film transition is due to the reorganization of adsorbed asphaltene molecules forming a cross−linked three−dimensional network of asphaltenes.

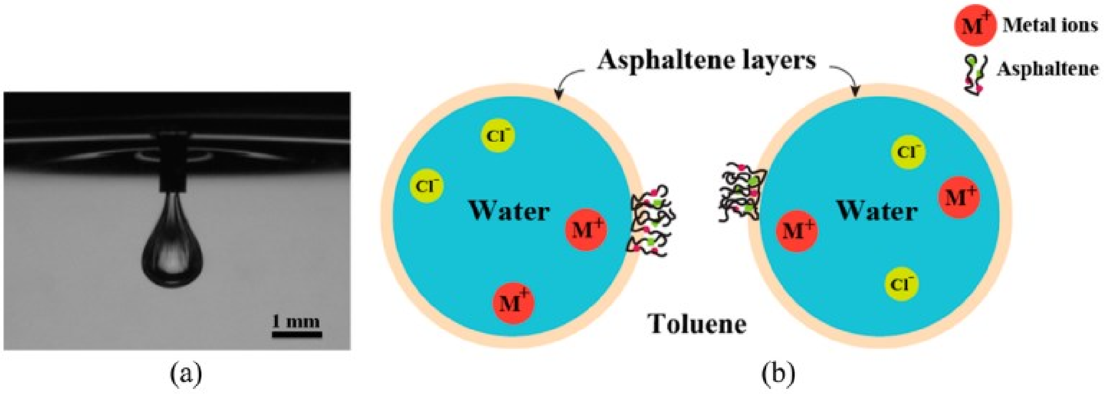

Figure 2.8 (a) Microscopic image of crumpled water droplet aged in asphaltene−in−toluene solution, (b) schematic of two emulsified water droplets interacting in toluene with asphaltenes adsorbed at interfaces, reprinted with permission from ref 70. Copyright 2016 American Chemical Society.

Studies showed that only a small part of asphaltenes actually stabilize W/O emulsions. Yang et al. demonstrated that more than 98 wt% asphaltenes could be removed without affecting W/O emulsion stability.[131] The asphaltenes irreversibly adsorbed at oil−water interfaces contain more polar groups than the asphaltenes remaining in the oil phase, indicating the critical role of polar interactions between asphaltenes and water in the asphaltene adsorption. Kilpatrick showed that less polar asphaltenes form weaker W/O emulsions.[132] The demulsifiers, such as ethylene oxide−propylene oxide (EO−PO) polymer[133] and ethylcellulose (EC)[134,135], can penetrate and soften asphaltene films by competing with asphaltene molecules for the polar interactions with active sites of water. As a result, the elastic (solid−like) oil−water interface is converted to a viscous (liquid−like) interface by the addition of demulsifiers. For the asphaltene−stabilized W/O emulsions, the appropriate hydrophile−lipophile balance (HLB) of a good demulsifier allows it to be well dispersed in oil phase while maintaining effective affinity to water. Feng et al. reported that EC with 4.5 wt% hydroxyl content exhibits the most effective demulsification behavior.[135] The EC−grafted Fe_3O_4 nanoparticles were synthesized by Peng and co−workers as demulsifiers. Due to their magnetic response, EC−grafted Fe_3O_4 nanoparticles exhibit enhanced water coalescence and recycle capability.[136,137] However, it should be emphasized that the overdosed demulsifiers alone can also stabilize the W/O emulsions.[133,138] Thus, it is necessary to determine the optimal dosage of demulsifiers in order to reach the best demulsification performance.

2.6 REFERENCES

(1) Dutta, P. K.; Holland, R. J. *Fuel* **1984**, *63*, 197–201.

(2) Strausz, O. P.; Lown, E. M. *The Chemistry of Alberta Oil Sands, Bitumens and Heavy Oils*; Alberta Energy Research Institute: Calgary, Alberta, Canada, 2003.

(3) Spiecker, P. M.; Gawrys, K. L.; Kilpatrick, P. K. *J. Colloid Interface Sci.* **2003**, *267*, 178–193.

(4) Masliyah, J. H.; Czarnecki, J.; Xu, Z. *Handbook on Theory and Practice of Bitumen Recovery from Athabasca Oil Sands*; Kingsley Knowledge Publishing: Calgary, Alberta, Canada, 2011.

(5) Akbarzadeh, K.; Bressler, D. C.; Wang, J.; Gawrys, K. L.; Gray, M. R.; Kilpatrick, P. K.; Yarranton, H. W. *Energy Fuels* **2005**, *19*, 1268–1271.

(6) Nordgård, E. L.; Sjoblom, J. *J Dispers. Sci.Technol.* **2008**, *29*, 1114–1122.

(7) Nordgåd, E. L.; Landsem, E.; Sjöblom, J. *Langmuir* **2008**, *24*, 8742–8751.

(8) Nordgård, E. L.; Sørland, G.; Sjöblom, J. *Langmuir* **2010**, *26*, 2352–2360.

(9) Alshareef, A. H.; Scherer, A.; Stryker, J. M.; Tykwinski, R. R.; Gray, M. R. *Energy Fuels* **2012**, *26*, 3592–3603.

(10) Sztukowski, D. M.; Yarranton, H. W. *Langmuir* **2005**, *21*, 11651–11658.

(11) Acevedo, S.; Méndez, B.; Rojas, A.; Layrisse, I.; Rivas, H. *Fuel* **1985**, *64*, 1741–1747.

(12) Artok, L.; Su, Y.; Hirose, Y.; Hosokawa, M.; Murata, S.; Nomura, M. *Energy Fuels* **1999**, *13*, 287–296.

(13) Andreatta, G.; Bostrom, N.; Mullins, O. C. *Langmuir* **2005**, *21*, 2728–2736.

(14) Zeng, H.; Song, Y. Q.; Johnson, D. L.; Mullins, O. C. *Energy Fuels* **2009**, *23*, 1201–1208.

(15) Klein, G. C.; Kim, S.; Rodgers, R. P.; Marshall, A. G.; Yen, A.; Asomaning, S. *Energy Fuels* **2006**, *20*, 1965–1972.

(16) Klein, G. C.; Kim, S.; Rodgers, R. P.; Marshall, A. G.; Yen, A. *Energy Fuels* **2006**, *20*, 1973–1979.

(17) Qian, K.; Mennito, A. S.; Edwards, K. E.; Ferrughelli, D. T. *Rapid Commun. Mass Spectrom* **2008**, *22*, 2153–2160.

(18) Cunico, R. L.; Sheu, E. Y.; Mullins, O. C. *Pet. Sci. Technol.* **2004**, *22*, 787–798.

(19) Pomerantz, A. E.; Hammond, M. R.; Morrow, A. L.; Mullins, O. C.; Zare, R. N. *J. Am. Chem. Soc.* **2008**, *130*, 7216–7217.

(20) Wu, Q.; Pomerantz, A. E.; Mullins, O. C.; Zare, R. N. *Energy Fuels* **2014**, *28*, 475–482.

(21) Groenzin, H.; Mullins, O. C. *J. Phys. Chem. A* **1999**, *103*, 11237–11245.

(22) Badre, S.; Carla Goncalves, C.; Norinaga, K.; Gustavson, G.; Mullins, O. C. *Fuel* **2006**, *85*, 1–11.

(23) Mullins, O. C. *Annu. Rev. Anal. Chem.* **2011**, *4*, 393–418.

(24) Mikami, Y.; Liang, Y.; Matsuoka, T.; Boek, E. S. *Energy Fuels* **2013**, *27*, 1838–1845.

(25) Sharma, A.; Groenzin, H.; Tomita, A.; Mullins, O. C. *Energy Fuels* **2002**, *16*, 490–496.

(26) Ruiz−Morales, Y.; Wu, X.; Mullins, O. C. *Energy Fuels* **2007**, *21*, 944–952.

(27) Bouhadda, Y.; Bormann, D.; Sheu, E.; Bendedouch, D.; Krallafa, A.; Daaou, M. *Fuel* **2007**, *86*, 1855–1864.

(28) Dutta Majumdar, R.; Gerken, M.; Mikula, R.; Hazendonk, P. *Energy Fuels* **2013**, *27*, 6528–6537.

(29) Groenzin, H.; Mullins, O. C. *Energy Fuels* **2000**, *14*, 677–684.

(30) Buenrostro−Gonzalez, E.; Groenzin, H.; Lira−Galeana, C.; Mullins, O. C. *Energy Fuels* **2001**, *15*, 972–978.

(31) Schneider, M. H.; Andrews, A. B.; Mitra−Kirtley, S.; Mullins, O. C. *Energy Fuels* **2007**, *21*, 2875–2882.

(32) Sabbah, H.; Morrow, A. L.; Pomerantz, A. E.; Zare, R. N. *Energy Fuels* **2011**, *25*, 1597–1604.

(33) Borton, D.; Pinkston, D. S.; Hurt, M. R.; Tan, X.; Azyat, K.; Scherer, A.; Tykwinski, R.; Gray, M.; Qian, K.; Kenttämaa, H. I. *Energy Fuels* **2010**, *24*, 5548–5559.

(34) Schuler, B.; Meyer, G.; Peña, D.; Mullins, O. C.; Gross, L. *J. Am. Chem. Soc.* **2015**, *137*, 9870–9876.

(35) Chacón−Patiño, M. L.; Blanco−Tirado, C.; Orrego−Ruiz, J. A.; Gómez−Escudero, A.; Combariza, M. Y. *Energy Fuels* **2015**, *29*, 6330–6341.

(36) Schuler, B.; Fatayer, S.; Meyer, G.; Rogel, E.; Moir, M.; Zhang, Y.; Harper, M. R.; Pomerantz, A. E.; Bake, K. D.; Witt, M.; Peña, D.; Kushnerick, J. D.; Mullins, O. C.; Ovalles, C.; Van Den Berg, F. G. A.; Gross, L. *Energy Fuels* **2017**, *31*, 6856–6861.

(37) Acevedo, S.; Castro, A.; Negrin, J. G.; Fernández, A.; Escobar, G.; Piscitelli, V.; Delolme, F.; Dessalces, G. *Energy Fuels* **2007**, *21*, 2165–2175.

(38) Hosseini−Dastgerdi, Z.; Tabatabaei−Nejad, S. A. R.; Khodapanah, E.; Sahraei, E. *Asia−Pac. J. Chem. Eng.* **2015**, *10*, 1–14.

(39) Fenistein, D.; Barré, L. *Fuel* **2001**, *80*, 283–287.

(40) Pfeiffer, J. P.; Saal, R. N. J. *J. Phys. Chem.* **1940**, *44*, 139–149.

(41) Wang, X.; Zhang, R.; Liu, L.; Qiao, P.; Simon, S.; Sjöblom, J.; Xu, Z.; Jiang, B. *Energy Fuels* **2017**, *31*, 9201−9212.

(42) Czarnecki, J.; Tchoukov, P.; Dabros, T.; Xu, Z. *Can. J. Chem. Eng.* **2013**, *91*, 1365–1371.

(43) Yarranton, H. W. *J. Dispers. Sci. Technol.* **2005**, *26*, 5–8.

(44) Freer, E. M.; Radke, C. J. *J. Adhes.* **2004**, *80*, 481–496.

(45) Dickie, J. P.; Yen, T. F. *Anal. Chem.* **1967**, *39*, 1847–1852.

(46) Mullins, O. C. *Energy Fuels* **2010**, 2179–2207.

(47) Mullins, O. C.; Sabbah, H.; Eyssautier, J.; Pomerantz, A. E.; Barré, L.; Andrews, A. B.; Ruiz−Morales, Y.; Mostowfi, F.; McFarlane, R.; Goual, L.; Lepkowicz, R.; Cooper, T.; Orbulescu, J.; Leblanc, R. M.; Edwards, J.; Zare, R. N. *Energy Fuels*

2012, *26*, 3986–4003.

(48) Mostowfi, F.; Indo, K.; Mullins, O. C.; McFarlane, R. *Energy Fuels* **2009**, *23*, 1194–1200.

(49) Lisitza, N. V; Freed, D. E.; Sen, P. N.; Song, Y. Q. *Energy Fuels* **2009**, *23*, 1189–1193.

(50) Eyssautier, J.; Levitz, P.; Espinat, D.; Jestin, J.; Gummel, J.; Grillo, I.; Barré, L. *J. Phys. Chem. B* **2011**, *115*, 6827–6837.

(51) Anisimov, M. A.; Yudin, I. K.; Nikitin, V.; Nikolaenko, G.; Chernoutsan, A.; Toulhoat, H.; Frot, D.; Briolant, Y. *J. Phys. Chem.* **1995**, *99*, 9576–9580.

(52) Yudin, I. K.; Anisimov, M. A. Dynamic light scattering monitoring of asphaltene aggregation in crude oils and hydrocarbon solutions. In *Asphaltenes, Heavy Oils and Petroleomics*; Mullins, O. C.; Sheu, E. Y.; Hammami, A.; Marshall, A. G.; Eds. Springer: New York, 2007.

(53) Sheu, E. Y. *Energy Fuels* **2002**, *16*, 74–82.

(54) Dutta Majumdar, R.; Montina, T.; Mullins, O. C.; Gerken, M.; Hazendonk, P. *Fuel* **2017**, *193*, 359–368.

(55) Wang, S.; Xu, J.; Wen, H. *Comput. Phys. Commun.* **2014**, *185*, 3069–3078.

(56) Wang, J.; Ferguson, A. L. *J. Phys. Chem. B* **2016**, *120*, 8016–8035.

(57) Gray, M. R.; Tykwinski, R. R.; Stryker, M.; Tan, X. *Energy Fuels* **2011**, *25*, 3125–3134.

(58) Gawrys, K. L.; Blankenship, G. A.; Kilpatrick, P. K. *Langmuir* **2006**, *22*, 4487–4497.

(59) Headen, T. F.; Boek, E. S.; Jackson, G.; Totton, T. S.; Müller, E. A. *Energy Fuels* **2017**, *31*, 1108–1125.

(60) Agrawala, M.; Yarranton, H. W. *Ind. Eng. Chem. Res.* **2001**, *40*, 4664–4672.

(61) Zahabi, A.; Gray, M. R.; Dabros, T. *Energy Fuels* **2012**, *26*, 1009–1018.

(62) Dudášová, D.; Silset, A.; Sjöblom, J. *J. Dispers. Sci. Technol.* **2008**, *29*, 139–146.

(63) Alboudwarej, H.; Pole, D.; Svrcek, W. Y.; Yarranton, H. W. *Ind. Eng. Chem. Res.* **2005**, *44*, 5585–5592.

(64) Long, J.; Xu, Z.; Masliyah, J. H. *Langmuir* **2007**, *23*, 6182–6190.

(65) Wang, S.; Liu, J.; Zhang, L.; Masliyah, J.; Xu, Z. *Langmuir* **2010**, *26*, 183–190.

(66) Qiao, P.; Harbottle, D.; Li, Z.; Tang, Y.; Xu, Z. *Energy Fuels* **2018**, *32*, 10478−10485.

(67) Sedghi, M.; Goual, L.; Welch, W.; Kubelka, J. *J. Phys. Chem. B* **2013**, *117*, 5765–5776.

(68) Hoepfner, M. P.; Fávero, C. V. B.; Haji−Akbari, N.; Fogler, H. S. *Langmuir* **2013**, *29*, 8799–8808.

(69) Natarajan, A.; Xie, J.; Wang, S.; Liu, Q.; Masliyah, J.; Zeng, H.; Xu, Z. *J. Phys. Chem. C* **2011**, *115*, 16043–16051.

(70) Zhang, L.; Shi, C.; Lu, Q.; Liu, Q.; Zeng, H. *Langmuir* **2016**, *32*, 4886–4895.

(71) Torkaman, M.; Bahrami, M.; Dehghani, M. *Energy Fuels* **2017**, *31*, 11169–11180.

(72) Painter, P.; Veytsman, B.; Youtcheff, J. *Energy Fuels* **2015**, *29*, 2120–2133.

(73) Strausz, O. P.; Torres, M.; Lown, E. M.; Safarik, I.; Murgich, J. *Energy Fuels* **2006**, *20*, 2013–2021.

(74) Drummond, C.; Israelachvili, J. *J. Pet. Sci. Eng.* **2004**, *45*, 61–81.

(75) de la Cruz, J. L. M.; Argüelles−Vivas, F. J.; Matías−Pérez, V.; Durán−Valencia, C. d. l. A.; López−Ramirez, S. *Energy Fuels* **2009**, *23*, 5611–5625.

(76) Torres, C.; Treint, F.; Alonso, C.; Milne, A.; Lecomte, A. *Proceedings of the SPE/ICoTA Coiled Tubing Conference and Exhibition*; The Woodlands, TX, April

12−13, 2005; SPE−93272−MS, DOI: 10.2118/93272−MS.

(77) Gawel, I.; Bociarska, D.; Biskupski, P. *Appl. Catal., A* **2005**, *295*, 89–94.

(78) Yarranton, H. W.; Hussein, H.; Masliyah, J. H. *J. Colloid Interface Sci.* **2000**, *228*, 52–63.

(79) Tchoukov, P.; Yang, F.; Xu, Z.; Dabros, T.; Czarnecki, J.; Sjöblom, J. *Langmuir* **2014**, *30*, 3024–3033.

(80) Harbottle, D.; Chen, Q.; Moorthy, K.; Wang, L.; Xu, S.; Liu, Q.; Sjoblom, J.; Xu, Z. *Langmuir* **2014**, *30*, 6730–6738.

(81) Wattana, P.; Wojciechowski, D. J.; Bolaños, G.; Fogler, H. S. *Pet. Sci. Technol.* **2003**, *21*, 591–613.

(82) Andersen, S. I. *Energy Fuels* **1999**, *13*, 315–322.

(83) Kraiwattanawong, K.; Fogler, H. S.; Gharfeh, S. G.; Singh, P.; Thomason, W. H.; Chavadej, S. *Energy Fuels* **2007**, *21*, 1248–1255.

(84) Oh, K.; Ring, T. A.; Deo, M. D. *J. Colloid Interface Sci.* **2004**, *271*, 212–219.

(85) Angle, C. W.; Long, Y.; Hamza, H.; Lue, L. *Fuel* **2006**, *85*, 492–506.

(86) Maqbool, T.; Balgoa, A. T.; Fogler, H. S. *Energy Fuels* **2009**, *23*, 3681–3686.

(87) Wang, J. X.; Buckley, J. S. *Energy Fuels* **2001**, *15*, 1004–1012.

(88) Huggins, M. L. *J. Chem. Phys.* **1941**, *9*, 440.

(89) Flory, P. J. *J. Chem. Phys.* **1942**, *10*, 51–61.

(90) Subramanian, S.; Simon, S.; Sjoblom, J. *J. Dispers. Sci. Technol.* **2016**, *37*, 1027–1049.

(91) Chapman, W. G.; Jackson, G.; Gubbins, K. E. *Mol. Phys.* **1988**, *65*, 1057–1079.

(92) Chapman, W. G.; Gubbins, K. E.; Jackson, G.; Radosz, M. *Fluid Phase Equilib.*

1989, *52*, 31–38.

(93) Wertheim, M. S. *J. Stat. Phys.* **1984**, *35*, 19–34.

(94) Wertheim, M. S. *J. Stat. Phys.* **1984**, *35*, 35–47.

(95) Wertheim, M. S. *J. Stat. Phys.* **1986**, *42*, 459–476.

(96) Wertheim, M. S. *J. Stat. Phys.* **1986**, *42*, 477–492.

(97) Gross, J.; Sadowski, G. *Ind. Eng. Chem. Res.* **2001**, *40*, 1244–1260.

(98) David Ting, P.; Hirasaki, G. J.; Chapman, W. G. *Pet. Sci. Technol.* **2003**, *21*, 647–661.

(99) Gonzalez, D. L.; Ting, P. D.; Hirasaki, G. J.; Chapman, W. G. *Energy Fuels* **2005**, *19*, 1230–1234.

(100) Spiecker, P. M.; Gawrys, K. L.; Trail, C. B.; Kilpatrick, P. K. *Colloids Surf., A.* **2003**, *220*, 9–27.

(101) Anisimov, M. A.; Ganeeva, Y. M.; Gorodetskii, E. E.; Deshabo, V. A.; Kosov, V. I.; Kuryakov, V. N.; Yudin, D. I.; Yudin, I. K. *Energy Fuels* **2014**, *28*, 6200–6209.

(102) Chang, C. L.; Fogler, H. S. *Langmuir* **1994**, *10*, 1749–1757.

(103) Chang, C. L.; Fogler, H. S. *Langmuir* **1994**, *10*, 1758–1766.

(104) Goual, L.; Sedghi, M. *J. Colloid Interface Sci.* **2015**, *440*, 23–31.

(105) Nassar, N. N.; Hassan, A.; Pereira−Almao, P. *Energy Fuels* **2011**, *25*, 1566–1570.

(106) Cortés, F. B.; Mejía, J. M.; Ruiz, M. A.; Benjumea, P.; Riffel, D. B. *Energy Fuels* **2012**, *26*, 1725–1730.

(107) Franco, C. A.; Nassar, N. N.; Ruiz, M. A.; Pereira−Almao, P.; Cortés, F. B. *Energy Fuels* **2013**, *27*, 2899–2907.

(108) Shojaati, F.; Riazi, M.; Mousavi, S. H.; Derikvand, Z. *Colloids Surf., A.* **2017**, *531*,

99–110.

(109) Akbarzadeh, K.; Hammami, A.; Kharrat, A.; Zhang, D.; Allenson, S.; Creek, J.; Kabir, S.; Jamaluddin, A. J.; Marshall, A. G.; Rodgers, R. P.; Mullins, O. C.; Solbakken, T. *Oilfield. Rev.* **2007**, *19*, 22–43.

(110) Adams, J. J. *Energy Fuels* **2014**, *28*, 2831–2856.

(111) Pernyeszi, T.; Patzkó, Á.; Berkesi, O.; Dékány, I. *Colloids Surf., A.* **1998**, *137*, 373–384.

(112) Saada, A.; Siffert, B.; Papirer, E. *J. Colloid Interface Sci.* **1995**, *174*, 185–190.

(113) Jada, A.; Debih, H. *Compos. Interfaces* **2009**, *16*, 219–235.

(114) Dudášová, D.; Simon, S.; Hemmingsen, P. V.; Sjöblom, J. *Colloids Surf., A.* **2008**, *317*, 1–9.

(115) Hannisdal, A.; Ese, M.−H.; Hemmingsen, P. V.; Sjöblom, J. *Colloids Surf., A.* **2006**, *276*, 45–58.

(116) Turgman−Cohen, S.; Smith, M. B.; Fischer, D. A.; Kilpatrick, P. K.; Genzer, J. *Langmuir* **2009**, *25*, 6260–6269.

(117) Fritschy, G.; Papirer, E. *Fuel* **1978**, *57*, 701–704.

(118) Hassan, A.; Ahmed, S.; Ali, M. A.; Hamid, H.; Inui, T. *Appl. Catal., A* **2001**, *220*, 59–68.

(119) Nassar, N. N.; Hassan, A.; Pereira−Almao, P. *J. Colloid Interface Sci.* **2011**, *360*, 233–238.

(120) Araújo, R. S.; Azevedo, D. C. S.; Cavalcante, C. L.; Jiménez−López, A.; Rodríguez−Castellón, E. *Microporous Mesoporous Mater.* **2008**, *108*, 213–222.

(121) Nassar, N. N. *Energy Fuels* **2010**, *24*, 4116–4122.

(122) Ekholm, P.; Blomberg, E.; Claesson, P.; Auflem, I. H.; Sjöblom, J.; Kornfeldt, A. *J.*

Colloid Interface Sci. **2002**, *247*, 342–350.

(123) Goual, L.; Horváth−Szabó, G.; Masliyah, J. H.; Xu, Z. *Langmuir* **2005**, *21*, 8278–8289.

(124) Rudrake, A.; Karan, K.; Horton, J. H. *J. Colloid Interface Sci.* **2009**, *332*, 22–31.

(125) Balabin, R. M.; Syunyaev, R. Z.; Schmid, T.; Stadler, J.; Lomakina, E. I.; Zenobi, R. *Energy Fuels* **2011**, *25*, 189–196.

(126) Castillo, J.; Goncalves, S.; Fernández, A.; Mujica, V. *Opt. Commun.* **1998**, *145*, 69–75.

(127) Acevedo, S.; Castillo, J.; Fernández, A.; Goncalves, S.; Ranaudo, M. A. *Energy Fuels* **1998**, *12*, 386–390.

(128) Labrador, H.; Fernández, Y.; Tovar, J.; Muñoz, R.; Pereira, J. C. *Energy Fuels* **2007**, *21*, 1226–1230.

(129) Zhang, L. Y.; Lopetinsky, R.; Xu, Z.; Masliyah, J. H. *Energy Fuels* **2005**, *19*, 1330–1336.

(130) Bouriat, P.; Kerri, N. El; Graciaa, A.; Lachaise, J. *Langmuir* **2004**, *20*, 7459–7464.

(131) Yang, F.; Tchoukov, P.; Pensini, E.; Dabros, T.; Czarnecki, J.; Masliyah, J.; Xu, Z. *Energy Fuels* **2014**, *28*, 6897–6904.

(132) Kilpatrick, P. K. *Energy Fuels* **2012**, *26*, 4017–4026.

(133) Pensini, E.; Harbottle, D.; Yang, F.; Tchoukov, P.; Li, Z.; Kailey, I.; Behles, J.; Masliyah, J.; Xu, Z. *Energy Fuels* **2014**, *28*, 6760–6771.

(134) Hou, J.; Feng, X.; Masliyah, J.; Xu, Z. *Energy Fuels* **2012**, *26*, 1740–1745.

(135) Feng, X.; Wang, S.; Hou, J.; Wang, L.; Cepuch, C.; Masliyah, J.; Xu, Z. *Ind. Eng. Chem. Res.* **2011**, *50*, 6347–6354.

(136) Peng, J.; Liu, Q.; Xu, Z.; Masliyah, J. *Adv. Funct. Mater.* **2012**, *22*, 1732–1740.

(137) Peng, J.; Liu, Q.; Xu, Z.; Masliyah, J. *Energy Fuels* **2012**, *26*, 2705–2710.

(138) Yang, F.; Tchoukov, P.; Qiao, P.; Ma, X.; Pensini, E.; Dabros, T.; Czarnecki, J.; Xu, Z. *Colloids Surf., A.* **2018**, *540*, 215–223.

CHAPTER 3 FRACTIONATION OF ASPHALTENES IN UNDERSTANDING THEIR ROLE IN PETROLEUM EMULSION STABILITY AND FOULING

3.1 INTRODUCTION

3.1.1 Saturates, Aromatics, Resins, and Asphaltenes (SARA)

Derived from ancient fossilized organisms, petroleum crude oil is a complex organic mixture comprised of saturated and unsaturated hydrocarbons with small amounts of heteroatoms (nitrogen, oxygen, and sulfur) and metallic constituents.[1] The characterization of crude oil is critical not only to oil processing from upstream reservoir exploration to downstream refining design, but also for prediction and management of environmental exposure.[2] Due to the complex nature of crude oil, it is almost impossible to identify individual molecules present in it. Bulk properties of crude oil, such as density [or American Petroleum Institute (API) gravity], viscosity, and boiling point, are often measured to give a fast assessment of crude oil, in the context of various types of oil separation processes based on boiling point (distillation), solubility (precipitation), and chromatography (adsorption).[3] These physical properties are determined by chemical compositions and structures as well as molecular weights of the crude oil components.

SARA fractionation uses a combination of solubility and chromatographic separation, which separates the crude oil into fractions of saturates (S), aromatics (A), resins (R), and asphaltenes (A) according to their polarizability and polarity (Figure 3.1).[4–6] In SARA fractionation, asphaltenes are first precipitated using *n*−alkanes, such as *n*−pentane or *n*−heptane.[4,7] After removal of asphaltenes, the remaining SARA fractions are sequentially obtained by eluting the remaining components, collectively called maltenes. Maltenes are adsorbed onto a chromatographic column using various solvents of particular polarity. Saturates consisting mainly of nonpolar linear, branched, and cyclic alkanes are removed by flushing the maltenes with *n*−alkanes through the column, with all other remaining components adsorbed onto the column.[4,8] The aromatic fraction is separated (washed off) from the adsorbent in the column using aromatic solvent, such as benzene; whereas resins are eluted from the column with polar solvent, such as methanol and chloroform. Aromatics contain compounds with one or more aromatic rings in which heteroatoms are normally embedded.[4,9] Resins and asphaltenes are operationally defined as two solubility classes containing various types of polar components with aromatic rings.[4,10,11] Resins are soluble in *n*−heptane and *n*−pentane, but insoluble in liquid propane; whereas asphaltenes are insoluble in *n*−alkanes, but soluble in toluene. The polarizability of all SARA fractions increases from saturates to asphaltenes.

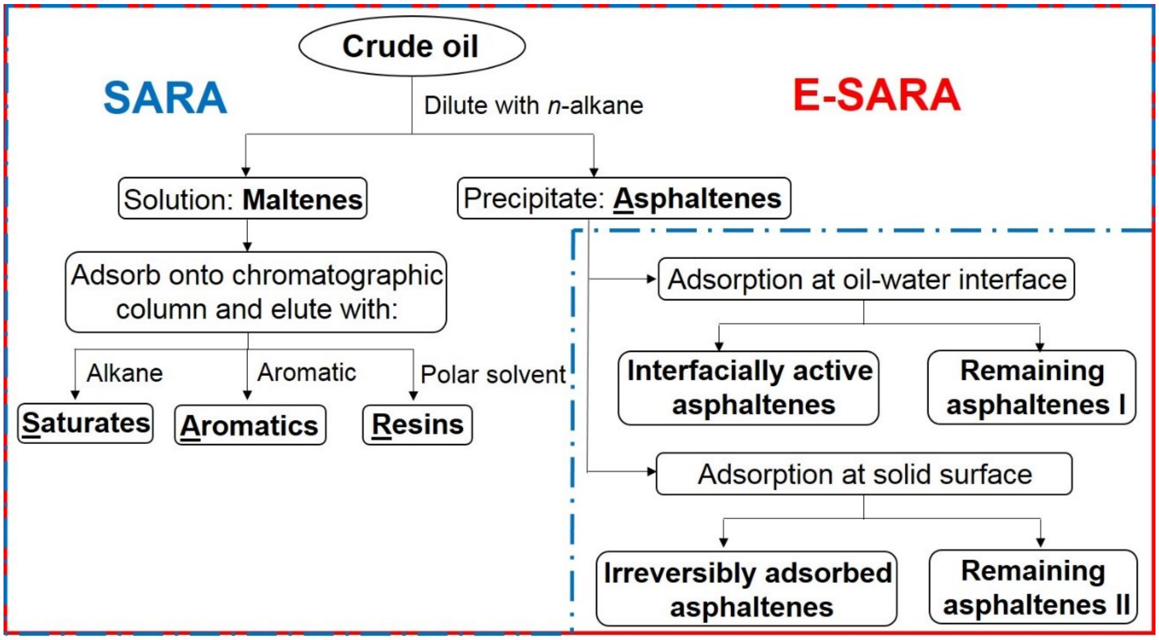

Figure 3.1 Comparison of conventional SARA and extended−SARA (E−SARA) analysis.

SARA analysis does not provide sharp boundaries between the various fractions. The yield of each of the fractions in chromatography depends upon the eluting solvent and adsorbent (column materials) used. For example, the mass fraction of asphaltenes recovered using *n*−heptane is lower than that using *n*−pentane as a result of their higher solubility in *n*−heptane than in *n*−pentane.[12] Moreover, the results of SARA analysis using different techniques and/or from different laboratories can vary greatly.[13,14] Despite these ambiguities, SARA analysis has become a widespread characterization method of crude oil. SARA analysis has successfully guided the processing and refining paths of crude oils based on the quantity of asphaltenes in crude oils. Asphaltenes precipitate when the temperature/pressure changes, or the oil loses its light components, is mixed with a paraffinic solvent, or is blended with a paraffinic crude.[4,15] Such precipitation may lead to the deposition of asphaltenes in production wells and pipelines (Figure 3.2a), resulting in the flow restriction, or even bringing oil production to a halt.[4,15–20] In addition, asphaltenes play a significant role in the stabilization of water−in−oil (W/O) emulsions[21–26] (Figure 3.2b) which lead to severe corrosion problems in production and transportation due to the dissolved salts and entrained fine solids carried by emulsified water droplets.[4] Moreover, crude oil with a high content of asphaltenes tends to form coke when heated, which is highly detrimental to heat exchangers and catalyst beds in upgrading and refining.[4,19,27,28] Because of its simplicity, SARA analysis is a reasonable first step in characterizing oils, providing warning for potential asphaltene−related losses suffered by the oil industry.

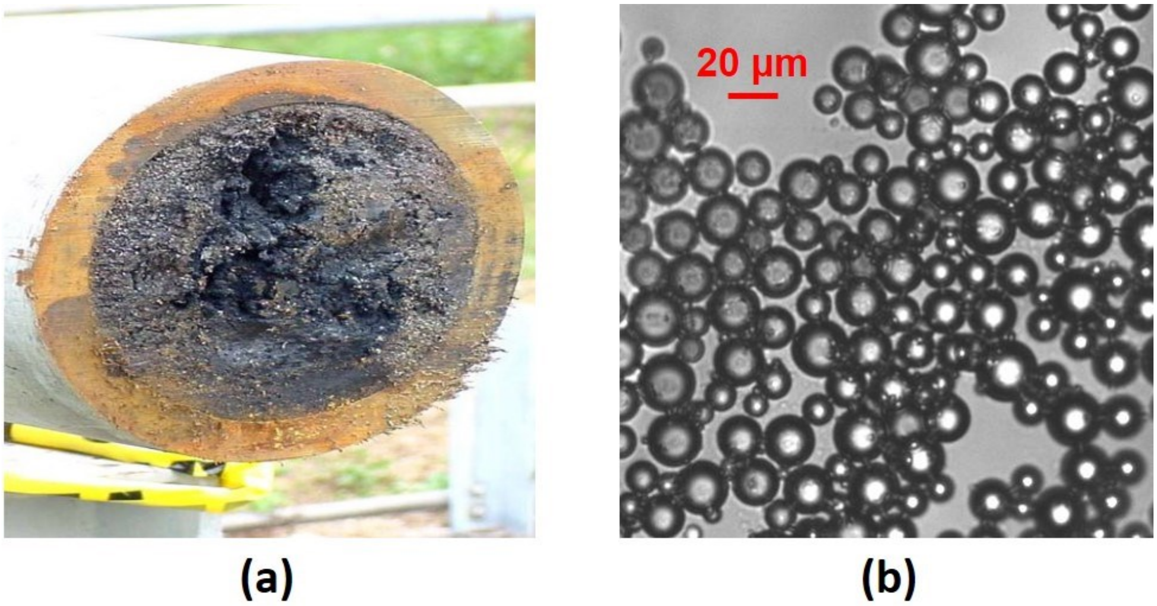

Figure 3.2 (a) The pipeline was plugged with asphaltenes, reprinted with permission from ref 20. Copyright 2005 Society of Petroleum Engineers. (b) Microscope image of a typical W/O emulsion stabilized by asphaltenes, prepared by homogenizing 20 mL of DI water in 100 mL of 10 g/L asphaltene−in−toluene solution at 30000 rpm for 5 min.

3.1.2 Asphaltenes

Asphaltenes are not a specific family of chemicals with a common functional group. Individual molecules in the spectra of asphaltenes may have distinct chemical structures.

Until very recently, the average molecular mass of asphaltenes was reported to span 6 orders of magnitude from less than 1000 up to tens of millions of daltons.[29] However, this has now been refined, and the well−accepted molecular weight of asphaltenes is between 500 and 1000 Da, with an average molecular weight of ∼750 Da, depending upon the source of oil.[30] Asphaltenes consist mainly of carbon, hydrogen, nitrogen, oxygen and sulfur, with trace amounts of metals such as vanadium, nickel and iron. While the elemental composition of asphaltenes is well−recognized, there had been a long−standing debate as to whether the asphaltene compounds comprised of one polycyclic aromatic hydrocarbon (PAH) core with peripheral alkyl and naphthenic groups, or they were composed of multiple cross−linked PAHs, known as the island model and archipelago model, respectively. A recent study by Schuler et al. indicated that asphaltenes are dominated by one large fused aromatic hydrocarbon ring with peripheral alkyl substituents. With the combination of atomic force microscopy (AFM) and scanning tunneling microscopy (STM), they identified the dominance of island structures in more than 100 asphaltene molecules.[31]

Aggregation behavior of asphaltenes has been another subject of controversy that receives substantial attention. Asphaltenes are known for their inevitable self−aggregation, even in good solvents, such as toluene.[32,33] The aggregation of asphaltenes is enhanced with decreasing solvent aromaticity.[34,35] Dickie and Yen[36] and later Mullins[37] proposed a stepwise aggregation model of asphaltenes, known as the Yen−Mullins model,[38] including formation of asphaltene nanoaggregates and clusters. According to Yen−Mullins model, asphaltene molecules are dominated by island architecture with a most likely molecular weight of ∼750 Da, as supported by recent mass spectral analysis.[39–41] Approximately six asphaltene molecules form a nanoaggregate via π−π stacking of their PAH cores. The asphaltene nanoaggregates can further associate to form clusters with aggregation numbers of approximately eight. The aliphatic side chains around PAH cores are believed to impose a steric repulsion that limits the aggregation number. The sizes of the asphaltene nanoaggregates and clusters are estimated to be around 2 and 5 nm, respectively. More recent work by Gray et al. proposed the formation of complex macromolecular aggregates of asphaltenes through a three−dimensional "supramolecular assembly model".[42] The authors suggested that asphaltene aggregation is a cumulative effect of various intermolecular interactions, including aromatic π−π stacking, acid−base interactions, hydrogen bonding, metal coordination complexes and hydrophobic pockets (Figure 3.3). Such multi−cooperative association would explain the porous structures of asphaltene aggregates with a range of different sizes and shapes, exhibiting polydispersity in population. Molecular dynamic (MD) simulation studies confirmed that asphaltene aggregation results in the formation of complex structures both in the bulk and at the oil−water interface.[43–46] The strong self−aggregation of asphaltenes facilitates the adsorption of asphaltenes at oil−water interfaces, which is crucial for the stabilization of oil−water petroleum emulsions. It also enhances the asphaltene adsorption onto mineral and metallic surfaces, giving rise to plugging and fouling in upstream and downstream processing facilities.

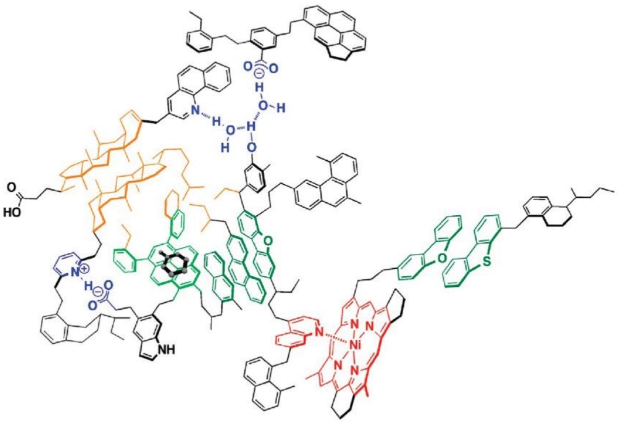

Figure 3.3 Possible intermolecular interactions between asphaltenes: acid−base interactions and hydrogen bonding (blue), metal coordination complex (red), a hydrophobic pocket (orange), π−π stacking (face−to−face dark green; within a clathrate containing toluene, light green), reprinted with permission from ref 42. Copyright 2011 American Chemical Society.

3.1.3 Asphaltene Adsorption

The interfacial activities of asphaltenes have long been studied due to the processing challenges encountered once asphaltenes begin to accumulate at oil−water and oil−solid interfaces. Earlier studies have shown that a water droplet aged in a diluted crude oil or asphaltene solution experiences crumpling upon volume reduction, which is attributed to the irreversible asphaltene adsorption at the oil−water interface.[35,47,48] Following the time−dependent adsorption of asphaltenes, Freer and Radke[49] completed several fluid exchanges with pure solvent, and the authors reported only a marginal increase in the oil−water interfacial tension (∼1.5 mN/m), confirming the irreversible adsorption of most asphaltene molecules. After washing, the frequency−dependent responses of interfacial dilatational moduli [storage (E′) and loss (E″) moduli] of the asphaltene film were in excellent agreement with the Maxwell model for irreversibly adsorbed species. When the surface pressure isotherms of asphaltene films were studied, Yarranton et al.[50] showed the lower film compressibility with increasing aging time. The formation of solid−like (elastic dominant) asphaltene films at the oil−water interfaces has been shown to significantly hinder the coalescence of two contacting water droplets, such that, when two droplets interact and undergo significant compression, they continue to remain stable without coalescence.[48,51]

The correlation between interfacial dilatational elasticity and overall emulsion stability has been qualitatively proven by several researchers,[49,50,52–56] although there is clear disagreement at high asphaltene concentrations where emulsion stability increases and E′ decreases. The discrepancy between the interfacial dilatational rheology and emulsion stability is believed to be associated with a change in the interfacial layer structure, transitioning from a compact and rigid monolayer to a collapsed interfacial layer dominated by three−dimensional structures.[55] More recently, the shear rheological responses [storage (G′) and loss (G″) modulus] of asphaltene films have been studied following the introduction of interfacial geometries.[54,51,57] With a biconical bob geometry, Spiecker and Kilpatrick investigated the evolution of the shear elasticity (G′) of interfacial asphaltene films.[54,57] It has been shown that stronger asphaltene films of higher elasticity and yield stress are more favored under conditions such as high asphaltene concentration, low solvent aromaticity, and asphaltenes of high polarity. Using a double−wall ring geometry, Harbottle et al. showed that asphaltene films exhibit time−dependent viscoelasticity, transitioning from liquid−like films (G″ > G′) at short aging times to solid−like films (G′ > G″) at longer aging times.[51] The transition in shear rheological responses corresponds to a transition in the observed droplet stability, with droplets coalescing rapidly within seconds in the liquid−like state and remaining stable without coalescence in the solid−like state. The contributing factor to the enhanced droplet stability is the development of a yield stress in the asphaltene network, which must be overcome to initiate the mobility within asphaltene films and subsequent droplet coalescence. The authors directly compared the shear and dilatational rheological responses, confirming that shear is the dominate mode of interfacial deformation due to the high energy cost associated with dilatational deformation. The importance of yield stress has also been underlined by thin liquid film (TLF) drainage experiments, where photo−interferometry is used to accurately measure the thickness of draining asphaltene films.[58] Following interfacial aging, the drainage kinetics is significantly retarded and thick asphaltene films with extended lifetimes are formed. The deviation between experiment and theory (Stefan−Reynolds equation) is addressed by accounting for the liquid film yield stress, i.e., resisting force as two asphaltene films interact.

The interaction of asphaltenes with solid surfaces has also received significant scientific attention as a result of its importance in preventing pipeline blockages and wettability modifications of fine solids. The oil wettability of fine clays increases with asphaltene adsorption, increasing the potential for clays to stabilize W/O emulsions.[19,26,59] A range of experimental techniques have been adopted to study the adsorption of asphaltenes onto several different substrates, including silica,[60–62] alumina,[61,62] iron oxide,[63] gold,[43,51,60,64–67] stainless steel,[66] glass,[68] and clay minerals.[69–78] Using quartz crystal microbalance (QCM), asphaltene adsorption and film formation have been studied in real time.[51,60,61,64–66] X-ray photoelectron spectroscopy (XPS),[65,75] X-ray diffraction (XRD),[72,74,75] small−angle X-ray scattering (SAXS),[74] Fourier transform infrared spectroscopy (FTIR)[71,72,74] and Fourier transform ion cyclotron resonance mass spectrometry (FT−ICR MS)[73] have been applied to characterize the surface modification by asphaltene adsorption. It is however not straightforward to compare the results from different adsorption studies since asphaltene adsorption is a complex process affected by many aspects, such as source of asphaltenes, type of solvents (quality and composition), moisture content of solvents, flow condition, and temperature, etc. The adsorption process often follows a Langmuir−type isotherm, although the mechanism for film formation and factors that contribute to mono− and multilayer films continue to be debated.[51,60,64–67,70,75] The detailed discussion on adsorption "isotherms" is outside the scope of this paper. Needless to say, adsorbed asphaltenes have been shown to be very stable. Removal of adsorbed asphaltenes by solvent washing has proven mostly unsuccessful, with only partial removal reported for aggressive cleaning strategies using solvent such as toluene, benzene, chloroform, andacetone.[60,69,78,79] The irreversibility of asphaltene adsorption is a big problem that can eventually lead to pipeline blockage and equipment fouling.

3.2 EXTENDED−SARA (E−SARA)

Asphaltenes are defined by solubility rather than any analyzed chemical properties. Despite its simplicity, such a generalized definition has often limited our knowledge regarding the asphaltene−induced problems in crude oil processing. It has been reported that, rather than whole asphaltenes, only a fraction of asphaltenes is more likely to contribute to the stabilization of W/O emulsions.[26,80–86] The asphaltenes adsorbed onto clays have also been found to be different in composition from whole asphaltenes.[70,75–77] Therefore, it is important to find ways to extract and study these particular asphaltenes subfractions, which are mainly responsible for the relevant issues of interest. The fractionation of asphaltenes allows for the investigation of these asphaltene subfractions, thereby providing necessary information to improve our understanding of the governing mechanisms and develop efficient mitigating approaches to the related problems. Most existing studies on the asphaltene fractionation are based on their solubility by precipitating different subfractions of asphaltenes using a mixture of aromatic and aliphatic solvents in varying ratios.[25,87,88] However, it is more instructive to fractionate asphaltene molecules according to their problematic properties of research interest, i.e. adsorption potential. Here, we introduce a new concept of E−SARA (Figure 3.1), the fractionation of asphaltenes based on their adsorption at oil−water and oil−solid interfaces. Through the studies of resulting asphaltene subfractions, E−SARA enables the identification of key functional groups that govern asphaltene adsorption at the solid surface and partition at the oil−water interface, thus providing a greater understanding of the molecular mechanisms of observed challenges caused by asphaltene subfractions isolated by E−SARA analysis. With such an approach, new routes to mitigate asphaltenes stabilizing oil−water emulsions and adsorbing onto solid surfaces (flow assurance and fouling) can be sought.

3.2.1 E−SARA Fractionation Based on Asphaltene Adsorption at Oil−Water Interfaces

One of the major problems encountered in crude oil or heavy oil production is the formation of stable W/O emulsions. Resolution of these emulsions and water removal from oil feed to upgrading facilities are important steps in the petroleum industry. A great deal of research has been focused on understanding the stabilization mechanisms of W/O emulsions..[21–26] It has been identified that asphaltenes play a key role in the emulsion stabilization; however, the exact mechanism is not entirely clear. As pointed out by Czarnecki et al.,[83,84] the understanding that asphaltenes stabilize the emulsions in way similar to surfactants by lowering interfacial tension and giving rise of surface forces to prevent droplet coalescence is discounting the facts that asphaltenes as a whole do not have amphiphilic characters and their structures are dominated by hydrophobic groups with few polar functionalities. The authors suggested that in fact only a small subfraction of asphaltenes is responsible for W/O emulsion stabilization, and blaming the asphaltenes as a whole is detrimental for the deep understanding of the underlying mechanisms.

Therefore, it is important to isolate and characterize interfacially active components of asphaltenes that irreversibly accumulate at the oil−water interface. Wu developed an effective method to collect the interfacial materials (IM) of bitumen adsorbed at the surfaces of heavy water (D_2O) droplets dispersed in the W/O emulsion.[81] In this method, D_2O is mixed with heptol 50/50 (a mixture of heptane and toluene at 1:1 volume ratio)−diluted bitumen to form a stable W/O emulsion. Regular deionized (DI) water is then added in the emulsion, followed by the centrifugation of the resulting mixture. After centrifugation, the emulsified heavy water droplets containing IM pass through the oil−water interface into DI water layer and finally settle down to form a cake on the bottom of the vessel as a result of the density difference. The DI water layer acts as a barrier to reduce bitumen contamination on the surfaces of heavy water droplets. The IM of bitumen are recovered by drying the wet cake. Through the characterization using FT−ICR MS, Stanford et al. reported that sulfur− and oxygen−containing species are enriched in the IM in comparison with parent bitumen.[82] Jarvis et al. isolated the IM of crude oils based their interactions with the immobilized water layers on the hydrated silica surface.[89] The interactions between oil compounds and silica substrate are inhibited by the water monolayers generated on the silica gel surface. The mixture of hydrated silica gel and heptol 50/50−diluted crude oil is loaded on the column at the beginning of the isolation. After the removal of non−interacting oil components by flushing the column with heptol 50/50, the IM solution is obtained by eluting the column using methanol/toluene (10:25 v/v) solution, followed by the extraction with dichloromethane to minimize silica contamination. The solvent of IM solution is then evaporated upon drying under N_2. The IM isolated using this wet silica technique show chemical functionalities similar to those obtained by Wu's heavy water method. These isolation techniques provide valuable information on interfacially active components of crude oils. In this line of thinking, our group developed an original method to extract the subfraction of asphaltenes which is really involved in the stabilization of W/O emulsions, i.e. the asphaltene species that irreversibly adsorb at oil−water interfaces.[85,86]

3.2.1.1 Fractionation procedure

Asphaltenes are fractionated based on their affinity to toluene−water interface.[85] The entire fractionation procedure is schematically represented in Figure 3.4. Pentane−extracted asphaltenes from Athabasca coker feed bitumen (Syncrude Canada, Ltd., Canada) refer to whole asphaltenes (WA) in this work. WA are first dissolved in toluene at a concentration of 10 g/L, followed by homogenizing the WA−in−toluene solution with 10% (v/v) water at 30000 rpm for 5 min. The resulting emulsion is then left for 24 h for equilibration purpose. Through the centrifugation (20000 g), the cake of emulsified water droplets is separated from the continuous oil phase. No apparent coalescence or free water is observed during centrifugation. The asphaltenes remaining in the oil supernatant are named as remaining asphaltenes (RA). Water droplets are then washed with an excessive amount of clean toluene until a clear washing toluene is observed, indicating the complete removal of asphaltenes trapped within the cake and loosely bound at the oil−water interface. After evaporation of water in a vacuum oven at 60 °C, the asphaltenes adsorbed at the surfaces of water droplets are isolated and named as interfacially active asphaltenes (IAA). The extracted IAA subfraction is estimated to be less than 2 wt% of WA.

3.2.1.2 Chemical compositions

The IAA subfraction is heavier than RA according to the results of electrospray ionization mass spectrometry (ESI−MS).[86] The molecular weight distribution of IAA peaks within the range of 1000−1200 Da, while the average molecular weight of RA is centered around 700−750 Da, showing good agreement with recent asphaltene studies.[30] The elemental analysis shows similar carbon, hydrogen, nitrogen, and sulfur contents of IAA and RA; however, the oxygen content of IAA (5.54 wt%) is 3 times higher than that of RA (1.68 wt%). A higher oxygen content of IAA is linked to the presence of sulfoxide groups, as indicated from FTIR spectra, in which the IAA subfraction exhibits a pronounced peak at 1020 cm^{-1}. Further analysis is conducted using ^{1}H and ^{13}C nuclear magnetic resonance (NMR) spectroscopy. All carbon types present in the asphaltene samples are determined using an original method developed at CanmetENERGY,[90] which allows for the calculation of average segment lengths of hydrocarbon chains and average cluster sizes of aromatic and cycloparaffinic rings. On the basis of the data collected, the typical molecular structures for IAA and RA are represented, respectively (Figure 3.5). On average, IAA molecules have lower aromatic content and higher paraffinic content than RA. No significant difference is observed between WA and RA, which is reasonable considering that the RA subfraction comprises more than 98 wt% of WA.

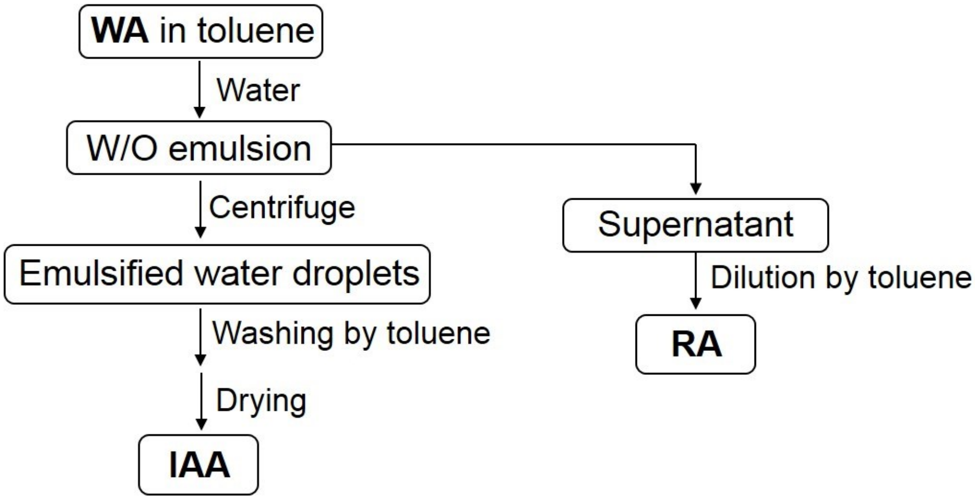

Figure 3.4 E−SARA fractionation based on asphaltene adsorption at toluene−water interfaces.

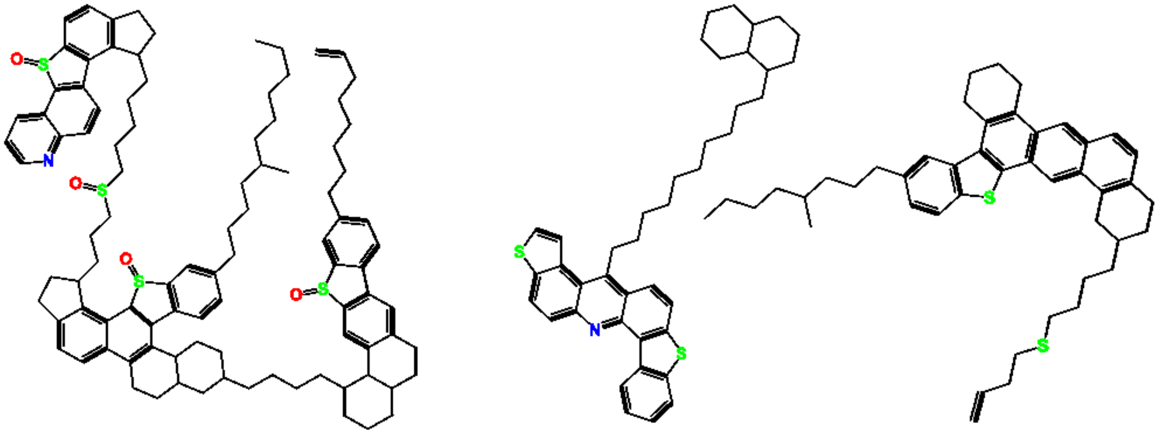

Figure 3.5 Molecular representations of IAA (left) and RA (right), reprinted with permission from ref 86. Copyright 2015 American Chemical Society.

3.2.1.3 Interfacial properties

The interfacial tension of 0.1 g/L IAA−in−toluene solution against water is measured to be 24.0 mN/m after 1 h, in comparison to 29.5 mN/m for RA under the same conditions, indicating that IAA are more interfacially active than RA.[85] In addition, interfacial pressure−area isotherms suggest that IAA form a rigid layer with low compressibility below 0.5 m/mN, even at the initial stage of compression. In contrast, RA films are soft with high compressibility. Furthermore, the relaxation of the IAA and RA interfacial layers is performed by reducing the interfacial area until reaching the same target pressure of 20 mN/m. The relaxation of the interfacial pressure is recorded for 20 min. The results indicate that the interfacial pressure decrease is approximately 10 and 40% for IAA and RA, respectively. In comparison with RA, the smaller reduction of interfacial pressure exhibited by IAA is interpreted as an indication of irreversible adsorption and less rearrangement freedom of adsorbed molecules.

3.2.1.4 Emulsion stability and oil film properties

Despite the fact that IAA molecules represent only a small subfraction of WA, bottle tests show that the removal of IAA dramatically decreases the stability of W/O emulsion.[85] In addition, the stability of oil films formed by IAA−, RA−, and WA−in−toluene solutions are studied using TLF technique. Directly studying the thin oil layers that separate water phases, it has been shown that IAA form very stable films, which do not rupture for 20 min; however, the average lifetime for WA and RA films is ~500 and less than 20 s, respectively. Such values agree well with emulsion stability results obtained from bottle tests. Microscopic images reveal that RA and IAA emulsion films have significantly different morphology and film thickness. The dark background of the RA film indicates that the film thickness is about 30−40 nm. RA films rupture in less than 1 min, and no apparent aging effects are observed. In contrast to RA films, the IAA films are much thicker (above 100 nm) with a significant variation in the thickness inferred by the Newton fringes. These thick lenses confirm the formation of aggregates in the IAA films, which is not observed before 30 min of aging. These films are similar to asphaltene−in−toluene films, as reported by Tchoukov et al.[58] The authors proposed that self−association of asphaltenes is not limited to nanoaggregates but also forms extended macrostructures in the film with gel−like rheological properties. As indicated by MD simulations, such formation and extension of the asphaltene network upon aging are believed to be related to hydrogen bonding interactions mainly induced by sulfoxide groups present in IAA. IAA molecules could form hydrogen bonds with water molecules, resulting in the adsorption at the interface. In addition, hydrogen bonding interactions between neighboring IAA molecules could provide a pathway for the formation of supramolecular structures.

3.2.2 E−SARA Fractionation Based on Asphaltene Adsorption at Solid Surfaces

Despite a great number of chemically distinct compounds acting as the building blocks of asphaltenes, they do not contribute equally to the formation of asphaltene deposits within pipelines and wellbores. Detailed chemical analysis on these subfractions of asphaltenes showed that the asphaltenes extracted from solid deposits contain a higher concentration of metals (vanadium, nickel, and iron) and more polar fractions than the asphaltenes separated from parent crude oils in the same field.[91] In comparison with their oil counterpart, asphaltenes in solid deposits are more prone to form aggregates in toluene. Heteroatoms (nitrogen, oxygen, and sulfur), largely contained in the ring systems, have also been found to be enriched in asphaltenes adsorbed onto clays than in bulk asphaltenes.[75–77] The amount of asphaltenes adsorbed onto kaolinite was reported to increase with increasing nitrogen and sulfur contents in asphaltenes.[77] The presence of heteroatoms in the form of polar functional groups in asphaltenes plays an important role in asphaltene−adsorbent interactions, presumably mainly through hydrogen bonding.[19,63,70] Water, as the most common hydrogen bonding molecule, can compete with asphaltenes for surface adsorption or even desorb the pre−adsorbed asphaltenes.[63] Few asphaltenes have been found to adsorb onto silica particles following hydrophobic treatment due to the hindered hydrogen bonding interactions between the silanol groups on the silica surface and polar groups of asphaltenes.[70] In addition, the asphaltenes with a higher degree of aromaticity show enhanced affinity to adsorbents in both computational[92] and real adsorption studies.[75–77] Although intriguing, it remains unclear as to the correlation between specific structures and solid adsorption behaviors of asphaltenes. Therefore, it would be informative to fractionate asphaltenes based on their adsorption characteristics to better understand the governing mechanisms of asphaltene adsorption on solid surfaces. However, the incomplete recovery of asphaltenes from the adsorbent limits the application of adsorption−based fractionation. Recently, Sjöblom group developed a new fractionation procedure of asphaltenes based on asphaltene adsorption onto calcium carbonate ($CaCO_3$) with a good recovery of 98−99 wt%.[93]

3.2.2.1 Fractionation procedure

Three different subfractions of asphaltenes are isolated from whole asphaltenes according to their adsorption strengths (Figure 3.6). The first subfraction, named as *bulk* asphaltenes, is obtained from the supernatant after centrifugation of the mixture of $CaCO_3$ and asphaltene−in−toluene solution. *Adsorbed* asphaltenes, which are defined as another subfraction of asphaltenes, are then collected from the supernatant following the centrifugation of tetrahydrofuran (THF) and asphaltene−adsorbed $CaCO_3$ obtained from previous step. $CaCO_3$ recovered here is mixed with 50/50 (v/v) THF/$CHCl_3$, followed by the addition of HCl or acetic acid (AA) solution. The organic and aqueous layers are separated subsequently. The last subfraction of asphaltenes, called *irreversibly−adsorbed* asphaltenes, is extracted from the organic layer. The use of different acids (HCl or acetic acid) has a negligible effect on the composition and structure of *irreversibly−adsorbed* asphaltenes. Similar elemental analysis results (Table 3.1) and FTIR spectra are observed for both *irreversibly−adsorbed*^{HCl} and *irreversibly−adsorbed*^{AA} asphaltenes. This separation method of asphaltenes is reproducible and quantitative with a recovery of 98−99 wt% of the *whole* asphaltenes used.

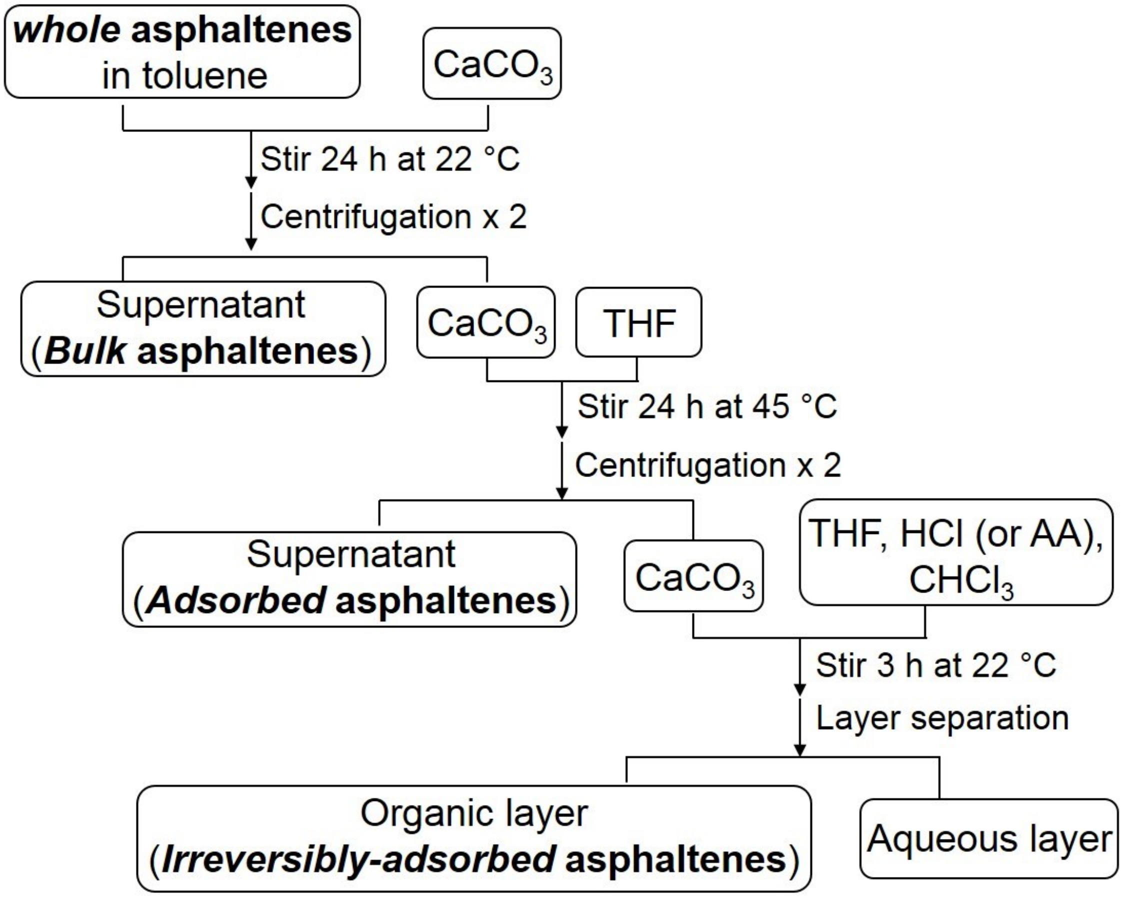

Figure 3.6 Procedure of asphaltene fractionation based on asphaltene adsorption onto $CaCO_3$, adapted with permission from ref 93. Copyright 2016 Elsevier.

3.2.2.2 Chemical compositions

The elemental analysis indicates that all the asphaltene subfractions have similar H/C ratio, nitrogen and sulfur contents (Table 3.1). As shown in FTIR spectra, they all have resembling absorption peaks in the region of $-CH_3$ and $-CH_2$ stretching vibration (2950 cm^{-1} and 2830 cm^{-1}), suggesting the presence of similar alkyl groups. However, the oxygen content of asphaltene subfractions varies significantly in the range of 2.33 to 4.22 with *irreversibly−adsorbed* asphaltenes containing the maximum amount of oxygen. *Adsorbed* asphaltenes have more oxygen than *bulk* asphaltenes. Such trend is also reflected by FTIR spectra in which *irreversibly−adsorbed* asphaltenes exhibit the highest adsorption intensity around 1700 cm^{-1}, indicating the highest concentration of carbonyl, carboxylic acid or derivative groups present in them. This adsorption band at 1700 cm^{-1} is found not induced by the contamination of $CaCO_3$. In addition, *irreversibly−adsorbed* asphaltenes have the lowest nickel and vanadium contents while the variations are comparatively less between *bulk* and *adsorbed* asphaltenes. It should be noted that, compared with *whole* asphaltenes, the fractionation procedure caused the overall increase of oxygen and calcium due to the oxidation and contamination by $CaCO_3$, as well as the loss of nickel, vanadium and iron resulting from acid treatment and water washing.

Table 3.1 Elemental analysis of *whole* asphaltenes and asphaltene subfractions. Adapted with permission from ref 93. Copyright 2016 Elsevier.

Element	*Whole* asphaltenes	Asphaltene subfractions				Mass balance of element (%)
		Bulk	*Adsorbed*	*Irreversibly-adsorbed*^{HCl}	*Irreversibly-adsorbed*^{AA}	
H/C ratio	1.145	1.137	1.139	1.194	1.186	/
N (wt%)	1.32	1.20	1.40	1.35	1.36	-3.0
S (wt%)	1.96	1.91	2.28	2.14	2.13	+4.5
O (wt%)	1.85	2.33	3.27	4.22	3.79	+58.4
Ni (ppm)	77	65	87	40	53	-13
V (ppm)	256	227	266	128	146	-15
Fe (ppm)	96	25	19	<30	<30	-75
Ca (ppm)	1402	6613	3366	655	434	+193

3.2.2.3 Adsorption properties

Irreversibly−adsorbed asphaltenes exhibit the ability to form viscoelastic multilayers on the stainless steel surface, while both *bulk* and *adsorbed* asphaltenes form rigid layers on the surface, as detected by QCM with dissipation (QCM−D) measurements. The adsorption of all the asphaltene subfractions has been found quite strong onto the stainless steel surface. In addition, they do not reach the saturation on the surface within the concentration range tested (0.01−1.5 g/L in xylene), unlike *whole* asphaltenes which exhibit maximum saturation when their concentration is higher than 0.05 g/L in xylene. The highest amount of adsorption (~8 mg/m^2) is obtained by *irreversibly−adsorbed* asphaltenes among three asphaltene subfractions with *bulk* asphaltenes showing the least (~4 mg/m^2), based on the calculated results from Sauerbrey equation. Such adsorption difference could be attributed to the concentration of carboxylic acid groups (*irreversibly−adsorbed* > *adsorbed* > *bulk*), since carboxylic acids tend to interact with chromium (III) oxide on the stainless steel surface thereby inducing the asphaltene adsorption. However, the enhanced adsorption could also result from the diminished interactions between asphaltene subfractions due to the fractionation. This is supported by the fact that the adsorption amount by *whole* asphaltenes is lower than any of the asphaltene subfractions. Further investigations concerning the interactions between asphaltene subfractions and their detailed structural information are therefore required to clarify the mechanism of asphaltene adsorption on stainless steel.

3.3 KEY EXPERIMENTAL TECHNIQUES USED IN E−SARA FRACTIONATION

3.3.1 Thin Liquid Film (TLF) Technique

The TLF technique developed by Scheludko and Exerowa[94] provides a convenient way to directly probe the interfacial film stability. The thin oil film sandwiched between two water phases closely resembles the real situation of W/O emulsions. The TLF technique uses the reflected light to obtain film imaging. Based on the image interference pattern and the light intensity change over time, a number of film parameters (e.g. film thickness and film lifetime) can be measured. The disjoining pressure isotherm, which describes the surface forces between oil−water interfaces as a function of separation, is routinely measured by applying external pressure on the interfacial film. The positive disjoining pressure acts to separate the surfaces, thus increasing emulsion stability; whereas a negative disjoining pressure causes fast film thinning, which eventually induces film rupture when a critical thickness is reached.

For the studies of asphaltene−stabilized W/O emulsions, the oil often refers to asphaltene solution. Using TLF technique (Figure 3.7),[95] a thin oil film is generated in a Scheludko−Exerowa cell housed in a chamber (1) kept at constant temperature (±0.1 °C). The film holder is made from a porous glass plate with a 0.8 mm diameter hole drilled in it. It is soaked in the oil phase and then immersed into an aqueous phase. The oil film is formed in the center of the hole when the oil is withdrawn through the capillary. Pressure transducers Pg and Pr, controlled via a Syringe Drive−PSD/2 (Hamilton, U.S.A.) (5), allow for the control of film diameter and thickness as well as provide information on the film disjoining pressure. The oil film is observed by reflected light using an inverted microscope (Axio Observer, Carl Zeiss, Germany) (2). A high−resolution digital camera (DFC500, Leica, Germany) (3) is used for recording film drainage process. A photodiode (Hamamatsu, Japan) (4) enables the photo−interferometric measurements of the film thickness. A custom−build LabVIEW program (6) is used to control the experiment and record the data. The porous glass plate is made hydrophobic by soaking it for 24 h in 20 vol % dichlorodimethylsilane in cyclohexene solutions prior to use.

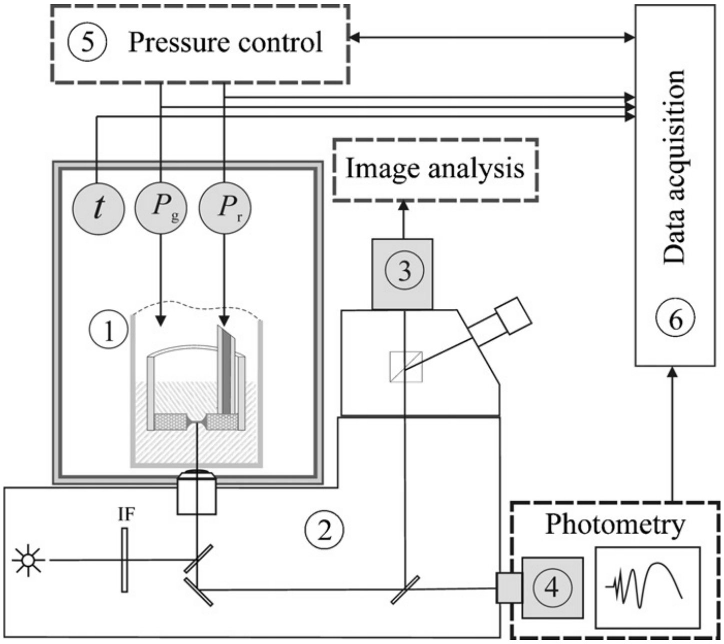

Figure 3.7 TLF experimental setup, reprinted with permission from ref 95. Copyright 2010 Elsevier.

Film Thickness. The film thickness is calculated using the formula proposed by Scheludko and Platikanov,[96] assuming a uniform refractive index throughout the film:

$$h = \left(\frac{\lambda}{2\pi n_f}\right) \sin^{-1}\left(\frac{\Delta}{1+[4N(1-N)^2](1-\Delta)}\right)^{1/2} \tag{3−1}$$

where $\Delta = (I - I_{min})/(I_{max} - I_{min})$, $N = (n_f - n_s)^2/(n_f + n_s)^2$; h is the calculated film thickness; I refers to the intensity of the reflected light from the film; I_{max} and I_{min} correspond to the maximum and minimum light intensity, respectively; n_f and n_s are the refractive indexes of the thin film liquid and the surrounding liquid, respectively; λ is the wavelength of the incident light.

Film Drainage. For the thin film stabilized by surfactants, Scheludko proposed that film interfaces could be effectively immobilized due to Gibbs−Marangoni effect,[97] and therefore the rate of film thinning, $V = -\,dh/dt$, can be described by Stephan−Reynolds equation (SRE) for the squeezing flow between two circular disks:

$$V_{Re} = -\frac{dh}{dt} = \frac{2h^3\Delta P}{3\mu R^2}, \quad \Delta P = P_\gamma - \prod h \tag{3−2}$$

where μ is the viscosity of film liquid, R is the film radius, and ΔP is the pressure difference that drives film drainage. The pressure difference consists of capillary pressure P_γ and disjoining pressure $\prod h$.

3.3.2 Quartz Crystal Microbalance with Dissipation Monitoring (QCM−D)

The QCM−D measures the amount of asphaltenes adsorbed on difference surfaces based on the piezoelectricity. A piezoelectric quartz crystal coated with surface materials of interest is sandwiched between two metal electrodes in the QCM−D. The crystal starts to oscillate upon excitation by applying an AC voltage across the electrodes. Its oscillation frequency depends on the mass adsorbed on the crystal surface. Through Sauerbrey equation,[98] the adsorbed mass can be calculated by monitoring the oscillation frequency change:

$$\Delta m = -C\Delta f/n \tag{3−3}$$

where Δm is the adsorbed mass, C is the crystal sensitivity constant, Δf is the frequency change, and n is the harmonic overtone number of the crystal sensor (n =1, 3, 5…13). It should be noted that Sauerbrey equation is only applicable when the following conditions are met: 1) the adsorbed mass is rigidly attached, 2) the adsorbed mass is distributed evenly over the crystal, and 3) the Δm is much smaller than the mass of the sensor crystal itself (<1%).

In addition to mass measurement, QCM−D can also provide the information concerning structural (viscoelastic) properties of the adsorbed materials on the crystal surface. In the case of asphaltene adsorption on the solid surface from oil phase, the viscoelasticity of the asphaltene film can be estimated from the energy dissipation shift (ΔD) of the crystal sensor. ΔD is measured by recording the response of a freely oscillating crystal sensor that has been vibrated at its resonance frequency. According to Stockbridge,[99] ΔD in a liquid medium can the given by:

$$\Delta D = 1/(\rho_q t_q)\sqrt{\rho_l \eta_l / 2\pi f} \tag{3−4}$$

where ρ_q and t_q are the density and the thickness of the quartz crystal, respectively, and ρ_l and η_l are the density and the viscosity of the liquid, respectively. The rigid adsorbed layer gives no change in dissipation, as opposed to the dissipation increase brought by a soft layer due to its internal friction and the frictional energy created when it slips on the electrodes. In addition to ΔD, the motional resistance (ΔR) of the crystal can also be used as a measure of dissipation in other QCMs.

3.4 CONCLUSIONS

Asphaltenes are generally recognized as a primary contribution to several major challenges encountered in petroleum processing from the reservoir to the refinery. They are notorious for the stabilization of undesirable W/O emulsions and the formation of solid deposits resulting in fouling and flow−assurance issues. As the oil industry is increasingly turning to unconventional oil resources such as heavy oil, extra heavy oil and oil sands bitumen which contain a large amount of asphaltenes, understanding the role of problematic asphaltenes is of immense scientific and economic importance. Defined as a solubility class by SARA analysis, asphaltenes comprise a broad range of molecules with distinct chemical structures and properties. Considering asphaltenes as a whole is noted to impede the understanding of corresponding mechanisms of asphaltene adsorption at oil−water interfaces and solid surfaces. Therefore, E−SARA is proposed as the solution−oriented fractionation of asphaltenes depending on their interfacial activities and adsorption characteristics. Through the determination of active components of asphaltenes, E−SARA enables the identification of key functional groups which participate in asphaltene adsorption. For instance, the stabilization of W/O emulsions by asphaltenes has been found mainly due to the IAA subfraction, which accounts less than 2 wt% of whole asphaltenes. The high interfacial activity of IAA molecules, and their ability to produce rigid film with aging effects, are linked with their high content of sulfoxide groups which induce the hydrogen bonding interactions between IAA molecules and water as well as neighbouring IAA molecules. In another study concerning the fractionation of asphaltenes based on adsorption onto $CaCO_3$, the whole asphaltenes show lower adsorption ability onto stainless steel surface than fractionated asphaltenes, in which carbonyl, carboxylic acid or derivative groups play an important role. Thus, E−SARA optimizes the investigation of complex asphaltene systems by distinguishing subfractions of asphaltenes and allowing the correlation of specific functional groups with certain asphaltene characteristics. Under the guidance of the concept of E−SARA fractionation, asphaltene molecules which have critical influences in the relevant systems of interest could be targeted and analyzed. Although the precise chemical structures and molecular associations of active components of asphaltenes remain largely unclear, E−SARA paves the road for future investigation to obtain in−depth understanding of asphaltene behaviors. With the aid of other analytical techniques and computational studies, the exact mechanisms involved are expected to be fully established.

3.5 REFERENCES

(1) Berkowitz, N. *Fossil Hydrocarbons: Chemistry and Technology*; Academic Press: San Diego, 1997.

(2) Bissada, K. K. A.; Tan, J.; Szymczyk, E.; Darnell, M.; Mei, M. *Org. Geochem.* **2016**, *95*, 21–28.

(3) Speight, J. G. *Handbook of Petroleum Analysis*; Wiley−Interscience: New York, 2001.

(4) Masliyah, J. H.; Czarnecki, J.; Xu, Z. *Handbook on Theory and Practice of Bitumen Recovery from Athabasca Oil Sands*; Kingsley Knowledge Publishing: Calgary, 2011.

(5) Jewell, D. M.; Weber, J. H.; Bunger, J. W.; Plancher, H.; Latham, D. R. *Anal. Chem.* **1972**, *44*, 1391–1395.

(6) Jewell, D. M.; Albaugh, E. W.; Davis, B. E.; Ruberto, R. G. *Ind. Eng. Chem. Fundam.* **1974**, *13*, 278–282.

(7) Sheu, E. Y. *Energy Fuels* **2002**, *16*, 74–82.

(8) Santos, R. G.; Loh, W.; Bannwart, A. C.; Trevisan, O. V. *Braz. J. Chem. Eng.* **2014**, *31*, 571–590.

(9) Nikookar, M.; Omidkhah, M. R.; Pazuki, G. R. *Pet. Sci. Technol.* **2008**, *26*, 1904–1912.

(10) Cho, Y.; Kim, Y. H.; Kim, S. *Anal. Chem.* **2011**, *83*, 6068–6073.

(11) Cho, Y.; Na, J.−G.; Nho, N.−S.; Kim, S.; Kim, S. *Energy Fuels* **2012**, *26*, 2558–2565.

(12) Langevin, D.; Argillier, J.−F. *Adv. Colloid Interface Sci.* **2016**, *233*, 83–93.

(13) Fan, T.; Buckley, J. S. *Energy Fuels* **2002**, *16*, 1571–1575.

(14) Kharrat, A. M.; Zacharia, J.; Cherian, V. J.; Anyatonwu, A. *Energy Fuels* **2007**, *21*, 3618–3621.

(15) Akbarzadeh, K.; Hammami, A.; Kharrat, A.; Zhang, D.; Allenson, S.; Creek, J.; Kabir, S.; Jamaluddin, A. J.; Marshall, A. G.; Rodgers, R. P.; Mullins, O. C.; Solbakken, T. *Oilfield. Rev.* **2007**, *19*, 22–43.

(16) Drummond, C.; Israelachvili, J. *J. Pet. Sci. Eng.* **2004**, *45*, 61–81.

(17) Vafaie−Sefti, M.; Mousavi−Dehghani, S. A. *Fluid Phase Equilib.* **2006**, *247*, 182–189.

(18) Syunyaev, R. Z.; Balabin, R. M.; Akhatov, I. S.; Safieva, J. O. *Energy Fuels* **2009**, *23*, 1230–1236.

(19) Adams, J. J. *Energy Fuels* **2014**, *28*, 2831–2856.

(20) Torres, C. A.; Treint, F.; Alonso, C.; Milne, A.; Lecomte, A. *Proceedings of the SPE/ICoTA Coiled Tubing Conference and Exhibition*; The Woodlands, TX, April 12−13, 2005; SPE−93272−MS, DOI: 10.2118/93272−MS.

(21) McLean, J. D.; Kilpatrick, P. K. *J. Colloid Interface Sci.* **1997**, *196*, 23–34.

(22) Yan, Z.; Elliott, J. A. W.; Masliyah, J. H. *J. Colloid Interface Sci.* **1999**, *220*, 329–337.

(23) Yarranton, H. W.; Hussein, H.; Masliyah, J. H. *J. Colloid Interface Sci.* **2000**, *228*, 52–63.

(24) Gafonova, O. V.; Yarranton, H. W. *J. Colloid Interface Sci.* **2001**, *241*, 469–478.

(25) Spiecker, P. M.; Gawrys, K. L.; Kilpatrick, P. K. *J. Colloid Interface Sci.* **2003**, *267*, 178–193.

(26) Kilpatrick, P. K. *Energy Fuels* **2012**, *26*, 4017–4026.

(27) Gawel, I.; Bociarska, D.; Biskupski, P. *Appl. Catal., A* **2005**, *295*, 89–94.

(28) Marchal, C.; Abdessalem, E.; Tayakout−Fayolle, M.; Uzio, D. *Energy Fuels* **2010**, *24*, 4290–4300.

(29) Mullins, O. C.; Martínez−Haya, B.; Marshall, A. G. *Energy Fuels* **2008**, *22*, 1765–1773.

(30) Mullins, O. C. *Annu. Rev. Anal. Chem.* **2011**, *4*, 393–418.

(31) Schuler, B.; Meyer, G.; Peña, D.; Mullins, O. C.; Gross, L. *J. Am. Chem. Soc.* **2015**,

137, 9870–9876.

(32) Merino−Garcia, D.; Andersen, S. I. *Pet. Sci. Technol.* **2003**, *21*, 507–525.

(33) Yarranton, H. W. *J. Dispers. Sci. Technol.* **2005**, *26*, 5–8.

(34) Wang, S.; Liu, J.; Zhang, L.; Masliyah, J.; Xu, Z. *Langmuir* **2010**, *26*, 183–190.

(35) Zhang, L.; Shi, C.; Lu, Q.; Liu, Q.; Zeng, H. *Langmuir* **2016**, *32*, 4886–4895.

(36) Dickie, J. P.; Yen, T. F. *Anal. Chem.* **1967**, *39*, 1847–1852.

(37) Mullins, O. C. *Energy Fuels* **2010**, *24*, 2179–2207.

(38) Mullins, O. C.; Sabbah, H.; Eyssautier, J.; Pomerantz, A. E.; Barré, L.; Andrews, A. B.; Ruiz−Morales, Y.; Mostowfi, F.; McFarlane, R.; Goual, L.; Lepkowicz, R.; Cooper, T.; Orbulescu, J.; Leblanc, R. M.; Edwards, J.; Zare, R. N. *Energy Fuels* **2012**, *26*, 3986–4003.

(39) Rodgers, R. P.; Marshall, A. G. In *Asphaltenes, Heavy Oils and Petroleomics*; Mullins, O. C., Sheu, E. Y., Hammami, A., Marshall, A. G., Eds.; Springer: New York, 2007.

(40) Pinkston, D. S.; Duan, P.; Gallardo, V. A.; Habicht, S. C.; Tan, X.; Qian, K.; Gray, M.; Mullen, K.; Kenttämaa, H. I. *Energy Fuels* **2009**, *23*, 5564–5570.

(41) Borton, D.; Pinkston, D. S.; Hurt, M. R.; Tan, X.; Azyat, K.; Scherer, A.; Tywinsky, R.; Gray, M.; Qian, K.; Kenttämaa, H. I. *Energy Fuels* **2010**, *24*, 5548−5559.

(42) Gray, M. R.; Tykwinski, R. R.; Stryker, M.; Tan, X. *Energy Fuels* **2011**, *25*, 3125–3134.

(43) Sedghi, M.; Goual, L.; Welch, W.; Kubelka, J. *J. Phys. Chem. B* **2013**, *117*, 5765–5776.

(44) Mikami, Y.; Liang, Y.; Matsuoka, T.; Boek, E. S. *Energy Fuels* **2013**, *27*, 1838–1845.

(45) Gao, F.; Xu, Z.; Liu, G.; Yuan, S. *Energy Fuels* **2014**, *28*, 7368–7376.

(46) Liu, J.; Zhao, Y.; Ren, S. *Energy Fuels* **2015**, *29*, 1233–1242.

(47) Yeung, A.; Dabros, T.; Masliyah, J.; Czarnecki, J. *Colloids Surf., A.* **2000**, *174*, 169–181.

(48) Gao, S.; Moran, K.; Xu, Z.; Masliyah, J. *Energy Fuels* **2009**, *23*, 2606–2612.

(49) Freer, E. M.; Radke, C. J. *J. Adhes.* **2004**, *80*, 481–496.

(50) Yarranton, H. W.; Sztukowski, D. M.; Urrutia, P. *J. Colloid Interface Sci.* **2007**, *310*, 246–252.

(51) Harbottle, D.; Chen, Q.; Moorthy, K.; Wang, L.; Xu, S.; Liu, Q.; Sjoblom, J.; Xu, Z. *Langmuir* **2014**, *30*, 6730–6738.

(52) Sztukowski, D. M.; Yarranton, H. W. *Langmuir* **2005**, *21*, 11651–11658.

(53) Quintero, C. G.; Noïk, C.; Dalmazzone, C.; Grossiord, J. L. *Oil Gas Sci. Technol.* **2009**, *64*, 607–616.

(54) Verruto, V. J.; Le, R. K.; Kilpatrick, P. K. *J. Phys. Chem. B* **2009**, *113*, 13788–13799.

(55) Alvarez, G.; Poteau, S.; Argillier, J.−F.; Langevin, D.; Salager, J.−L. *Energy Fuels* **2009**, *23*, 294–299.

(56) Rane, J. P.; Pauchard, V.; Couzis, A.; Banerjee, S. *Langmuir* **2013**, *29*, 4750–4759.

(57) Spiecker, P. M.; Kilpatrick, P. K. *Langmuir* **2004**, *20*, 4022–4032.

(58) Tchoukov, P.; Yang, F.; Xu, Z.; Dabros, T.; Czarnecki, J.; Sjöblom, J. *Langmuir* **2014**, *30*, 3024–3033.

(59) Harbottle, D.; Liang, C.; El−thaher, N.; Liu, Q.; Masliyah, J.; Xu, Z. Particle−stabilized emulsions in heavy oil processing. In *Particle Stabilized Emulsions and Colloids: Formation and Application*; Ngai, T.; Bon, S. A. F., Eds.;

The Royal Society of Chemistry: London, UK, 2015.

(60) Zahabi, A.; Gray, M. R.; Dabros, T. *Energy Fuels* **2012**, *26*, 1009–1018.

(61) Dudášová, D.; Silset, A.; Sjöblom, J. *J. Dispers. Sci. Technol.* **2008**, *29*, 139–146.

(62) González, M. F.; Stull, C. S.; López−Linares, F.; Pereira−Almao, P. *Energy Fuels* **2007**, *21*, 234–241.

(63) Carbognani, L. *Pet. Sci. Technol.* **2000**, *18*, 335–360.

(64) Ekholm, P.; Blomberg, E.; Claesson, P.; Auflem, I. H.; Sjöblom, J.; Kornfeldt, A. *J. Colloid Interface Sci.* **2002**, *247*, 342–350.

(65) Rudrake, A.; Karan, K.; Horton, J. H. *J. Colloid Interface Sci.* **2009**, *332*, 22–31.

(66) Xie, K.; Karan, K. *Energy Fuels* **2005**, *19*, 1252–1260.

(67) Goual, L.; Abudu, A. *Energy Fuels* **2010**, *24*, 469–474.

(68) Acevedo, S.; Castillo, J.; Fernández, A.; Goncalves, S.; Ranaudo, M. A. *Energy Fuels* **1998**, *12*, 386–390.

(69) Clementz, D. M. *Clays Clay Miner.* **1976**, *24*, 312–319.

(70) Dudášová, D.; Simon, S.; Hemmingsen, P. V.; Sjöblom, J. *Colloids Surf., A.* **2008**, *317*, 1–9.

(71) Jada, A.; Debih, H.; Khodja, M. *J. Pet. Sci. Eng.* **2006**, *52*, 305–316.

(72) Jada, A.; Debih, H. *Compos. Interfaces* **2009**, *16*, 219–235.

(73) Klein, G. C.; Kim, S.; Rodgers, R. P.; Marshall, A. G.; Yen, A. *Energy Fuels* **2006**, *20*, 1973–1979.

(74) Pernyeszi, T.; Patzkó, Á.; Berkesi, O.; Dékány, I. *Colloids Surf., A.* **1998**, *137*, 373–384.

(75) Tu, Y.; Kung, J.; McCracken, T.; Kotlyar, L.; Kingston, D.; Sparks, B. *Clay Sci.*

2006, *12*, 194–198.

(76) Tu, Y.; Woods, J.; Kung, J.; McCracken, T.; Kotlyar, L.; Sparks, B.; Dong, M. *Clay Sci.* **2006**, *12*, 183–187.

(77) Tu, Y.; Woods, J.; McCracken, T.; Kotlyar, L.; Sparks, B.; Chung, K. *Clay Sci.* **2006**, *12*, 188–193.

(78) Czarnecka, E.; Gillott, J. E. *Clays Clay Miner.* **1980**, *28*, 197–203.

(79) Hannisdal, A.; Ese, M.−H.; Hemmingsen, P. V.; Sjöblom, J. *Colloids Surf., A.* **2006**, *276*, 45–58.

(80) Xu, Y.; Dabros, T.; Hamza, H.; Shefantook, W. *Pet. Sci. Technol.* **1999**, *17*, 1051–1070.

(81) Wu, X. *Energy Fuels* **2003**, *17*, 179–190.

(82) Stanford, L. A.; Rodgers, R. P.; Marshall, A. G.; Czarnecki, J.; Wu, X. A.; Taylor, S. *Energy Fuels* **2007**, *21*, 973–981.

(83) Czarnecki, J.; Tchoukov, P.; Dabros, T. *Energy Fuels* **2012**, *26*, 5782–5786.

(84) Czarnecki, J.; Tchoukov, P.; Dabros, T.; Xu, Z. *Can. J. Chem. Eng.* **2013**, *91*, 1365–1371.

(85) Yang, F.; Tchoukov, P.; Pensini, E.; Dabros, T.; Czarnecki, J.; Masliyah, J.; Xu, Z. *Energy Fuels* **2014**, *28*, 6897–6904.

(86) Yang, F.; Tchoukov, P.; Dettman, H.; Teklebrhan, R. B.; Liu, L.; Dabros, T.; Czarnecki, J.; Masliyah, J.; Xu, Z. *Energy Fuels* **2015**, *29*, 4783−4794.

(87) Fossen, M.; Kallevik, H.; Knudsen, K. D.; Sjöblom, J. *Energy Fuels* **2007**, *21*, 1030–1037.

(88) Kharrat, A. M. *Energy Fuels* **2009**, *23*, 828–834.

(89) Jarvis, J. M.; Robbins, W. K.; Corilo, Y. E.; Rodgers, R. P. *Energy Fuels* **2015**, *29*,

7058–7064.

(90) Japanwala, S.; Chung, K. H.; Dettman, H. D.; Gray, M. R. *Energy Fuels* **2002**, *16*, 477–484.

(91) Wattana, P.; Fogler, H. S.; Yen, A.; Carmen Garcia, M. D.; Carbognani, L. *Energy Fuels* **2005**, *19*, 101–110.

(92) Alvarez−Ramírez, F.; García−Cruz, I.; Tavizón, G.; Martínez−Magadán, J. M. *Pet. Sci. Technol.* **2004**, *22*, 915–926.

(93) Subramanian, S.; Simon, S.; Gao, B.; Sjöblom, J. *Colloids Surf., A.* **2016**, *495*, 136–148.

(94) Exerowa, D.; Ivanov, I.; Scheludko, A. *Issledovaniya v Oblasti Poverkhnostnykh Sil*; Nauka: Moscow, Russia, 1964.

(95) Tchoukov, P.; Czarnecki, J.; Dabros, T. *Colloids Surf., A.* **2010**, *372*, 15–21.

(96) Scheludko, A.; Platikanov, D. *Kolloid−Z.* **1961**, *175*, 150–158.

(97) Scheludko, A. *Adv. Colloid Interface Sci.* **1967**, *1*, 391–464.

(98) Martin, S. J.; Granstaff, V. E.; Frye, G. C. *Anal. Chem.* **1991**, *63*, 2272–2281.

(99) Stockbridge, C. D. *Vacuum Microbalance Techniques*; Plenum Press: New York, 1966.

CHAPTER 4 ASPHALTENE SUBFRACTIONS RESPONSIBLE FOR STABILIZING WATER−IN−CRUDE OIL EMULSIONS. EFFECT OF SOLVENT AROMATICITY

4.1 INTRODUCTION

Stable water−in−oil (W/O) emulsions are highly undesirable in the petroleum industry since they contribute to the enhanced corrosion of downstream processing equipment, and impact production capacity due to difficulties associated with emulsion breaking.[1−3] As such, extensive research efforts have been focused on studying the stabilizing potential of the numerous surface active species native to crude oils, including asphaltenes, naphthenic acids, resins, and fine clays.[2,4] While each component provides some stabilizing potential, overwhelmingly asphaltenes are frequently identified to be a major contributor to stabilizing W/O petroleum emulsions.[1−10] However, it has been shown that not all asphaltenes contribute equally to the stabilization of W/O petroleum emulsions.[2,11] Bitumen washing experiments by Xu et al. showed that less than 2 wt% of Athabasca bitumen is actually responsible for the stabilization of W/O petroleum emulsions.[12] Considering that asphaltenes account for 17−20 wt% of Athabasca bitumen, it is clear that only a small fraction of asphaltenes can be classified as “problematic” and readily stabilize W/O emulsions.[13] Fourier transform ion cyclotron resonance mass spectrometry (FT−ICR MS) was used by Stanford and coworkers[14] to characterize the interfacially active materials extracted from diluted bitumen using the heavy water method proposed by Wu.[15] The asphaltenes irreversibly adsorbed at the oil−water interface were found to contain a higher content of heteroatoms (nitrogen, oxygen and sulfur). Differences in asphaltene chemical composition have also been observed when considering asphaltene deposition onto solid surfaces.[16] Wattana et al. characterized asphaltenes extracted from solid deposits, and found that the deposited asphaltenes contain more metals (vanadium, nickel and iron) and polar fractions than asphaltenes separated from the parent crudes.[17] Differences in chemical composition were also noted by Rogel et al. who reported that asphaltenes extracted from crude oils are less aromatic and more soluble than those present in the deposits.[18]

Additional research conducted by Tu et al. confirmed that asphaltenes remaining in solution contain less amount of nitrogen and sulfur than those adsorbed onto clays.[19–21]

It becomes evident that studying fractionated asphaltenes could provide more insights to mitigate asphaltene−related issues, which can be achieved by focusing on the physicochemical properties of asphaltene subfractions that actually cause the problems. Asphaltene precipitation in solvents of low aromaticity has frequently been used to separate asphaltene subfractions.[22–24] Spiecker and coworkers precipitated whole asphaltenes in mixtures of heptane and toluene to obtain two asphaltene subfractions of precipitates and solubles.[22] In comparison with the soluble subfraction, the precipitates exhibit a lower H/C ratio and a larger amount of nitrogen, nickel, vanadium and iron. The stability of W/O emulsions is greatly enhanced by large asphaltene aggregates formed from the precipitate subfraction. Östlund et al. fractionated whole asphaltenes using a mixture of methylene chloride and *n*−pentane.[23] The authors noted that asphaltenes of lower aromaticity could be precipitated out of solutions by solvents of decreasing methylene chloride to *n*−pentane ratios, albeit the heteroatom content remained unchanged. While most of the asphaltene fractionation research to date has considered differences in solubility, it is more informative to fractionate asphaltene molecules according to their adsorption characteristics at oil−water and oil−solid interfaces, which is crucial to provide insights on the most troublesome asphaltene subfractions.

E−SARA concept proposed by our group describes the fractionation of asphaltenes based on their interfacial activity and adsorption characteristics, providing an effective route to study the physicochemical properties of the most troublesome asphaltene subfractions.[25] Subramanian et al. fractionated asphaltenes based on asphaltene adsorption onto calcium carbonate. The study showed that asphaltenes adsorbed onto calcium carbonate contain a higher amount of carbonyl, carboxylic acid, and/or derivative groups than unadsorbed asphaltenes.[26] Compared with the whole asphaltenes, the asphaltene subfraction deposited onto calcium carbonate preferentially adsorbs onto stainless steel surfaces, forming thicker asphaltene layers. By isolating emulsified water droplets, Yang et al. recovered the asphaltene subfraction irreversibly adsorbed at the toluene−water interface, naming it as “interfacially active asphaltenes” or IAA.[27] The asphaltene subfraction remaining in the bulk oil phase was termed “remaining asphaltenes” or RA. The IAA subfraction exhibits a higher interfacial activity than the RA subfraction, with the IAA producing thicker and more rigid interfacial films, and exhibiting a strong aging effect on interfacial properties and W/O emulsion stability. This research confirmed the notion that only a small subfraction of asphaltenes is responsible for the stabilization of W/O petroleum emulsions.

The ability of asphaltenes to stabilize W/O petroleum emulsions is closely related to the self−aggregation of asphaltene molecules, which facilitates the formation of viscoelastic films at oil−water interfaces, thus providing the stabilizing mechanism to inhibit water droplet coalescence.[27–30] Asphaltene aggregation is known to be affected by solvent aromaticity,[6,7,9] with aliphatic solvents promoting the flocculation and precipitation of asphaltenes. Eley et al. reported that the highest stability of W/O emulsions occurs when the solvent condition approaches the asphaltene solubility limit.[31] Using atomic force microscopy (AFM), Wang and co−workers showed that the interactions between adsorbed asphaltene films in toluene are dominated by steric repulsion.[32] Adding *n*−heptane significantly reduces the repulsive force, accompanied by an increasing adhesion force. When using surface forces apparatus (SFA) to study the interactions between asphaltene films deposited on mica in solvents of different aromaticity, Natarajan et al.[33] and Zhang et al.[34] obtained similar results with Wang et al. All of these studies highlighted the effect of solvent aromaticity on asphaltene aggregation. It is therefore essential to study the effect of solvent aromaticity on the composition of the IAA subfraction of asphaltenes and physical properties of interfacial asphaltene films in relation to the stability of W/O petroleum emulsions that are of great scientific and practical importance. Following the E−SARA concept, whole asphaltenes (WA) are fractionated into IAA and RA by emulsifying water in asphaltene solutions prepared using solvents of different aromatic contents (toluene and heptol 50/50). Heptol 50/50 used in this work refers to the mixture of *n*−heptane and toluene at a 1:1 volume ratio. The composition and molecular structure of asphaltene subfractions have been determined by elemental analysis, Fourier transform infrared (FTIR) spectroscopy, and X-ray photoelectron spectroscopy (XPS), with the chemical structure determined being related to the physical properties of asphaltene subfractions including interfacial tension, interfacial shear rheology, crumpling ratio, and emulsion stability.

4.2 MATERIALS AND METHODS

4.2.1 Chemicals

Vacuum distillation feed bitumen from Syncrude Canada, Ltd. (Canada) was used to precipitate WA. Optima^{TM}−grade toluene, Optima^{TM}−grade *n*−heptane, certified *n*−pentane (Fisher Scientific, Canada) were used as received. Toluene and *n*−heptane were chosen as standard solvents, with the aromaticity of the solvent being adjusted by adding an equal volume of *n*−heptane to toluene (heptol 50/50). These solvents represent the boundary of the asphaltene solubility spectra[35] that is commonly encountered in oil industry. Deionized (DI) water with a resistivity of 18.2 MΩ·cm was used throughout the study. WA were extracted from bitumen using an excess volume of *n*−pentane (40:1 by volume) and further washed with *n*−pentane until the supernatant appeared clear. The fine mineral solids in the resultant asphaltene precipitates were removed by centrifuging the asphaltene−in−toluene solution at 20000 g for 20 min. Further details on asphaltene precipitation can be found in Tchoukov et al.[29]

4.2.2 E−SARA Fractionation Based on Asphaltene Adsorption at Oil−Water Interface

WA were fractionated into two subfractions using the method shown in Figure 4.1. In the toluene−based fractionation, 10 mL of DI water was emulsified in 100 mL of 10 g/L WA−in−toluene solution using a VWR 250 homogenizer (VWR, Canada) operating at 30000 rpm for 5 min. The W/O emulsion was left undisturbed overnight before centrifuging at 20000 g for 10 min. A brown sediment cake of stable water droplets was separated by carefully removing the supernatant using a transfer pipette. The sediment cake was consecutively washed (6 times) with 40 mL of fresh toluene until the supernatant appeared colorless, confirming the removal of any entrapped asphaltene−in−toluene solution or loosely bound asphaltenes. During each wash, the sediment cake was dispersed by shaking for 5 min and left undisturbed for 1 h prior to removing the supernatant. The supernatants from each wash were collected and combined with the supernatant obtained following centrifugation. The solvent was evaporated from the supernatants at 60 °C under a reduced pressure to obtain asphaltene precipitates, termed toluene−extracted remaining asphaltenes (T−RA). The washed cake was dried in a vacuum oven at 60 °C overnight to evaporate water and toluene. After evaporation, the resulting asphaltene subfraction was collected and termed toluene−extracted interfacially active asphaltenes (T−IAA). Heptol 50/50−based fractionation was performed by following the same procedure. WA were fully solubilized in heptol 50/50 and visual inspection of the solution confirmed no asphaltene precipitation after centrifugation of the solution at 20,000 g for 10 min.[36] The two asphaltene subfractions obtained were termed heptol 50/50−extracted interfacially active asphaltenes (HT−IAA) and heptol 50/50−extracted remaining asphaltenes (HT−RA). The fractional yields of T−IAA and HT−IAA were 1.1 ± 0.3 wt% and 4.2 ± 0.3 wt%, respectively. It was noted that the fractional yields of T−IAA and HT−IAA remained unchanged as the use of DI water was increased from 10 to 20 mL during the emulsification, showing the abundance of oil−water interfacial area during the extraction of IAA subfractions. All four asphaltene subfractions (T−IAA, T−RA, HT−IAA and HT−RA) were redissolved in toluene for further analysis, including measurements of interfacial tension, interfacial shear rheology, crumpling ratio and emulsion stability (bottle test).

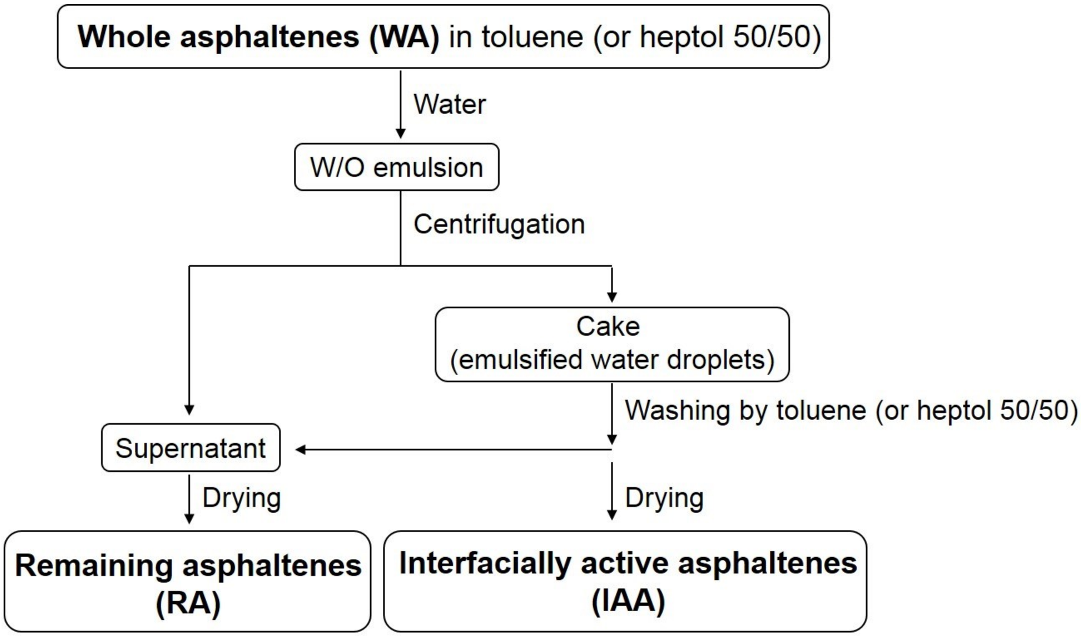

Figure 4.1 E−SARA fractionation of asphaltenes based on asphaltene adsorption at oil−water interfaces.

4.2.3 Elemental Analysis

The carbon, hydrogen, nitrogen, sulfur and oxygen contents of asphaltene subfractions were analyzed using a FLASH 2000 CHNS/O analyzer (Thermo Scientific, U.S.A.). The standard method recommended by the instrument manufacturer was used, in which 5 mg of each asphaltene subfraction was analyzed.

4.2.4 Fourier Transform Infrared (FTIR) Spectroscopy

FTIR spectra of the asphaltene subfractions were obtained using a Nicolet 8700 FTIR spectrometer (Thermo Scientific, U.S.A.), equipped with a Smart iTR Attenuated Total Reflection (ATR) sampling accessory in the spectral range between 4000 cm^{-1} and 800 cm^{-1}, with a spectral resolution of 4 cm^{-1}. A single spectrum was obtained from a total of 128 scans. For semi−quantitative analysis, all FTIR spectra obtained were normalized with respect to the absorption band at 2780−3000 cm^{-1}, which is assigned to the aliphatic C−H stretching vibration.

4.2.5 X-ray Photoelectron Spectroscopy (XPS)

XPS analysis of the asphaltene subfractions was performed using a Kratos Axis 165 spectrometer (Kratos, U.K.) under ultrahigh vacuum conditions (the base pressure of the instrument is ~ 5×10^{-10} Torr), with a monochromatic Al Kα X-ray source (1486.6 eV) at 15 kV anode potential and 20 mA emission current. The spectrometer was calibrated by the binding energy (84.0 eV) of Au $4f_{7/2}$ with reference to the Fermi level. High−resolution scans were performed at a pass energy of 20.0 eV, with a step of 0.1 eV and dwell time of 200 ms for C 1s, N 1s, S 2p and O 1s spectra to indicate the distribution of chemical bonds present in asphaltene subfractions. The core−level lines of XPS spectra were fitted using Gaussian and Lorentzian functions by Casa XPS software to determine peak positions, widths, areas and intensities.

4.2.6 Interfacial Tension Measurement

The water−oil dynamic interfacial tension was measured using an Attension Theta tensiometer (Biolin Scientific, Finland) at a constant temperature (23 ± 1 °C). A gastight syringe with an inverted 18−gauge needle was used to generate a 20 μL oil droplet (0.1 g/L fractionated asphaltene−in−toluene solution) in a quartz cuvette filled with 10 mL of DI water. Even though the asphaltene concentration in heavy crude oil can greatly exceed the concentration used in the current study,[13] 0.1 g/L asphaltene in solvent was chosen to better elucidate the dynamics of asphaltene adsorption (interfacial tension) and the dynamic nature of asphaltene film formation (interfacial shear rheology). Prior to the measurement, the syringe was first thoroughly rinsed with toluene, acetone and DI water, and then dried using nitrogen. The cuvette was sealed to minimize any solvent loss and atmospheric disturbances during the measurement. Interfacial tension was recorded at a rate of 5 fps. All experiments were repeated five times to obtain a statistical certainty of a typical experimental error less than 2%.

4.2.7 Interfacial Shear Rheology

The viscoelasticity of films formed by asphaltene subfractions at the toluene−water interfaces was determined using an AR−G2 stress−controlled rheometer (TA Instruments, Canada), equipped with a Pt/Ir double−wall ring (DWR) geometry and a circular Delrin trough. The DWR geometry has a square−edged cross−section, allowing the geometry to "pin" the toluene−water interface. The Delrin trough was placed on a Peliter plate for temperature control. The shear viscoelasticity [storage modulus (G') and loss modulus (G'')] of asphaltene interfacial films was measured using the harmonic oscillation of the DWR geometry while keeping the interfacial area constant. Details on the measurement technique are given elsewhere.[30,37]

All shear rheological measurements were conducted at a constant temperature of 23 ± 0.1 °C. Pipetted first into the Delrin trough was 19.2 mL of DI water as the sub−phase. The DWR geometry was then positioned at the air−water interface, before adding 15 mL of 0.1 g/L fractionated asphaltene−in−toluene solution. Finally, the Delrin trough was covered with a Teflon cap to prevent solvent evaporation and atmospheric disturbances. Aging experiments were performed over 12 h with the measurements at a frequency of 0.5 Hz and 0.5% strain amplitude which were within the linear viscoelastic region, identified by preliminary experiments. Following the aging, frequency sweeps were conducted, in which the frequency was increased from 0.001 to 0.1 Hz at a constant strain amplitude of 0.5%.

4.2.8 Crumpling Ratio

The mechanical response of the asphaltene−stabilized interface was qualitatively evaluated by the crumpling ratio (CR). An oil droplet (0.1 g/L fractionated asphaltene−in−toluene solution) was generated following the procedure outlined in Section 2.6 and aged for 1 h in DI water. The oil droplet volume was then slowly decreased at a rate of 20 μL/min and the CR was determined as $CR = A_f / A_i$, where A_f is the projected area of the oil droplet when crumpling is first observed upon contraction, and A_i is the initial projected area of the oil droplet. Sequential droplet images were recorded at 100 fps using an Attension Theta tensiometer (Biolin Scientific, Finland) and analyzed using ImageJ software to determine A_i and A_f, and hence the crumpling ratio. All experiments were completed at a constant temperature of 23 ± 1 °C and repeated five times to obtain a statistical certainty of a typical experimental error less than 2%.

4.2.9 Emulsion Stability by Bottle Test

W/O emulsions were prepared by mixing 10 mL of 0.1 g/L fractionated asphaltene−in−toluene solution and 1 mL of DI water using a VWR 250 homogenizer (VWR, Canada) at 30,000 rpm for 5 min. Optical microscope [Axiovert 200 microscope (Carl Zeiss, Germany)] images of the settled water droplets recovered from the glass vial, 1 cm above the base, were used to determine the droplet size distribution immediately following emulsification and after 1 h aging. Asphaltene depletion in the bulk oil phase was measured 1 h after emulsification using a Shimadzu UV−3600 spectrophotometer (Shimadzu, U.S.A.). The supernatant absorbance (removed at 1 cm below the air−solution interface) was converted to the concentration according to Beer−Lambert law. The calibration curves for asphaltene subfractions were determined based on the absorbance measured at 409 nm, for fractionated asphaltene−in−toluene solutions in the concentration range between 0.02 g/L and 0.1 g/L.

4.3 RESULTS

4.3.1 Elemental Composition and Structure Analysis

4.3.1.1 Elemental Analysis

The elemental composition of asphaltene subfractions is summarized in Table 4.1. HT−RA and T−RA are shown to have similar elemental compositions as anticipated, since both RA subfractions are the dominant species in WA. The fractional yield of HT−IAA is 4.2 ± 0.3 wt%, while the yield of T−IAA is lower at 1.1 ± 0.3 wt%. The H/C ratio varies between 1.16 and 1.20, confirming that all asphaltene subfractions have similar aromaticity. The nitrogen content varies slightly among asphaltene subfractions. However, the two IAA subfractions are quite different from the RA subfractions in terms of sulfur and particularly the oxygen content. Both HT−IAA (9.72 wt% S) and T−IAA (9.78 wt% S) contain higher sulfur content than HT−RA (8.74 wt% S) and T−RA (8.76 wt% S). Furthermore, a significantly higher oxygen content was found in T−IAA (5.62 wt% O), followed by HT−IAA (3.71 wt% O), in comparison with lower oxygen contents in T−RA (1.37 wt% O) and HT−RA (1.34 wt% O). Enrichment of oxygen and oxygen−sulfur species in interfacial materials of crude oil has been reported in previous studies.[14,38] O_2, O_4 and O_3S classes were found to be enriched in the multilayer asphaltene films stabilizing W/O emulsions at low bitumen concentration in heptol 50/50.[14] Likewise, in contrast to the less competitive adsorption of N class species, O_2 and O_4S were found as the two most abundant classes in interfacially active species collected from crude oils of different origins.[38]

Table 4.1 Elemental composition of asphaltene subfractions.

Asphaltene subfraction	Element (wt%)					H/C ratio
	C	H	N	S	O	
HT−RA	80.61	8.04	1.11	8.74	1.34	1.20
T−RA	80.67	8.03	1.12	8.76	1.37	1.19
HT−IAA	77.79	7.53	1.13	9.72	3.71	1.16
T−IAA	75.91	7.48	1.12	9.78	5.62	1.18

4.3.1.2 FTIR Spectroscopy

In general, most of the sulfur−bearing functional groups in asphaltenes are thiophenes, sulfides and sulfoxides which contain both sulfur and oxygen, while oxygen is present mainly in the forms of hydroxyl, carbonyl and carboxyl groups.[6] FTIR spectroscopy was used to determine the major functional groups contained in asphaltene subfractions. All FTIR spectra were normalized using the strong absorbance peak of the aliphatic C−H stretching vibration in the range of 2780 cm^{-1} to 3000 cm^{-1}, enabling comparison of the relative amounts of functional groups among the four asphaltene subfractions (Figure 4.2). The absorbance band observed between 1460 cm^{-1} and 1380 cm^{-1} corresponds to the aliphatic C−H bending vibration, and the band at 1600 cm^{-1} is assigned to the aromatic C=C stretching vibration. These bands are similar in intensity for all asphaltene subfractions, suggesting the presence of similar hydrocarbon backbones. No noticeable bands were observed for the N−H stretching between 3100 cm^{-1} and 3500 cm^{-1} (not shown in Figure 4.2), indicating that nitrogen atoms are mainly embedded in the aromatic rings for all the asphaltene subfractions. The main difference between the spectra of asphaltene subfractions is seen in the spectral range of 1020 cm^{-1} to 1040 cm^{-1}, which is attributed to the stretching vibration of sulfoxide group. T−IAA appear to exhibit a higher intensity of sulfoxides than HT−IAA, while HT−RA and T−RA show similar but much weaker absorbance, confirming the lower oxygen and sulfur contents of two RA subfractions as revealed also by elemental analysis. The oxygen and sulfur present in IAA subfractions at higher contents, particularly in T−IAA, exist mainly in the form of sulfoxides. The enrichment of sulfoxide groups in the IAA subfractions was also observed in our previous study (see earlier paper in the series),[39] although the WA used were from a different source of bitumen. In addition, the C−O bond (C−O stretching at 1100 cm^{-1}) along with hydroxyl (O−H bending at 910 cm^{-1}) and carbonyl (C=O stretching at 1700 cm^{-1}) groups also contribute to the high oxygen content of T−IAA and HT−IAA, but to a lesser extent. Between the two IAA subfractions, T−IAA exhibit a higher amount of oxygen−containing groups than HT−IAA, which is in good agreement with the differences in oxygen content shown by elemental analysis.

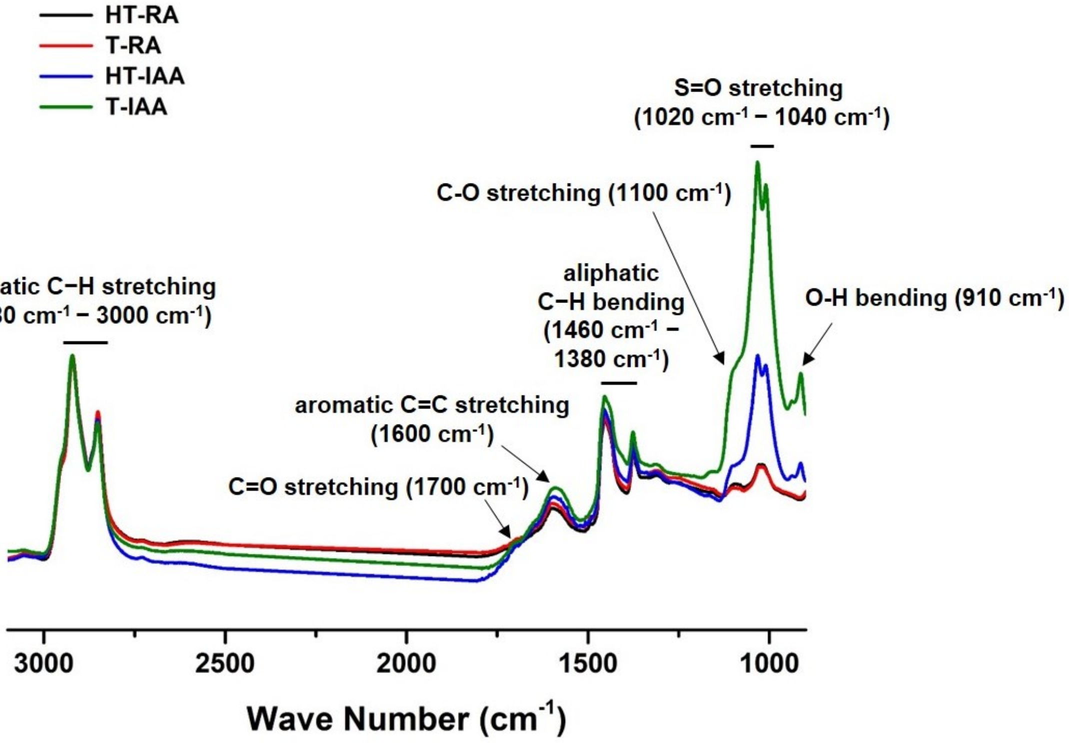

Figure 4.2 FTIR spectra of asphaltene subfractions.

4.3.1.3 XPS Analysis

High resolution XPS spectra over C 1s, N 1s, S 2p and O 1s regions were acquired to investigate the type and the relative proportion of chemical bonds present in asphaltene subfractions (Table 4.2). The C 1s spectra of asphaltene subfractions were fitted as two peaks with binding energies of 284.8 and 285.8 eV. The main C 1s peak at 284.8 eV represents a systematic carbon bond (C−H or C−C bond), while the sub−peak at 285.8 eV is attributed to carbon in a C−O environment.[40,41] From Table 4.2, it is worth noting that among the four asphaltene subfractions, T−IAA subfraction has the highest relative concentration of C−O bonds, followed by HT−IAA, HT−RA and T−RA.

The N 1s spectra confirm that nitrogen atoms are present in the forms of pyridinic (398.7 eV) and pyrrolic (400.2 eV) nitrogen[40–43] and in similar concentrations for all asphaltene subfractions. The data is in good agreement with the results from FTIR analysis which showed nitrogen atoms of asphaltene subfractions to be mainly embedded in the aromatic rings. XPS analysis reconfirms that nitrogen−containing species are not enriched in the different asphaltene subfractions obtained by E−SARA fractionation based on asphaltene adsorption at oil−water interfaces.

In the S 2p spectra, $2p_{3/2}$ and $2p_{1/2}$ components of a single species were fitted with a 2:1 relative intensity and separated in binding energy by 1.2 eV. Two pairs of S 2p peaks were observed in the S 2p spectra of HT−RA and T−RA. The major S $2p_{3/2}$ peak was found at a binding energy of 164.0 eV, which corresponds to the presence of thiophenic sulfur,[40–43] while the minor S $2p_{3/2}$ peak appearing at 163.2 eV indicates the presence of a small amount of alkyl sulfides.[44,45] However, in the S 2p spectra of HT−IAA and T−IAA, in addition to the two S $2p_{3/2}$ peaks at 163.2 and 164.0 eV, a third S $2p_{3/2}$ peak was measured at 166.0 eV, which is corresponding to sulfoxides.[42,44,45] Despite the fact that most of the sulfur atoms are present in the form of thiophenes and alkyl sulfides for all asphaltene subfractions, a large amount of sulfur atoms form sulfoxides in IAA subfractions. T−IAA have a higher relative concentration of sulfoxides than HT−IAA, which agrees well with the FTIR results (Figure 4.2). The absence of this XPS peak in the RA subfractions indicates that the amount of IAA in the RA subfractions is below the detection limit of XPS, typically below 0.5 wt%.

The narrow band O 1s spectra of T−IAA and HT−IAA were deconvoluted, which resulted in two O 1s peaks at 531.5 and 533.0 eV. These peaks are attributed to C=O type and C−O type of oxygen, respectively.[15,40] Based on the studies by Wu,[15] Rudrake et al.[40] and Abdallah and Taylor,[46] both peaks at binding energies of 532.4 and 533.4 eV in the O 1s spectra of HT−RA and T−RA are attributed to C−O type oxygen in different chemical environments, indicating a negligible amount of C=O bonds in HT−RA and T−RA. These results suggest that IAA subfractions have a greater amount of carbonyl functional groups than RA subfractions, which is consistent with the findings from FTIR analysis.

Table 4.2 XPS spectral features of C 1s, N 1s, S $2p_{3/2}$ and O 1s in asphaltene subfractions.

Element	Binding energy (eV)	Chemical bond	Concentration (%)^a of chemical bond	Element	Binding energy (eV)	Chemical bond	Concentration (%)^a of chemical bond
		HT-RA				**HT-IAA**	
C 1s	284.8	C-H or C-C	92.35	C 1s	284.8	C-H or C-C	88.81
	285.8	C-O	7.65		285.8	C-O	11.19
N 1s	398.7	pyridinic	43.96	N 1s	398.7	pyridinic	44.39
	400.2	pyrrolic	56.04		400.2	pyrrolic	55.61
S $2p_{3/2}$	163.2	sulfidic	20.01	S $2p_{3/2}$	163.2	sulfidic	23.26
	164.0	thiophenic	79.99		164.0	thiophenic	57.50
O 1s	532.4	C-O	91.49		166.0	sulfoxide	19.24
	533.4	C-O	8.51	O 1s	531.5	C=O	42.29
					533.0	C-O	57.71
		T-RA				**T-IAA**	
C 1s	284.8	C-H or C-C	93.58	C 1s	284.8	C-H or C-C	87.13
	285.8	C-O	6.42		285.8	C-O	12.87
N 1s	398.7	pyridinic	43.91	N 1s	398.7	pyridinic	44.28
	400.2	pyrrolic	56.09		400.2	pyrrolic	55.72
S $2p_{3/2}$	163.2	sulfidic	19.55	S $2p_{3/2}$	163.2	sulfidic	23.36
	164.0	thiophenic	80.45		164.0	thiophenic	54.21
O 1s	532.4	C-O	92.13		166.0	sulfoxide	22.43
	533.4	C-O	7.87	O 1s	531.5	C=O	34.01
					533.0	C-O	65.99

^{a}The concentration of the element in each chemical state was calculated from the peak area ratio of the element at each specific binding state.

4.3.2 Interfacial Properties

4.3.2.1 Interfacial Tension

The water−oil (0.1 g/L fractionated asphaltene−in−toluene solution) dynamic interfacial tension is shown in Figure 4.3. For all asphaltene subfractions, the interfacial tension decreases rapidly after droplet production, followed by a slower reduction at longer aging times. Such behavior is often attributed to the diffusion controlled adsorption of asphaltenes, followed by the relaxation and reorganization of the interfacially adsorbed asphaltenes.[47,48] It is not surprising to observe that T−IAA were more interfacially active than HT−IAA, and the least interfacially active subfractions were HT−RA and T−RA. The high interfacial activity of IAA subfractions, notably T−IAA, can be attributed to a significantly higher amount of polar functional groups in IAA subfractions, which exist mainly in the form of sulfoxides. Due to the electronegativity difference between oxygen and sulfur, electron density is drawn from the sulfur atom to the oxygen atom in S=O bond, making the sulfoxide group a strong hydrogen bond acceptor. The hydrogen bonding of these polar functional groups with water is responsible for the interfacial activity of asphaltene molecules.[39] The T−IAA subfraction has the highest content of sulfoxides along with other oxygen−containing functional groups, making it the most interfacially active subfraction. While the sulfoxide content of HT−IAA is lower than that of T−IAA, this asphaltene subfraction contains more sulfoxides than HT−RA and T−RA, and thus shows a higher interfacial activity. The interfacial tension of WA was studied at an equivalent concentration (0.1 g/L) to T−IAA and HT−IAA, corresponding to 9.1 g/L and 2.4 g/L of WA for T−IAA and HT−IAA, respectively (concentrations determined from the average fractional yields of IAA subfractions, 1.1 wt% for T−IAA and 4.2 wt% for HT−IAA). The interfacial tension of WA showed a high degree of similarity to the corresponding data measured using HT−IAA and T−IAA only, confirming the dominating influence of IAA subfractions on the interfacial activity of WA. On the other hand, the interfacial tension of WA at an equivalent concentration (0.1 g/L) to T−RA and HT−RA (data not shown) was found to be only slightly (2%) lower than the values measured for the two RA subfractions alone, which could be considered essentially to be within the experimental error. Considering the fact that T−RA accounted for 98.9 ± 0.3 wt% of WA and HT−RA accounted for 95.8 ± 0.3 wt% of WA, this result is not unexpected as the amount of IAA in this case is negligible.

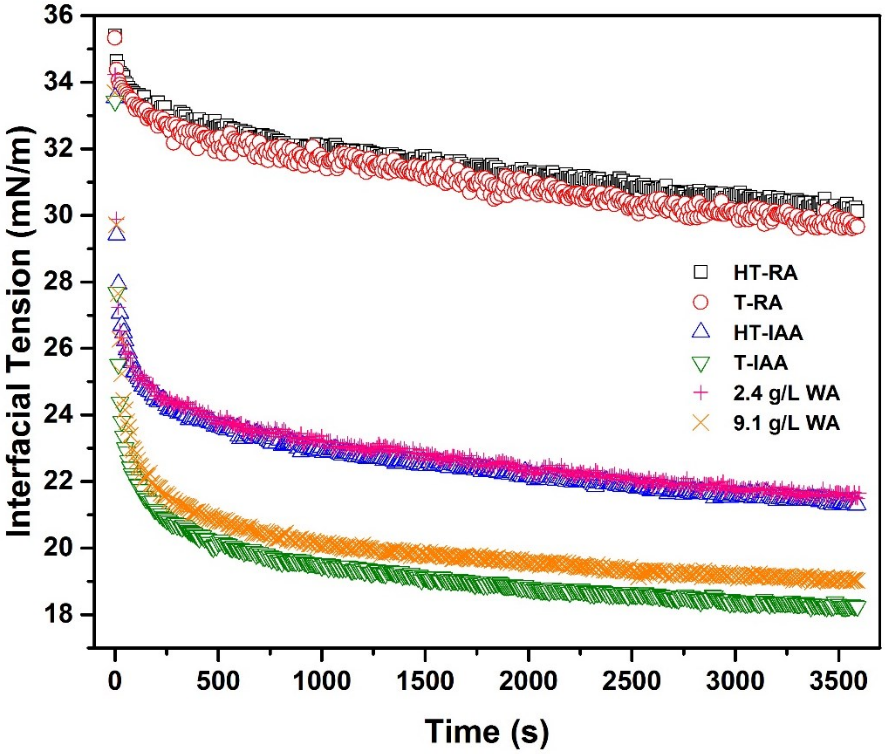

Figure 4.3 Dynamic interfacial tension between DI water and 0.1 g/L or equivalent (2.4 and 9.1 g/L WA−in−toluene) fractionated asphaltene−in−toluene solution.

4.3.2.2 Interfacial Shear Rheology

It has been shown that the viscoelasticity of interfacial asphaltene films is strongly related to the stability of W/O emulsions.[30,49,50] Contacting water droplets coalesce rapidly when the film remains viscous dominant. However, as the film becomes elastic dominant, water droplets become stable and do not coalescence.[30] To understand the role of interfacially active asphaltenes in stabilizing W/O emulsions, the viscoelastic moduli (G': elastic modulus; G'': viscous modulus) of asphaltene−stabilized films were measured as a function of aging time and the results are shown in Figure 4.4. For T−IAA, the G'' contribution developed at a decreasing rate while G' remained unmeasurable until t = 7,500 s. The $G'$of T−IAA interfacial film continued to build up, exhibiting a viscous−to−elastic transition ($G' = G''$) at t = 14600 s, after which the film can be considered elastic dominant or "solid−like". HT−IAA showed a similar aging profile, producing an elastic dominant interfacial film, albeit with a longer time to reach the transition ($G' = G''$) as compared with T−IAA. In contrast, no measurable G' was obtained for HT−RA and T−RA, confirming that interfacial films composed of RA subfractions remained purely viscous even after 12 h of aging. From the shear rheology measurements, it is readily evident that the IAA subfractions are the major contributor to the formation of elastic dominant asphaltene films at oil−water interfaces.

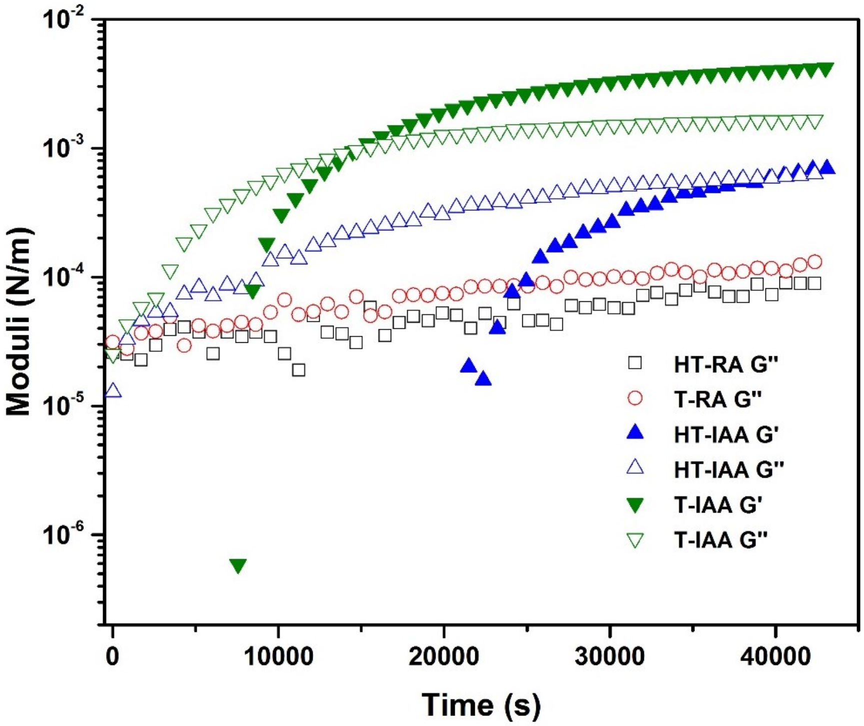

Figure 4.4 Time dependence of G' and G'' of interfacial films formed by asphaltene subfractions at toluene−water interfaces.

The mechanical strength of the asphaltene−stabilized interfacial film can also be inferred from the power−law dependence of G' and G'' on the angular frequency of shear oscilations.[37,51] For a viscous dominant film ($G' < G''$), both G' and G'' exhibit strong dependence on the angular frequency (ω). However, as the interface begins to strengthen ($G' > G''$), the viscoelastic moduli respond as a function of ω^n with n between 0 and 1, showing weak dependence on the frequency. For a fully cross−linked system ($G' \gg G''$), G' and G'' are entirely independent of the frequency with $n = 0$. The degree of cross−linking for T−IAA and HT−IAA interfacial films was evaluated by the frequency response of the asphaltene−stabilized interface after 12 h of aging. The frequency was increased from 0.001 Hz to 0.1 Hz with a constant strain amplitude of 0.5%. As shown in Figure 4.5, G' and G'' exhibit a weak dependence on angular frequency with n smaller than 1 for both T−IAA and HT−IAA interfacial films. Furthermore, the power exponents of the T−IAA interfacial film were smaller than those of the HT−IAA interfacial film, indicating that the T−IAA interfacial film is more cross−linked, supporting the higher shear elasticity measured for the T−IAA interfacial film.

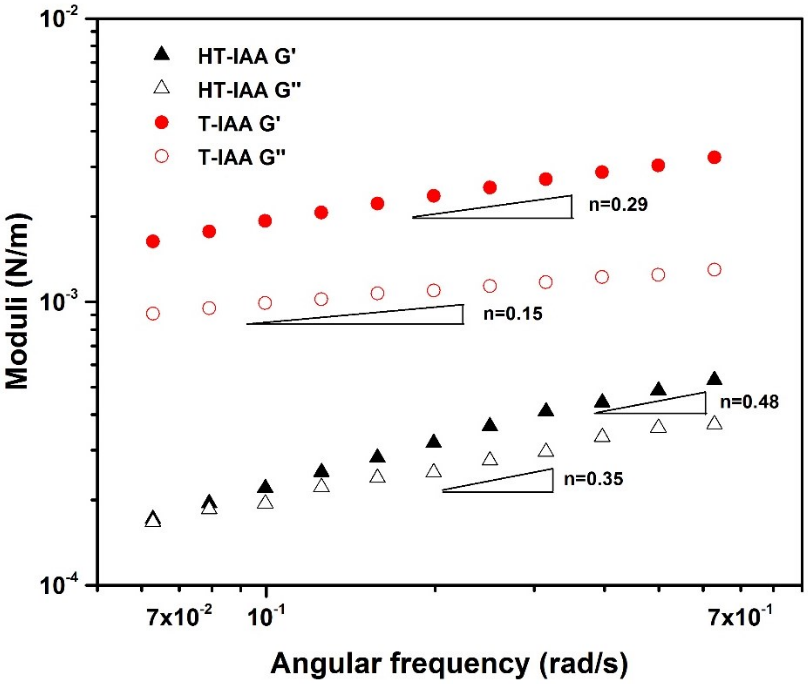

Figure 4.5 Frequency dependence of G' and G'' of interfacial films formed by HT−IAA and T−IAA at toluene−water interfaces.

4.3.2.3 Crumpling Ratio

The formation of solid−like asphaltene interfacial films was further confirmed by the crumpling ratio measurement. Due to the irreversible adsorption of asphaltenes and formation of rigid asphaltene films that resist in−plane shear, asphaltene−stabilized interfaces buckle during droplet volume reduction when the compressive yield of the film is surpassed.[34,52,53] The crumpling ratios of oil droplets (0.1 g/L fractionated asphaltene−in−toluene solutions) aged in DI water for 1 h were measured and the results are summarized in Table 4.3. Unlike interfacial shear rheology where the interfacial area remains constant, the crumpling ratio measurement relies on reducing the interfacial area, with more rigid films exhibiting a higher crumpling ratio. The highest crumpling ratio was observed for T−IAA (0.58), followed by HT−IAA (0.38). This result is consistent with the interfacial shear rheology data which shows that the T−IAA subfraction contains more interfacially active asphaltenes. These asphaltenes interact to form rigid films at oil−water interfaces. Interestingly, the HT−RA (0.24) and T−RA (0.25) subfractions resulted in a measurable crumpling ratio, even though the corresponding interfacial shear rheology confirmed a purely viscous film after 12 h aging. The measurable crumpling ratios suggest that the RA subfractions contain a number of IAA molecules which may have not been completely removed during the fractionation due to the limited interfacial area at the given water−to−oil ratio. The presence of a small fraction of IAA in the RA subfractions is also evident by the slight reduction in the oil−water interfacial tension (Figure 4.3).

Table 4.3 Crumpling ratios of oil droplets (0.1 g/L fractionated asphaltene−in−toluene solutions) aged for 1 h in DI water.

Asphaltene subfraction	Crumpling ratio
HT−RA	0.24
T−RA	0.25
HT−IAA	0.38
T−IAA	0.58

4.3.3 Emulsion Stability by Bottle Test

The emulsion stabilizing potential of different asphaltene subfractions was studied by the conventional bottle test method, wherein 10 mL of 0.1 g/L fractionated asphaltene−in−toluene solutions and 1 mL of DI water were homogenized at 30,000 rpm for 5 min. The stability of W/O emulsion against coalescence can be qualitatively evaluated based on the size distribution of water droplets, with smaller water droplets indicating reduced droplet−droplet coalescence and more stable emulsions. The settled water droplets were collected at a depth of 1 cm above the base of the sample vial, and the droplet size distribution was determined from microscopic images (analyzing 100 water droplets using ImageJ). Immediately following emulsification, the initial 50% passing size (D_{50}) was found to be similar for all emulsions, with slight variability in the narrow size range of 14−17 µm. With aging, droplets began to settle and coalesce in the densely packed bed at the bottom of the sample vial.

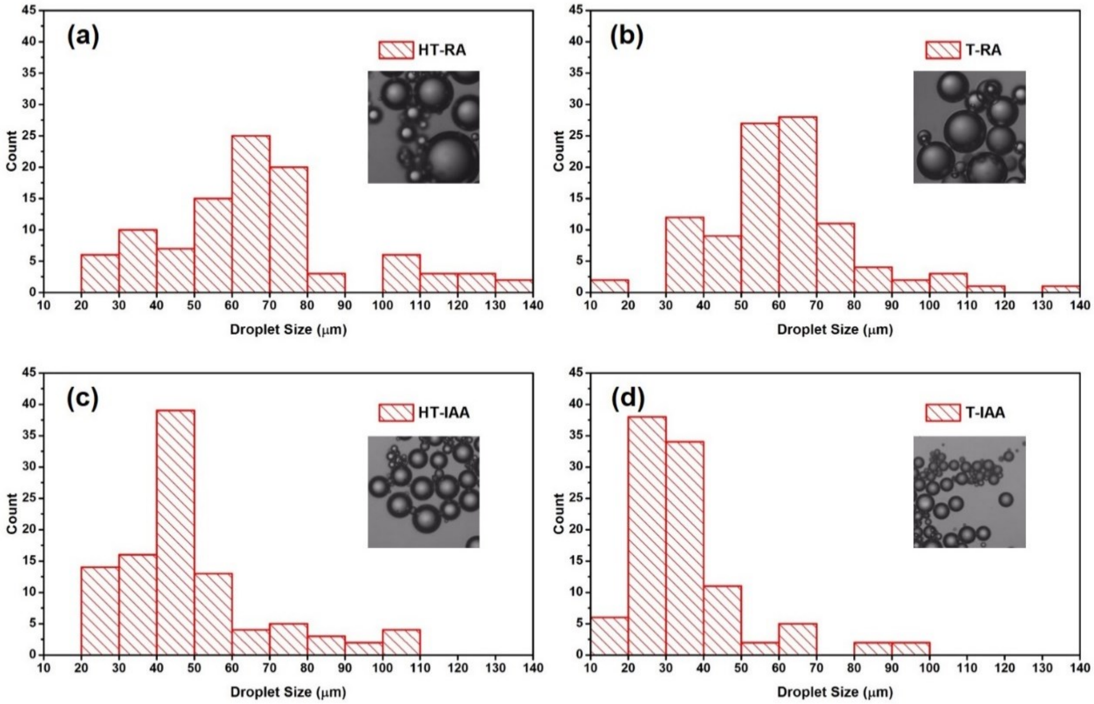

Figure 4.6 Size distribution of settled water droplets from W/O emulsions stabilized by a) HT−RA, b) T−RA, c) HT−IAA, and d) T−IAA 1 h after emulsification. Inset: Microscopic images of water droplets collected at a depth of 1 cm above the vial base.

Figure 4.6 shows the size distribution of water droplets 1 h after emulsification. The majority of water droplets stabilized by T−IAA were in the size range of 20−40 µm, in contrast to 40−50 µm for droplets stabilized by HT−IAA. Differences in the droplet size distributions confirm that T−IAA−stabilized water droplets were more resistant to coalescence than those stabilized by HT−IAA. Moreover, much larger water droplets were observed in emulsions prepared using HT−RA and T−RA, with the droplet size distribution in the range of 60−70 µm and 50−70 µm, respectively. Free water dropout was observed only for the emulsions prepared using HT−RA and T−RA 12 h after emulsification.

Therefore, W/O emulsions prepared using RA subfractions were significantly less stable against coalescence than those prepared using IAA subfractions, underlining the enhanced stabilizing potential of IAA.

The remaining asphaltene concentration in the supernatant 1 h after emulsification was measured by ultraviolet (UV)−visible (Vis) spectroscopy. The concentration of asphaltenes in the oil phase equaled 0.035 g/L for HT−IAA and 0.005 g/L for T−IAA, confirming that 65 wt% of HT−IAA and 95 wt% of T−IAA were adsorbed at the oil−water interface during emulsification. However, 84 wt% of HT−RA and 82 wt% of T−RA remained in the oil phase, clearly demonstrating that the presence of a small amount of IAA molecules in RA subfractions was not sufficient to stabilize W/O emulsions.

W/O emulsions prepared using T−IAA and HT−IAA can be considered stable since free water dropout was not observed after 12 h aging. Hence, the asphaltene "blocking" coverage to prevent water droplet coalescence can be estimated as follows. Based on the definition of droplet Sauter mean diameter[54,55], d_{32} is given by

$$d_{32} = \frac{\sum n_i d_i^3}{\sum n_i d_i^2} \tag{1}$$

where n_i is the number frequency of water droplets of diameter d_i. d_{32} for HT−IAA and T−IAA was determined to be 62.8 μm and 50.1 μm, respectively. Assuming that asphaltenes stabilize W/O emulsions by forming a dense monolayer of asphaltene molecules,[54–57] the surface mass coverage (Γ_{asp}) of asphaltenes can be approximated by

$$\Gamma_{asp} = \frac{M'_{asp}}{A_w} \tag{2}$$

where M'_{asp} is the mass of asphaltenes adsorbed at the oil−water interface, and the total interfacial area (A_w) of the emulsion can be obtained from the Sauter mean diameter and the total volume of emulsified water (V_w)

$$A_w = \frac{6V_w}{d_{32}} \tag{3}$$

By combining Eqs. (2) and (3), Γ_{asp} can be expressed as

$$\Gamma_{asp} = \frac{M'_{asp} d_{32}}{6V_w} = \frac{(1-\alpha_w)(C^{i}_{asp} - C''_{asp}) d_{32}}{6\alpha_w} \qquad (4)$$

where α_w is the volume fraction of water, C^{i}_{asp} is the initial concentration of asphaltenes in the oil phase before emulsification, and C''_{asp} is the concentration of asphaltenes remaining in the oil phase 1 h after emulsification. Previous research studying WA showed a critical blocking coverage of ~3.5 mg/m^2, which was independent of the emulsification method.[54,55] Based on the calculation, the Γ_{asp} value for HT−IAA and T−IAA was found to be 6.8 and 7.9 mg/m^2, respectively, which is higher than the value of 3.5 mg/m^2 reported for WA.

4.4 DISCUSSION

Four asphaltene subfractions were prepared using the E−SARA method.[25,27] The influence of solvent aromaticity on the interfacial activity of asphaltenes and the subsequent effect on the physicochemical properties of IAA subfractions were determined. Table 4.4 compares the physicochemical properties of the four asphaltene subfractions: T−IAA, HT−IAA, T−RA and HT−RA.

The amount of IAA was significantly influenced by the solvent aromaticity, with more IAA being recovered when the emulsion was prepared using heptol 50/50. Since the solubility of asphaltenes is reduced in less aromatic solvents,[28] asphaltenes partition more favorably at the oil−water interface from heptol 50/50 than from toluene solutions,[58] thus contributing to the higher yield of HT−IAA than that of T−IAA. In spite of similar H/C ratio and nitrogen content for all asphaltene subfractions, the elemental analysis highlighted substantial differences in oxygen content. The oxygen content of T−IAA was one and a half times that of HT−IAA, and three times that of T−RA and HT−RA. As revealed by FTIR and XPS analysis, the high oxygen content of IAA subfractions manifested through the presence of sulfoxide groups, with the sulfoxide content being a single identifier for IAA subfractions.[38,59,60] The polar oxygenated sulfur− and carbon−containing groups were found to enhance the interfacial adsorption of asphaltenes mainly through hydrogen bonding,[39,61] although the decreased solvent aromaticity also promoted interfacial adsorption, as highlighted by the lower amount of oxygen and sulfoxide groups in HT−IAA as compared with T−IAA. However, the reduced solvency of asphaltenes in heptol 50/50 encourages lesser interfacially active asphaltenes to partition at the oil−water interface. Therefore, when two asphaltene subfractions were re−dissolved in toluene at the same concentration (0.1 g/L), the HT−IAA subfraction contains comparatively less IAA than the T−IAA subfraction, and was shown to be less interfacially active. Both IAA subfractions are considerably more interfacially active than the two RA subfractions. The IAA subfractions packed densely at the toluene−water interface (Γ_{asp} = 7.9 mg/m^2 for T−IAA; 6.8 mg/m^2 for HT−IAA), with surface coverage being approximately twice the previously reported value for WA.[54,55] The surface coverage of asphaltenes at the oil−water interface is likely to be a contributing factor to the observed differences among the four asphaltene subfractions, providing a justification for the lowest interfacial tension and highest interfacial film rigidity formed by the T−IAA subfraction.

Table 4.4 Comparison of physicochemical properties of four asphaltene subfractions.

	T−IAA	HT−IAA	T−RA	HT−RA
Yield (wt%)	1.1 ± 0.3	4.2 ± 0.3	98.9 ± 0.3	95.8 ± 0.3
O (wt%)	5.62	3.71	1.37	1.34
S (wt%)	9.78	9.72	8.76	8.74
Sulfoxide (%)[a]	22.43	19.24	n/a	n/a
IFT (mN/m)[b] *(t = 1 h)*	18.27	21.33	29.66	30.14
G'/G"[b] *(t = 12 h)*	2.51	1.07	n/a	n/a
D_{50} (μm)[b] *(t = 1 h)*	35.6	43.5	58.2	64.2
Γ_{asp} (mg/m^2)[b]	7.9	6.8	n/a	n/a

[a]The sulfoxide percent was determined by the peak area ratio of sulfoxide from the XPS S 2p band of each asphaltene subfraction. [b]The oil phases were 0.1 g/L fractionated asphaltene−in−toluene solutions with DI water as the water phase.

4.5 CONCLUSION

Asphaltene fractionation by E−SARA according to their adsorption characteristics at oil−water interfaces was studied in solvents of different aromaticity: toluene and heptol 50/50. The research further supports the notion that not all asphaltene molecules contribute equally to stabilization of W/O petroleum emulsions. Despite the small proportion of IAA subfractions in WA, the IAA subfractions were recognized as the predominant contributor to the stabilization of W/O emulsions rather than the more abundant RA subfractions. The aromaticity of solvents (toluene vs heptol 50/50) had an insignificant impact on the elemental compositions of RA subfractions. However, larger amounts of sulfur and oxygen were observed in T−IAA than HT−IAA.

Even though both IAA (T−IAA and HT−IAA) subfractions were considered to be irreversibly adsorbed at oil−water interfaces, differences in their elemental compositions led to differences in asphaltene interfacial activity and properties of their interfacial films. The T−IAA subfraction formed a densely packed network that was more elastic and resistant to droplet−droplet coalescence than the system prepared using HT−IAA. As indicated by FTIR and XPS analysis, the oxygenated groups, in particular sulfoxides, play a critical role in the interfacial activity of asphaltenes. T−IAA contained the highest content of sulfoxides, followed by HT−IAA, then T−RA and HT−RA. The current research further elucidates that sulfoxide is the key functional group responsible for asphaltene adsorption at oil−water interfaces and subsequently the stabilization of W/O emulsions. Such knowledge is necessary to design smarter chemicals and processing strategies to mitigate asphaltene−related issues (emulsion stabilization, deposition, etc.) which begin when the interfacially active asphaltenes first adsorb or deposit at liquid−liquid or solid−liquid interfaces.

4.6 REFERENCES

(1) Sjöblom, J.; Aske, N.; Auflem, I. H.; Brandal, Ø.; Havre, T. E.; Sæther, Ø.; Westvik, A.; Johnsen, E. E.; Kallevik, H. *Adv. Colloid Interface Sci.* **2003**, *100*, 399–473.

(2) Kilpatrick, P. K. *Energy Fuels* **2012**, *26*, 4017–4026.

(3) Wong, S. F.; Lim, J. S.; Dol, S. S. *J. Pet. Sci. Eng.* **2015**, *135*, 498–504.

(4) Harbottle, D.; Liang, C.; El−thaher, N.; Liu, Q.; Masliyah, J.; Xu, Z. Particle−stabilized emulsions in heavy oil processing. In *Particle Stabilized Emulsions and Colloids: Formation and Application;* Ngai, T.; Bon, S. A. F., Eds.; The Royal Society of Chemistry: London, UK, 2015.

(5) Akbarzadeh, K.; Hammami, A.; Kharrat, A.; Zhang, D.; Allenson, S.; Creek, J.; Kabir, S.; Jamaluddin, A. J.; Marshall, A. G.; Rodgers, R. P.; Mullins, O. C.; Solbakken, T. *Oilfield. Rev.* **2007**, *19*, 22–43.

(6) Mullins, O. C. *Annu. Rev. Anal. Chem.* **2011**, *4*, 393–418.

(7) Langevin, D.; Argillier, J.−F. *Adv. Colloid Interface Sci.* **2015**, *233*, 83–93.

(8) McLean, J. D.; Kilpatrick, P. K. *J. Colloid Interface Sci.* **1997**, *196*, 23−34.

(9) Sheu, E. Y. *Energy Fuels* **2002**, *16*, 74–82.

(10) He, L.; Lin, F.; Li, X.; Sui, H.; Xu, Z. *Chem. Soc. Rev.* **2015**, *44*, 5446–5494.

(11) Czarnecki, J.; Tchoukov, P.; Dabros, T. *Energy Fuels* **2012**, *26*, 5782–5786.

(12) Xu, Y.; Dabros, T.; Hamza, H.; Shefantook, W. *Pet. Sci. Technol.* **1999**, *17*, 1051–1070.

(13) Czarnecki, J.; Tchoukov, P.; Dabros, T.; Xu, Z. *Can. J. Chem. Eng.* **2013**, *91*, 1365–1371.

(14) Stanford, L. A.; Rodgers, R. P.; Marshall, A. G.; Czarnecki, J.; Wu, X. A. *Energy Fuels* **2007**, *21*, 963–972.

(15) Wu, X. *Energy Fuels* **2003**, *17*, 179–190.

(16) Adams, J. J. *Energy Fuels* **2014**, *28*, 2831–2856.

(17) Wattana, P.; Fogler, H. S.; Yen, A.; Carmen Garcia, M. D. Carbognani, L. *Energy Fuels* **2005**, *19*, 101–110.

(18) Rogel, E.; Miao, T.; Vien, J.; Roye, M. *Fuel* **2015**, *147*, 155–160.

(19) Tu, Y.; Woods, J.; Kung, J.; McCracken, T.; Kotlyar, L.; Sparks, B.; Dong, M. *Clay Sci.* **2006**, *12*, 183–187.

(20) Tu, Y.; Kung, J.; McCracken, T.; Kotlyar, L.; Kingston, D.; Sparks, B. *Clay Sci.* **2006**, *12*, 194–198.

(21) Tu, Y.; Woods, J.; McCracken, T.; Kotlyar, L.; Sparks, B.; Chung, K. *Clay Sci.* **2006**, *12*, 188–193.

(22) Spiecker, P. M.; Gawrys, K. L.; Kilpatrick, P. K. *J. Colloid Interface Sci.* **2003**, *267*, 178–193.

(23) Östlund, J.−A.; Nydén, M.; Fogler, H. S.; Holmberg, K. *Colloids Surf., A.* **2004**, *234*, 95–102.

(24) Kharrat, A. M. *Energy Fuels* **2009**, *23*, 828–834.

(25) Qiao, P.; Harbottle, D.; Tchoukov, P.; Masliyah, J. H.; Sjoblom, J.; Liu, Q.; Xu, Z. *Energy Fuels* **2017**, *31*, 3330–3337.

(26) Subramanian, S.; Simon, S.; Gao, B.; Sjöblom, J. *Colloids Surf., A.* **2016**, *495*, 136–148.

(27) Yang, F.; Tchoukov, P.; Pensini, E.; Dabros, T.; Czarnecki, J.; Masliyah, J.; Xu, Z. *Energy Fuels* **2014**, *28*, 6897–6904.

(28) Tchoukov, P.; Czarnecki, J.; Dabros, T. *Colloids Surf., A.* **2010**, *372*, 15–21.

(29) Tchoukov, P.; Yang, F.; Xu, Z.; Dabros, T.; Czarnecki, J.; Sjöblom, J. *Langmuir* **2014**, *30*, 3024–3033.

(30) Harbottle, D.; Chen, Q.; Moorthy, K.; Wang, L.; Xu, S.; Liu, Q.; Sjoblom, J.; Xu, Z. *Langmuir* **2014**, *30*, 6730–6738.

(31) Eley, D. D.; Hey, M. J.; Symonds, J. D. *Colloids Surf.* **1988**, *32*, 87–101.

(32) Wang, S.; Liu, J.; Zhang, L.; Masliyah, J.; Xu, Z. *Langmuir* **2010**, *26*, 183–190.

(33) Natarajan, A.; Xie, J.; Wang, S.; Liu, Q.; Masliyah, J.; Zeng, H.; Xu, Z. *J. Phys. Chem. C* **2011**, *115*, 16043–16051.

(34) Zhang, L.; Shi, C.; Lu, Q.; Liu, Q.; Zeng, H. *Langmuir* **2016**, *32*, 4886–4895.

(35) Mannistu, K. D.; Yarranton, H. W.; Masliyah, J. H. *Energy Fuels* **1997**, *11*, 615–622.

(36) Vilas Bôas Fávero, C.; Maqbool, T.; Hoepfner, M.; Haji−Akbari, N.; Fogler, H. S. *Adv. Colloid Interface Sci.* **2016**, *244*, 267–280.

(37) Bi, J.; Yang, F.; Harbottle, D.; Pensini, E.; Tchoukov, P.; Simon, S.; Sjöblom, J.; Dabros, T.; Czarnecki, J.; Liu, Q.; Xu, Z. *Langmuir* **2015**, *31*, 10382−10391.

(38) Stanford, L. A.; Rodgers, R. P.; Marshall, A. G.; Czarnecki, J.; Wu, X. A.; Taylor, S. *Energy Fuels* **2007**, *21*, 973–981.

(39) Yang, F.; Tchoukov, P.; Dettman, H.; Teklebrhan, R. B.; Liu, L.; Dabros, T.; Czarnecki, J.; Masliyah, J.; Xu, Z. *Energy Fuels* **2015**, *29*, 4783−4794.

(40) Rudrake, A.; Karan, K.; Horton, J. H. *J. Colloid Interface Sci.* **2009**, *332*, 22–31.

(41) Abdallah, W. A.; Taylor, S. D. *J. Phys. Chem. C* **2008**, *112*, 18963–18972.

(42) Abudu, A.; Goual, L. *Energy Fuels* **2009**, *23*, 1237–1248.

(43) Siskin, M.; Kelemen, S. R.; Eppig, C. P.; Brown, L. D.; Afeworki, M. *Energy Fuels* **2006**, *20*, 1227–1234.

(44) Kozłowski, M. *Fuel* **2004**, *83*, 259–265.

(45) Liu, F.; Li, W.; Chen, H.; Li, B. *Fuel* **2007**, *86*, 360–366.

(46) Abdallah, W. A.; Taylor, S. D. *Nucl. Instrum. Methods Phys. Res., Sect. B* **2007**, *258*, 213–217.

(47) Jeribi, M.; Almir−Assad, B.; Langevin, D.; Hénaut, I.; Argillier, J. F. *J. Colloid*

Interface Sci. **2002**, *256*, 268–272.

(48) Pauchard, V.; Rane, J. P.; Zarkar, S.; Couzis, A.; Banerjee, S. *Langmuir* **2014**, *30*, 8381–8390.

(49) Spiecker, P. M.; Kilpatrick, P. K. *Langmuir* **2004**, *20*, 4022–4032.

(50) Pensini, E.; Harbottle, D.; Yang, F.; Tchoukov, P.; Li, Z.; Kailey, I.; Behles, J.; Masliyah, J.; Xu, Z. *Energy Fuels* **2014**, *28*, 6760–6771.

(51) Verruto, V. J.; Le, R. K.; Kilpatrick, P. K. *J. Phys. Chem. B* **2009**, *113*, 13788–13799.

(52) Gao, S.; Moran, K.; Xu, Z.; Masliyah, J. *Energy Fuels* **2009**, *23*, 2606–2612.

(53) Yeung, A.; Dabros, T.; Masliyah, J.; Czarnecki, J. *Colloids Surf., A.* **2000**, *174*, 169–181.

(54) Yarranton, H. W.; Hussein, H.; Masliyah, J. H. *J. Colloid Interface Sci.* **2000**, *228*, 52–63.

(55) Pauchard, V.; Roy, T. *Colloids Surf., A.* **2014**, *443*, 410–417.

(56) Sztukowski, D. M.; Jafari, M.; Alboudwarej, H.; Yarranton, H. W. *J. Colloid Interface Sci.* **2003**, *265*, 179–186.

(57) Rane, J. P.; Zarkar, S.; Pauchard, V.; Mullins, O. C.; Christie, D.; Andrews, A. B.; Pomerantz, A. E.; Banerjee, S. *Energy Fuels* **2015**, *29*, 3584–3590.

(58) Kiran, S. K.; Acosta, E. J.; Moran, K. *Energy Fuels* **2009**, *23*, 3139–3149.

(59) Muller, H.; Pauchard, V. O.; Hajji, A. A. *Energy Fuels* **2009**, *23*, 1280–1288.

(60) Jarvis, J. M.; Robbins, W. K.; Corilo, Y. E.; Rodgers, R. P. *Energy Fuels* **2015**, *29*, 7058–7064.

(61) Teklebrhan, R. B.; Ge, L.; Bhattacharjee, S.; Xu, Z.; Sjöblom, J. *J. Phys. Chem. B* **2014**, *118*, 1040–1051.

CHAPTER 5 MOLECULAR INTERACTIONS OF ASPHALTENE SUBFRACTIONS IN ORGANIC MEDIA OF VARYING AROMATICITY

5.1 INTRODUCTION

Frequently quantified by SARA (Saturates, Aromatics, Resins and Asphaltenes) analysis, asphaltenes are defined as a solubility class of petroleum molecules being soluble in aromatic solvents such as toluene but insoluble in *n*–alkanes such as *n*–pentane or *n*–heptane.[1] Despite their applications in coating and paving, asphaltenes are generally considered a nuisance.[2–4] Their ability to self–associate and partition at oil–solid and oil–water interfaces is the root cause of several major issues encountered during oil production and processing. The adsorption of asphaltenes onto solid surfaces can i) change reservoir wettability and plug wellbores,[5,6] and ii) block pipelines and foul equipment,[7] thereby reducing oil recovery and potentially halting oil production. On the other hand, the adsorption of asphaltenes to the oil–water interfaces significantly contributes to the stabilization of undesirable water–in–oil (W/O) emulsions, which pose severe corrosion problems to pipelines and refining facilities due to salts and fine solids associated with emulsified water droplets.[8–11] These asphaltene–induced problems are closely related to the inevitable self–aggregation behavior of asphaltenes as a result of the strong adsorption of asphaltene aggregates at oil−water interfaces or onto mineral and metallic surfaces.[1,2,12,13]

As a result of such important practical implications, the aggregation of asphaltenes has been the subject of extensive investigations for several decades. Asphaltenes are able to self–assemble at very low concentrations and in a good solvent such as toluene.[14] Fluorescence spectroscopic studies showed the gradual aggregation of asphaltenes with increasing asphaltene concentration.[15,16] Molecular dynamic simulations confirmed the formation of complex asphaltene aggregates both in the bulk oil phase and at the oil−water interface.[17–19] Chacón–Patiño et al.[20] and Yang et al.[21] reported that the asphaltene subfractions enriched in archipelago structures exhibit a higher tendency of self–association than those enriched in island structures. Mullins et al. proposed a step–wise asphaltene aggregation model in which asphaltene molecules begin to form nanoaggregates of ~2 nm, followed by further association of nanoaggregates to form clusters of ~5 nm.[22] Gray et al. proposed that asphaltenes self–associate to form a three–dimensional “supramolecular assembly” as a result of multiple intermolecular interactions, including aromatic π−π stacking, hydrogen bonding, acid−base interaction, metal coordination and association of hydrophobic pockets.[23]

Addition of an aliphatic solvent can greatly enhance asphaltene aggregation.[24] Sirota et al. reported that asphaltene molecules in a good solvent undergo a thermodynamic phase separation following the addition of an aliphatic solvent.[25] Wang et al. pioneered the colloidal force measurements between whole asphaltenes coated on silica in organic solvents of different aromaticity (toluene to *n*–heptane ratio) using an atomic force microscopy (AFM).[26,27] The increase of *n*–heptane content reduces long–range steric repulsion and induces weak adhesion between asphaltene molecules. Using mica as the substrate material, Natarajan et al.[28] and Zhang et al.[29] observed a similar trend when studying the molecular interactions between whole asphaltenes using a surface forces apparatus (SFA). The addition of *n*–heptane reduces the steric repulsion between asphaltenes, accompanied by an increase in adhesion force. Asphaltene films adsorbed on mica swell significantly in toluene in contrast to those films immersed in *n*–heptane.

As discussed more recently,[30–32] studying whole asphaltenes may restrict our ability to determine the physicochemical characteristics of the most interfacially active asphaltenes, i.e., the most troublesome asphaltene subfractions which preferentially deposit and partition at oil–solid[33–35] or oil–water[31,36–40] interfaces. The extended–SARA (E–SARA) analysis fractionates whole asphaltenes according to their interfacial behaviors and adsorption characteristics, allowing us to target specific asphaltene subfractions of varying interfacial activities.[32] Subramanian et al. fractionated whole asphaltenes using the E–SARA analysis by adsorbing asphaltenes onto calcium carbonate.[34] The authors showed that the asphaltene subfraction irreversibly adsorbed onto calcium carbonate exhibits the highest concentration of carbonyl and carboxylic acid groups, which agrees with the work of Clingenpeel et al.[41]

In our previous studies of E–SARA fractionation based on asphaltene adsorption at oil–water interfaces, a total of four different asphaltene subfractions were obtained using toluene and heptol 50/50 (a mixture of *n*–heptane and toluene at a 1:1 volume ratio) as the extracting solvent, respectively.[40] We found that the oxygenated groups, in particular sulfoxides, played a critical role in enhancing asphaltene adsorption at oil–water interfaces. Among the four asphaltene subfractions, the subfraction containing the highest amount of sulfoxides exhibited the highest interfacial activity, formed the most rigid interfacial films and contributed significantly to the stabilization of W/O emulsions.

Despite their critical importance in understanding molecular mechanisms of asphaltene–induced problems, no study has considered the molecular interactions between such interfacially active asphaltenes. The complex asphaltene interactions could be better understood by studying and comparing asphaltene subfractions of different interfacial activities and compositions, paving the way to correlate specific chemical functionalities with certain interaction characteristics. In the current work, the four different asphaltene subfractions were obtained according to the procedure outlined in our earlier study.[40] Dynamic light scattering (DLS) was used to measure the aggregation behaviors of these fractionated asphaltenes in organic solvents of varying aromaticity, while AFM colloidal force measurements were conducted to understand the mechanisms of their molecular interactions. Combined with the detailed characterizations of fractionated asphaltenes through elemental analysis and X-ray photoelectron spectroscopy (XPS), the results from this study provide molecular insights into the role of key functional groups in controlling asphaltene interactions.

5.2 MATERIALS AND METHODS

5.2.1 Materials

Whole asphaltenes were precipitated at a 40:1 (mL/g) *n*–pentane/bitumen ratio from vacuum distillation feed bitumen provided by Syncrude Canada, Ltd. (Canada). Optima^{TM}–grade *n*–pentane, Optima^{TM}–grade toluene, Optima^{TM}–grade *n*–heptane (Fisher Scientific, Canada) were used as received. Heptol 50/50 and heptol 70/30 were prepared by mixing *n*–heptane and toluene at a 1:1 and 7:3 volume ratio, respectively. Deionized (DI) water with a resistivity of 18.2 MΩ·cm was used throughout the study.

Asphaltene subfractions were obtained using the E–SARA fractionation method by adsorbing asphaltenes at oil–water interfaces. In brief, the W/O emulsion was prepared using DI water and whole asphaltene–in–solvent solution, agitated at 30 000 rpm for 5 min and allowed to stand still overnight. The supernatant was removed and the sediment cake (settled water droplets) of the emulsion was washed with fresh solvent until its supernatant appeared colorless. The cleaned sediment cake was then dried in a vacuum oven at 60 °C to obtain the interfacially active asphaltene subfraction, termed IAA. The asphaltenes which remained in the organic phase were considered as remaining asphaltenes (RA). Based on the different organic solvents used in the E–SARA fractionation, two IAA subfractions and two corresponding RA subfractions were collected as follows: toluene–extracted interfacially active asphaltenes (T–IAA), toluene–extracted remaining asphaltenes (T–RA), heptol 50/50–extracted interfacially active asphaltenes (HT–IAA), and heptol 50/50–extracted remaining asphaltenes (HT–RA). Further details on the E–SARA fractionation of whole asphaltenes can be found in our previous study.[40]

5.2.2 Dynamic Light Scattering (DLS)

The aggregation behaviors of fractionated asphaltenes were studied using the DLS technique. The mean hydrodynamic radius (R_h) of the particles (asphaltene aggregates) is correlated directly to their diffusion coefficient (D) according to the Stokes−Einstein equation

$$D = \frac{kT}{6\pi R_h \eta} \tag{5–1}$$

where k is the Boltzmann constant, T is the temperature, and η is the viscosity of solvent. For Brownian particles, their diffusion coefficient (D) is also related to their characteristic diffusion time (τ_D) through

$$D = \frac{1}{2\tau_D q^2} \tag{5–2}$$

where q is the scattering vector given by

$$q = (4\pi n/\lambda)sin(\theta/2) \tag{3}$$

with n being the refractive index of the medium in which the asphaltenes are dispersed, λ being the wavelength of the laser beam, and θ being the detection angle. The DLS technique can measure the time–dependent autocorrelation function $G(\tau)$ of the scattered light, which is a function of the characteristic diffusion time τ_D and the decay time τ between the measurements as given by

$$G(\tau) = b[1 + \epsilon \exp\left(-\frac{\tau}{\tau_D}\right)] \tag{4}$$

where b is the baseline correlation level relative to the total light scattering intensity, and ϵ is the coefficient which depends on the stray light and the aperture size. In the current study, aggregates of fractionated asphaltenes were found to exhibit Brownian motion with different diffusion rates. Combining Eqs. (1–4), the mean hydrodynamic radius R_h of the asphaltene aggregates can be deduced from the DLS data. In spite of the tendency for asphaltenes to interact with each other to form growing aggregates, the DLS is applicable to monitor the size of asphaltenes when the measurement time is much shorter than the characteristic aggregation time. Details of the DLS technique can be found in the relevant literature.[42,43]

A multifunctional ALV 5022 laser light scattering goniometer (ALV, Germany) in combination with an ALV SP–86 digital correlator (ALV, Germany) was used in the DLS experiments. A He–Ne laser (632.8 nm) with an output power of 22 mW was used as the light source. The optical cell was placed in an index–matching cell filled with high–purity, dust–free toluene. 2 mL of 0.04 g/L fractionated asphaltene–in–solvent (heptol 50/50 or heptol 70/30) solution was added into the optical cell. The asphaltene concentration of 0.04 g/L was chosen in this study to ensure that the fractionated asphaltenes do not precipitate in the solvents during the measurement. The scattering angle was set at 75° to minimize the effect of backscattering from the samples. The data acquisition time was chosen to be 60 s to ensure no significant changes in the aggregate size during the measurement interval, while retaining a good signal/noise ratio. The total measurement time was limited to 2 h to avoid the artifacts of aggregate sedimentation. A lag time of 60 s was allowed between any two consecutive measurements. All of the measurements were carried out at room temperature (22 ± 0.2 °C) and ambient pressure.

5.2.3 Elemental Analysis

A FLASH 2000 CHNS/O analyzer (Thermo Scientific, U.S.A.) was used to analyze the contents of carbon, hydrogen, nitrogen, sulfur and oxygen of asphaltene subfractions. The standard operational method recommended by the instrument manufacturer was followed. Asphaltene samples of ~5 mg were used for the analysis.

5.2.4 X-ray Photoelectron Spectroscopy (XPS)

A Kratos Axis 165 spectrometer (Kratos, U.K.) equipped with a monochromatic Al Kα X-ray source (1486.6 eV) at 15 kV anode potential and 20 mA emission current was used to perform XPS analysis on the asphaltene subfractions. All the XPS spectra were calibrated by the binding energy of Au $4f_{7/2}$ at 84.0 eV with reference to the Fermi level. Narrow scan spectra over the C 1s, S 2p, N 1s and O 1s regions were acquired with a pass energy of 20.0 eV and a dwell time of 200 ms. Casa XPS software was used to conduct peak deconvolutions and calculate atomic concentrations.

5.2.5 Colloidal Force Measurement using Atomic Force Microscopy (AFM)

AFM was used to measure the interaction forces between asphaltene subfractions in different organic solvents. Asphaltene subfractions were coated onto silica wafers and probe particles by dip–coating method. The silica wafers (NanoFab, University of Alberta, Canada) were cleaned using freshly prepared piranha solutions [3:1 (v/v) H_2SO_4/H_2O_2], soaked for 1 h and rinsed with DI water prior to their use. The AFM colloidal probe was made by attaching a silica microsphere ($D \approx 9$ μm, Whitehouse Scientific, U.K.) onto the apex of an AFM tipless silicon nitride cantilever (NP–O10, Bruker Scientific, U.S.A.) using a two–component epoxy glue (EP2LV, Master Bound, U.S.A.). The colloidal probes were kept under vacuum overnight and then exposed to an ultraviolet light for 30 min to remove residual organic contaminants. The spring constants of AFM cantilevers used in this study were ~0.24 N/m and did not change significantly during the force measurements (<10%). Prior to the force measurements, the treated probes and silica wafers were immersed in 0.1 g/L fractionated asphaltene–in–toluene solutions for 1 h, after which they were washed with pure toluene and then dried with gentle nitrogen gas blow. The fractionated asphaltene–coated silica wafers and colloidal probes were used for AFM colloidal force measurements. The clean and fractionated asphaltene–deposited silica wafers were imaged in air with a silicon tip at a scan rate of 1 Hz in ambient conditions of temperature and humidity using a Dimension Icon AFM (Bruker Scientific, U.S.A.) in tapping mode.

Interaction forces between fractionated asphaltenes immobilized on silica wafers and colloidal probes in organic solvents of varying aromaticity were measured using the same Dimension Icon AFM. The approach and retract velocity of the colloidal probe was fixed at 1 μm/s. Details of the AFM force measurement technique can be found in the open literature.[44–47] All interaction forces were normalized by the radius of the colloidal probe coated with the fractionated asphaltenes. Force measurements were conducted in toluene, heptol 50/50 and heptol 70/30 using a house–made liquid cell at a constant temperature of 22 ± 1 °C and ambient pressure. After the solvent was injected into the cell, the system was allowed to equilibrate for 15 min before initiating force measurements. A number of different surface locations on at least two independent samples for each asphaltene–asphaltene pair were chosen to ensure that representative interaction forces were captured.

5.3 RESULTS AND DISCUSSION

5.3.1 Aggregation of Fractionated Asphaltenes Monitored by DLS

The aggregation kinetics of fractionated asphaltenes were studied by DLS. The hydrodynamic radii of the aggregates of different asphaltene subfractions were measured as a function of time. At a concentration of 0.04 g/L in heptol 50/50, the T–IAA subfraction was found to be more prone to aggregation than any other subfractions, as shown in Figure 5.1a. The hydrodynamic radii of T–IAA aggregates quickly increased from around 500 nm, the largest initial size amongst the four fractionated asphaltenes, to almost 1600 nm after 2 h. The increase in size of HT–IAA aggregates was slower than that of T–IAA, while no significant size increase was observed for T–RA and HT–RA aggregates during the measurement time. The RA subfractions showed a much lower tendency to aggregate than the IAA subfractions. As an effective precipitant for asphaltenes, increasing the *n*–heptane content from heptol 50/50 to heptol 70/30 led to increased aggregation rates and enlarged ultimate aggregate sizes, as shown in Figure 5.1b. However, in comparison with the two IAA subfractions, the extent of enhanced aggregation was much smaller for T–RA and HT–RA.

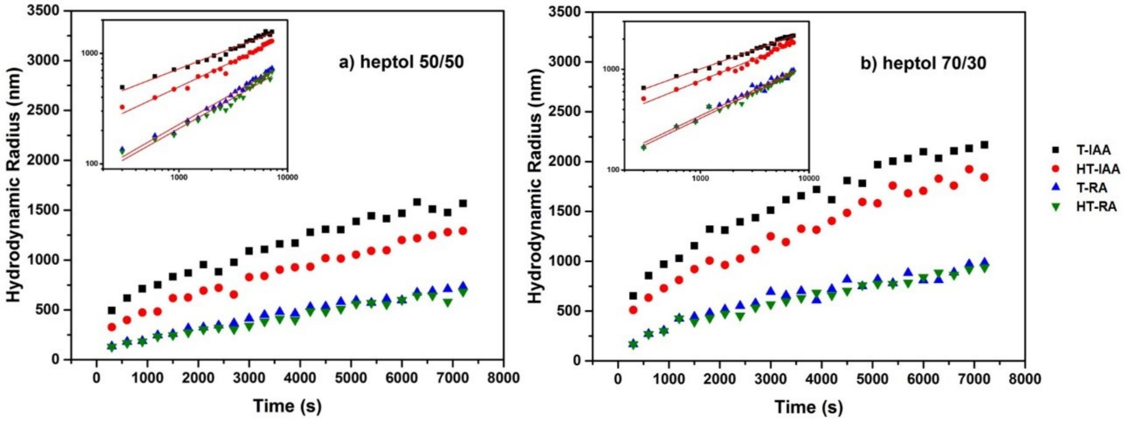

Figure 5.1 Time–dependent aggregation kinetics of 0.04 g/L fractionated asphaltenes in a) heptol 50/50 and b) heptol 70/30. Inset: data plotted on a log–log scale.

A linear relationship was observed between the hydrodynamic radii and aggregation time when plotted on a log–log scale (inset of Figure 5.1), indicating diffusion–limited aggregation for all asphaltene subfractions. The dependence of asphaltene aggregate size (R) on time (t) can be approximated as follows,

$$R = At^{\alpha} \tag{5–5}$$

where A is a constant determined by the size of initial asphaltene aggregates and the characteristic time of asphaltene nucleation.[48] The empirical fits showed that the T–RA and HT–RA had a similar α of 0.53 ± 0.02, while α was 0.45 ± 0.01 and 0.38 ± 0.01 for HT–IAA and T–IAA, respectively. The α of T–IAA was similar to the value reported for whole asphaltenes (0.36 ± 0.04),[48] suggesting that the T–IAA subfraction contributes significantly to asphaltene aggregation despite the fact that T–IAA accounts for only a small fraction of the whole asphaltenes as shown by its low fractional yield (1.1 ± 0.3 wt%), see Table 5.1.

Table 5.1 Elemental composition of four asphaltene subfractions.

	T–IAA	HT–IAA	T–RA	HT–RA
H/C ratio	1.19	1.20	1.18	1.18
N (wt%)	1.12	1.13	1.12	1.12
O (wt%)	5.64	3.70	1.38	1.33
S (wt%)	9.76	9.71	8.75	8.72
Sulfoxide (%)[a]	22.36	19.22	n/a	n/a
Fractional yield (wt%)	1.1 ± 0.3	4.2 ± 0.3	98.9 ± 0.3	95.8 ± 0.3

[a] Sulfoxide content determined by the peak area ratio of sulfoxide from the XPS S 2p band of each fractionated asphaltenes.

The differences in oxygen and sulfur contents among asphaltene subfractions caused their contrasting aggregation behaviors. The IAA subfractions, particularly T–IAA subfraction, featured higher oxygen and sulfur contents than the RA subfractions (Table 5.1). As determined by elemental analysis, the oxygen content of T–IAA was ~1.5 times greater than that of HT–IAA, and 3 times greater than those of both RA subfractions. Such significant differences in oxygen and sulfur content were highlighted by the higher content of oxygenated polar groups, in particular sulfoxides, present in the IAA subfractions than in the RA subfractions, as verified by XPS analysis given in Table 5.1. The higher amount of sulfoxides in IAA provide more binding sites among IAA molecules than RA molecules, leading to a higher probability of aggregation and hence larger aggregates of IAA than RA through polar/hydrogen binding. It is therefore reasonable to conclude that the polar sulfoxides significantly contribute to promoting asphaltene aggregation, as supported by previous studies showing that considerably larger asphaltene aggregates were formed by the more polar asphaltene subfractions.[49] Using isothermal titration calorimetry (ITC), Subramanian and co–workers reported that the asphaltene subfraction with higher concentrations of polar groups (carbonyl, carboxylic acid or derivative groups) showed a significantly higher aggregation tendency than other subfractions.[35] Similar results were also observed by Wang et al. using DLS.[50] The subfraction which was believed to be responsible for the aggregation of whole asphaltenes had the largest number of polar groups. The role of polar groups in enhancing asphaltene aggregation was also confirmed in studies of asphaltene model compounds.[50] In addition, by disrupting the interactions between the polar groups of asphaltene molecules, polar resins were found to be able to disperse asphaltenes.[51]

5.3.2 Characterization of Fractionated Asphaltene Films Deposited on Silica Wafers

Fractionated asphaltenes were coated onto silica wafers and colloidal probes in order to measure the interaction forces between asphaltene surfaces in organic media using an AFM. The successful and similar coatings of fractionated asphaltenes on both silica wafers and probes were confirmed by the identical interaction forces measured by AFM upon approach between asphaltene–coated wafer–bare probe, and bare wafer–asphaltene–coated probe pairs.[26,27] The morphological features of the asphaltene films dip–coated from asphaltene solutions onto silica wafers were characterized in air by AFM in tapping mode (Figure 5.2). In reference, the bare hydrophilic silica wafer was flat and featureless, as shown in Figure 5.2a. In comparison, deposited asphaltenes following rinsing with pure toluene exhibited a layer of asphaltene aggregates of irregular shapes, suggesting a strong irreversible adsorption of asphaltenes onto hydrophilic silica surfaces (Figure 5.2b–5.2e). Asphaltene aggregates of equivalent diameter between 60 and 180 nm were observed for the HT–RA and T–RA, while the size of aggregates formed by HT–IAA and T–IAA increased to between 200 and 400 nm, with the aggregates much more densely distributed. The root mean square roughness (Rq) of the dry asphaltene film gradually increased from ~1.1 to ~1.8 nm in the order of HT–RA, T–RA, HT–IAA and T–IAA. The results indicated the stronger aggregation of two IAA subfractions than that of two RA subfractions, which agreed well with the DLS data.

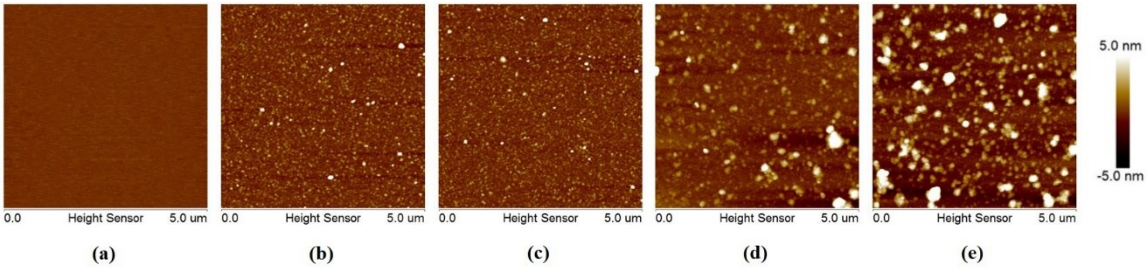

Figure 5.2 Tapping mode AFM imaging in air of clean bare silica surface (a) and silica surfaces coated with (b) HT–RA, (c) T–RA, (d) HT–IAA and (e) T–IAA.

Asphaltenes adsorb onto silica surfaces primarily through their polar functional groups.[52,53] The sulfoxide group was considered the single identifier for IAA subfractions[40] with the T–IAA containing more sulfoxides than the HT–IAA (Table 5.1). The presence of polar oxygenated functional groups allows the asphaltene molecules to arrange themselves more favorably on hydrophilic solid surfaces[53,54] and oil–water interfaces,[12,21,40] mainly through hydrogen bonding interactions. It is therefore not surprising to see that T–IAA molecules packed more densely on the hydrophilic silica surface than any other subfractions, resulting in the closest packing pattern amongst the four asphaltene subfractions.

5.3.3 Interaction Forces between Fractionated Asphaltenes in Organic Solvents

The interaction forces between immobilized asphaltene subfractions in toluene, heptol 50/50 and heptol 70/30 were measured using the AFM colloidal probe technique, to provide a fundamental understanding of asphaltene interactions in organic media. During approach, pure repulsion between two immobilized asphaltene surfaces was measured for all asphaltene subfractions. Since the electrostatic double–layer forces can be considered negligible in organic media, the observed repulsion was attributed to the steric repulsion between the immobilized asphaltene films.[26] Such interaction can be analyzed using the Alexander−de Gennes (AdG) scaling model, as asphaltenes exhibit similar steric interactions as swollen polymer brushes.[26–29] The AdG model is normally used to interpret the steric forces between surfaces coated with monodisperse and neutral polymer brushes in good solvents.[55,56] Since the absolute distance between the two substrate surfaces coated with asphaltene films is unknown in the AFM force measurements, the AdG model was modified to include a parameter ξ which describes the thickness of a fully compressed asphaltene film as follows,[26,27]

$$\frac{F(D)}{R} = \frac{16\pi kTL}{35s^3}\left[7\left(\frac{2L}{D+2\xi}\right)^{5/4} + 5\left(\frac{D+2\xi}{2L}\right)^{7/4} - 12\right]$$

$$\text{for } D + 2\xi < 2L \tag{5–6}$$

where D is the distance between two compressed asphaltene films (m), R is the radius of the probe, k is the Boltzmann constant, T is the temperature, L is the length of protruding asphaltenes without compression, s is the average distance between two grafting points on the surface, and ξ is the thickness of a fully compressed asphaltene film (Figure 5.3).

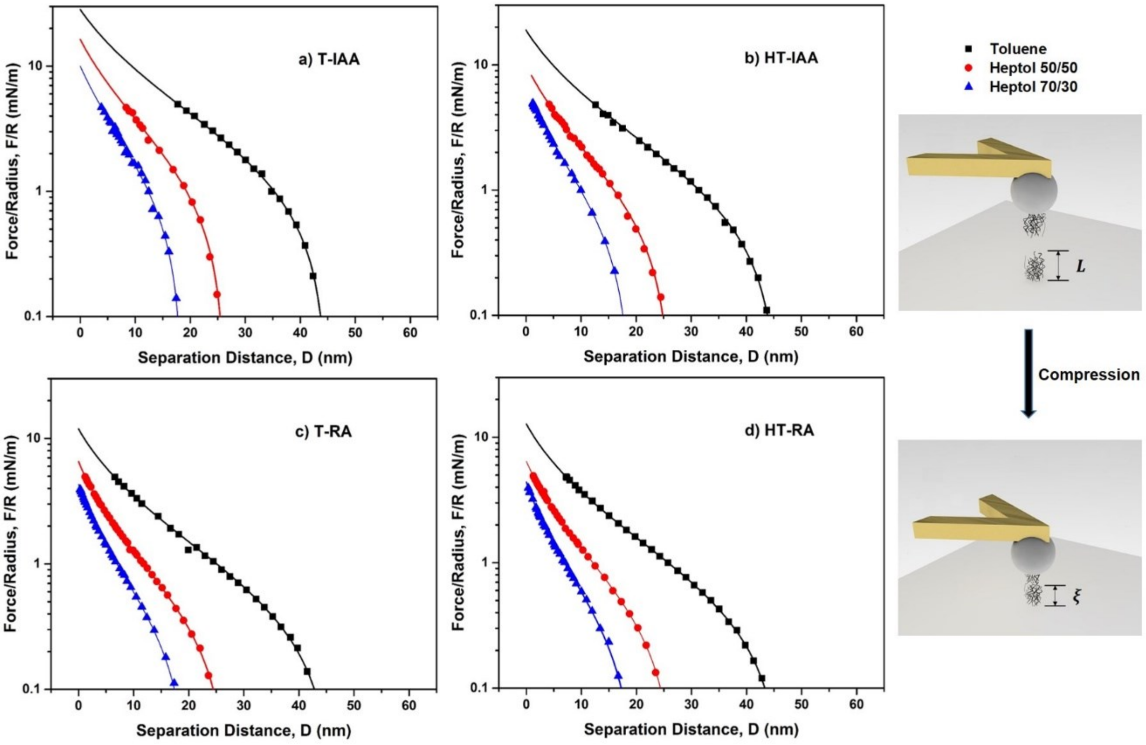

Figure 5.3 Measured force profiles (symbols) between two approaching fractionated asphaltene films (subfraction labelled in figure) immobilized on a silica colloidal probe and a flat silica substrate, respectively, in comparison with the best theoretical fit (solid lines) of the AdG model. Only one typical force profile has been reported for each condition to provide a clear illustration of the subfraction and solvent effect.

The measured repulsion was in good agreement with the AdG scaling model for all the cases (Figure 5.3), confirming that steric repulsion was the dominant interaction between asphaltene films during approach. Table 5.2 provides a summary of the fitting parameters L, s and ξ obtained for the four asphaltene subfractions under different conditions. The varying trends of the three fitting parameters are readily observed in Figure 5.4. For all the subfractions, the uncompressed size (L) of asphaltene films decreased with increasing *n*–heptane concentration, indicating a more dense conformation of asphaltenes induced by the addition of a poor solvent (*n*–heptane). For instance, L for T–IAA was reduced significantly from 41.9 to 19.5 nm as the solvent was changed from a good solvent (toluene) to a relatively poor solvent (heptol 70/30). Similar observations were previously noted when studying the molecular interactions between whole asphaltenes.[27,29] Likewise, ξ which describes the thickness of a fully compressed asphaltene film, was greater in toluene than in heptol 50/50 and heptol 70/30, for all the asphaltene subfractions. The smaller and denser asphaltene aggregates are less likely to repel each other when brought into contact, as verified by the decreasing magnitude and range of repulsive forces with increasing *n*–heptane content in the solvent. In terms of the average distance between the two grafting points on the surface, the largest s values were observed in toluene for all the cases, with only a slight reduction (~ 2%) observed between the cases of heptol 50/50 and heptol 70/30.

Table 5.2 Parameter values obtained by fitting the repulsive interactions (Figure 5.3) using the AdG model.

	Toluene			Heptol 50/50			Heptol 70/30		
	L (nm)	ξ (nm)	s (nm)	L (nm)	ξ (nm)	s (nm)	L (nm)	ξ (nm)	s (nm)
T–IAA	41.9	4.8	9.3	26.1	3.8	8.5	19.5	3.4	8.3
HT–IAA	42.0	4.4	11.1	25.8	3.6	10.2	19.1	2.9	10.1
T–RA	41.6	3.9	13.6	25.5	2.9	12.9	19.3	2.5	12.7
HT–RA	41.8	3.8	13.5	25.6	3.1	12.6	19.0	2.4	12.7

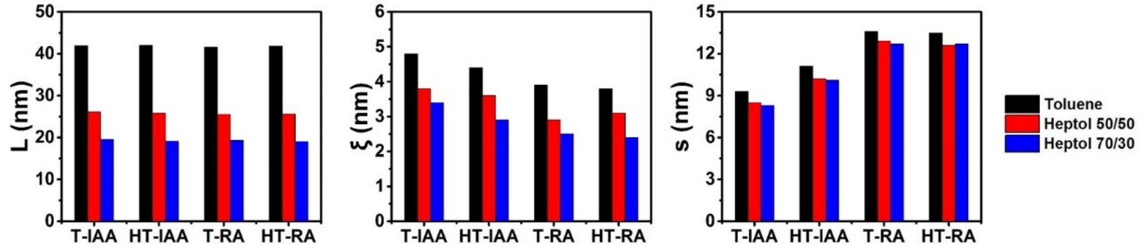

Figure 5.4 Varying trends of the AdG fitting parameters L, ξ and s of four asphaltene subfractions under different solvent conditions.

For different asphaltene subfractions under the same solvent conditions, L values were comparable, indicating little variation in the size of the uncompressed asphaltene films among the four subfractions. The fitted ξ values also showed little variation, all less than 5 nm which was close to the asphaltene film thickness (5 ± 1 nm) measured by ellipsometry in air. The ξ values of the two IAA subfractions were slightly larger than those determined for the two RA subfractions in the same solvent. Such differences were anticipated due to the higher polarity of IAA subfractions and hence less compressible nature of their films.[53] Unlike L and ξ, the s values varied significantly among the different asphaltene subfractions. The RA subfractions showed larger s values than the IAA subfractions. For example, in heptol 50/50, the s values of T–RA and HT–RA were 12.9 and 12.6 nm, respectively, whereas the s values for HT–IAA and T–IAA were reduced to 10.2 and 8.5 nm, respectively. According to the definition, s represents the mean distance between the two neighboring grafting points on the surface. Since polar interactions are the main mechanism for asphaltene adsorption onto silica,[52,53] more polar functional groups would lead to more grafting points of asphaltenes on the silica surface. The asphaltene subfraction with the highest polarity (number of polar groups) would hence exhibit the smallest s value. As discussed earlier, the primary difference among the four fractionated asphaltenes was the higher amount of sulfoxide groups present in the IAA subfractions. In comparison with the RA subfractions, the IAA subfractions also contained more of other oxygenated polar functional groups, such as carbonyl and hydroxyl groups, more so for T–IAA than HT–IAA.[40] The T–IAA subfraction was therefore expected to result in the smallest s value, followed by HT–IAA, and then the two RA subfractions. This trend was in good agreement with the order of fitted s values, indicating the predominant role of polar interactions in the adsorption of asphaltenes onto hydrophilic silica. As a result, the T–IAA molecules had the least freedom of movement on the silica, leading to their closest packing pattern, which was in good agreement with the results of AFM imaging (Figure 5.2).

Figure 5.4 shows the magnitude of the adhesion forces measured when separating two contacting immobilized asphaltene surfaces in toluene, heptol 50/50 and heptol 70/30. For all subfractions, adhesion forces between the immobilized asphaltene surfaces increased with increasing *n*–heptane content in the solvent. The fully expanded (swollen) asphaltene aggregates in toluene featured no adhesion (unmeasurable) between opposing asphaltene films upon separation. For instance, the adhesion force (F_{ad}/R) between the T–IAA films was unmeasurable in toluene, while it increased to ~0.29 mN/m in heptol 50/50, and further increased to ~0.41 mN/m in heptol 70/30. Increased adhesion between asphaltenes in more aliphatic solvents (addition of *n*–heptane) correlated well with the stronger aggregation tendency of asphaltenes in more aliphatic solvents measured by DLS (Figure 5.1).

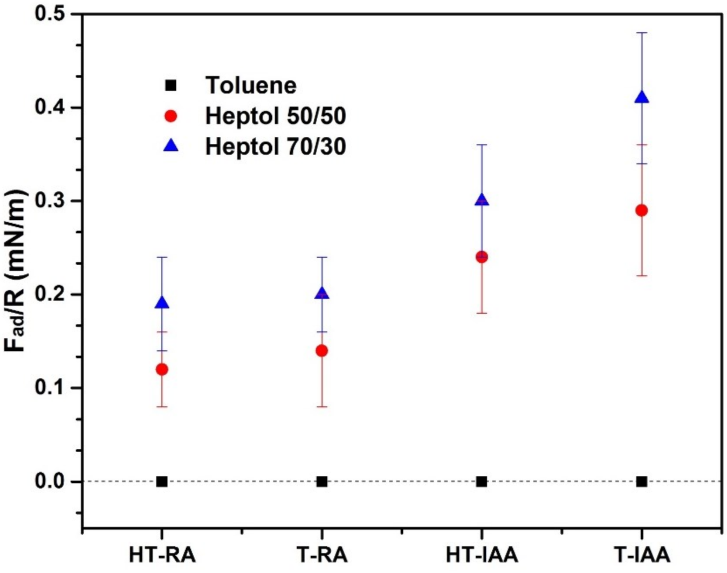

Figure 5.5 Normalized adhesion forces (F_{ad}/R) between equivalent asphaltene subfractions interacting in toluene, heptol 50/50 and heptol 70/30. The dotted line indicates zero adhesion.

Under the same solvent conditions, T–IAA and HT–IAA exhibited larger adhesion forces than the two RA subfractions. The stronger adhesions between IAA subfractions were attributed to their higher oxygen and sulfur contents (Table 5.1). The heteroatoms (N, O and S) embedded in the aromatic rings of asphaltenes could strengthen the aromatic interaction between asphaltenes,[17,57] which is considered to be the dominant driving force for asphaltene aggregation.[17,57,58] The presence of heteroatoms increases the polarity of asphaltenes and hence enhances the π–electron cloud density of aromatic rings, thus contributing to stronger π–π stacking interactions between the polyaromatic cores of asphaltenes. In addition, heteroatoms along the aliphatic side chains of asphaltenes also play a significant role in the aggregation of asphaltenes through polar interactions.[58–60] The density functional theory (DFT) calculations by da Costa et al. showed that hydrogen bonding was as important as π–π stacking interactions for asphaltene aggregation.[61] The higher oxygen and sulfur contents of the IAA subfractions can therefore be considered to be the primary cause for the enhanced association between neighboring asphaltene molecules. The AFM colloidal force measurements correlated well with the aggregation trend revealed by DLS, confirming the stronger binding interactions between the IAA subfractions than the RA subfractions, as well as the role of *n*–heptane in enhancing asphaltene aggregation.

5.4 CONCLUSION

The aggregation behaviors of four asphaltene subfractions (T–IAA, HT–IAA, T–RA and HT–RA) prepared using E–SARA fractionation were probed by DLS in organic media of varying aromaticity. The DLS results indicated a stronger aggregation tendency of the two IAA subfractions (especially T–IAA) than the two RA subfractions in a given solvent. Decreasing solvent aromaticity was found to promote asphaltene aggregation. AFM colloidal force measurements were conducted in order to obtain a molecular level understanding of asphaltene interactions, and the results showed a good correlation with the DLS findings. For all asphaltene subfractions, the solvent aromaticity significantly influenced the interaction forces between immobilized asphaltene films. As the solvent aromaticity decreased, asphaltene molecules adopted a more compressed conformation as verified by their collapsed sizes. The steric repulsion detected during the approach of two asphaltene films diminished with increasing *n*–heptane concentration. On the contrary, the adhesion forces measured during separation of two asphaltene surfaces in contact increased as the solvent changed from toluene to heptol 70/30. Under the same solvent conditions, IAA films were more likely to associate with each other than RA films as revealed during separation of two contacting asphaltene films. The greater aggregation tendency of IAA subfractions was attributed to their higher oxygen and sulfur contents. Compared with the RA subfractions, the presence of a larger number of oxygenated polar groups (particularly sulfoxides) greatly contributed to the stronger asphaltene aggregation by stronger π–π stacking interactions between large conjugated aromatic rings of asphaltenes, as well as hydrogen bonding interactions between polar groups of asphaltenes. The current study provides scientific insights into the molecular interactions between asphaltenes, specifically highlighting the contribution of sulfoxides which promote strong asphaltene aggregation.

5.5 REFERENCES

(1) Mullins, O. C. *Annu. Rev. Anal. Chem.* **2011**, *4*, 393–418.

(2) Akbarzadeh, K.; Hammami, A.; Kharrat, A.; Zhang, D.; Allenson, S.; Creek, J.; Kabir, S.; Jamaluddin, A. J.; Marshall, A. G.; Rodgers, R. P.; Mullins, O. C.; Solbakken, T. *Oilfield. Rev.* **2007**, *19*, 22–43.

(3) Adams, J. J. *Energy Fuels* **2014**, *28*, 2831–2856.

(4) Langevin, D.; Argillier, J.–F. *Adv. Colloid Interface Sci.* **2015**, *233*, 83–93.

(5) Drummond, C.; Israelachvili, J. *J. Pet. Sci. Eng.* **2004**, *45*, 61–81.

(6) Eskin, D.; Mohammadzadeh, O.; Akbarzadeh, K.; Taylor, S. D.; Ratulowski, J. *Can. J. Chem. Eng.* **2016**, *94*, 1202–1217.

(7) Torres, C.; Treint, F.; Alonso, C.; Milne, A.; Lecomte, A. *Proceedings of the SPE/ICoTA Coiled Tubing Conference and Exhibition*; The Woodlands, TX, April 12−13, 2005; SPE−93272−MS, DOI: 10.2118/93272−MS.

(8) Yarranton, H. W.; Hussein, H.; Masliyah, J. H. *J. Colloid Interface Sci.* **2000**, *228*, 52–63.

(9) Kilpatrick, P. K. *Energy Fuels* **2012**, *26*, 4017–4026.

(10) Tchoukov, P.; Yang, F.; Xu, Z.; Dabros, T.; Czarnecki, J.; Sjöblom, J. *Langmuir* **2014**, *30*, 3024–3033.

(11) Harbottle, D.; Chen, Q.; Moorthy, K.; Wang, L.; Xu, S.; Liu, Q.; Sjoblom, J.; Xu, Z. *Langmuir* **2014**, *30*, 6730–6738.

(12) Teklebrhan, R. B.; Ge, L.; Bhattacharjee, S.; Xu, Z.; Sjöblom, J. *J. Phys. Chem. B* **2014**, *118*, 1040–1051.

(13) Xiong, Y.; Cao, T.; Chen, Q.; Li, Z.; Yang, Y.; Xu, S.; Yuan, S.; Sjöblom, J.; Xu, Z. *J. Phys. Chem. C* **2017**, *121*, 5020–5028.

(14) Yarranton, H. W.; Ortiz, D. P.; Barrera, D. M.; Baydak, E. N.; Barré, L.; Frot, D.; Eyssautier, J.; Zeng, H.; Xu, Z.; Dechaine, G.; Becerra, M.; Shaw, J. M.; McKenna, A. M.; Mapolelo, M. M.; Bohne, C.; Yang, Z.; Oake, J. *Energy Fuels* **2013**, *27*, 5083–5106.

(15) Ghosh, A. K.; Srivastava, S. K.; Bagchi, S. *Fuel* **2007**, *86*, 2528–2534.

(16) Ghosh, A. K.; Chaudhuri, P.; Panja, S. S. *Fuel* **2016**, *185*, 164–170.

(17) Sedghi, M.; Goual, L.; Welch, W.; Kubelka, J. *J. Phys. Chem. B* **2013**, *117*, 5765–5776.

(18) Mikami, Y.; Liang, Y.; Matsuoka, T.; Boek, E. S. *Energy Fuels* **2013**, *27*, 1838–1845.

(19) Gao, F.; Xu, Z.; Liu, G.; Yuan, S. *Energy Fuels* **2014**, *28*, 7368–7376.

(20) Chacón–Patiño, M. L.; Rowland, S. M.; Rodgers, R. P. *Energy Fuels* **2018**, *32*, 314–328.

(21) Yang, F.; Tchoukov, P.; Dettman, H.; Teklebrhan, R. B.; Liu, L.; Dabros, T.; Czarnecki, J.; Masliyah, J.; Xu, Z. *Energy Fuels* **2015**, *29*, 4783−4794.

(22) Mullins, O. C. *Energy Fuels* **2010**, 2179–2207.

(23) Gray, M. R.; Tykwinski, R. R.; Stryker, M.; Tan, X. *Energy Fuels* **2011**, *25*, 3125–3134.

(24) Yarranton, H. W. *J. Dispers. Sci. Technol.* **2005**, *26*, 5–8.

(25) Sirota, E. B.; Lin, M. Y. *Energy Fuels* **2007**, *21*, 2809–2815.

(26) Wang, S.; Liu, J.; Zhang, L.; Xu, Z.; Masliyah, J. *Energy Fuels* **2009**, *23*, 862–869.

(27) Wang, S.; Liu, J.; Zhang, L.; Masliyah, J.; Xu, Z. *Langmuir* **2010**, *26*, 183–190.

(28) Natarajan, A.; Xie, J.; Wang, S.; Liu, Q.; Masliyah, J.; Zeng, H.; Xu, Z. *J. Phys. Chem. C* **2011**, *115*, 16043–16051.

(29) Zhang, L.; Shi, C.; Lu, Q.; Liu, Q.; Zeng, H. *Langmuir* **2016**, *32*, 4886–4895.

(30) Czarnecki, J.; Tchoukov, P.; Dabros, T. *Energy Fuels* **2012**, *26*, 5782–5786.

(31) Czarnecki, J.; Tchoukov, P.; Dabros, T.; Xu, Z. *Can. J. Chem. Eng.* **2013**, *91*, 1365–1371.

(32) Qiao, P.; Harbottle, D.; Tchoukov, P.; Masliyah, J. H.; Sjoblom, J.; Liu, Q.; Xu, Z. *Energy Fuels* **2017**, *31*, 3330−3337.

(33) Dudášová, D.; Simon, S.; Hemmingsen, P. V.; Sjöblom, J. *Colloids Surf., A.* **2008**, *317*, 1–9.

(34) Subramanian, S.; Simon, S.; Gao, B.; Sjöblom, J. *Colloids Surf., A.* **2016**, *495*, 136–148.

(35) Subramanian, S.; Humborstad, G.; Simon, S.; Xu, Z.; Sjöblom, J. *Colloids Surf., A.* **2017**, *514*, 79–90.

(36) Xu, Y.; Dabros, T.; Hamza, H.; Shefantook, W. *Pet. Sci. Technol.* **1999**, *17*, 1051–1070.

(37) Wu, X. *Energy Fuels* **2003**, *17*, 179–190.

(38) Yang, F.; Tchoukov, P.; Pensini, E.; Dabros, T.; Czarnecki, J.; Masliyah, J.; Xu, Z. *Energy Fuels* **2014**, *28*, 6897–6904.

(39) Jarvis, J. M.; Robbins, W. K.; Corilo, Y. E.; Rodgers, R. P. *Energy Fuels* **2015**, *29*, 7058–7064.

(40) Qiao, P.; Harbottle, D.; Tchoukov, P.; Wang, X.; Xu, Z. *Energy Fuels* **2017**, *31*, 9179−9187.

(41) Clingenpeel, A. C.; Rowland, S. M.; Corilo, Y. E.; Zito, P.; Rodgers, R. P. *Energy Fuels* **2017**, *31*, 5933–5939.

(42) Hassan, P. A.; Rana, S.; Verma, G. *Langmuir* **2015**, *31*, 3–12.

(43) Eyssautier, J.; Frot, D.; Barré, L. *Langmuir* **2012**, *28*, 11997–12004.

(44) Liu, J.; Xu, Z.; Masliyah, J. *Langmuir* **2003**, *19*, 3911–3920.

(45) Liu, J.; Xu, Z.; Masliyah, J. *AIChE J.* **2004**, *50*, 1917–1927.

(46) Liu, J.; Xu, Z.; Masliyah, J. *Colloids Surf., A.* **2005**, *260*, 217–228.

(47) Long, J.; Zhang, L.; Xu, Z.; Masliyah, J. H. *Langmuir* **2006**, *22*, 8831–8839.

(48) Anisimov, M. A.; Ganeeva, Y. M.; Gorodetskii, E. E.; Deshabo, V. A.; Kosov, V. I.; Kuryakov, V. N.; Yudin, D. I.; Yudin, I. K. *Energy Fuels* **2014**, *28*, 6200–6209.

(49) Spiecker, P. M.; Gawrys, K. L.; Kilpatrick, P. K. *J. Colloid Interface Sci.* **2003**, *267*, 178–193.

(50) Wang, X.; Zhang, R.; Liu, L.; Qiao, P.; Simon, S.; Sjöblom, J.; Xu, Z.; Jiang, B. *Energy Fuels* **2017**, *31*, 9201−9212.

(51) Spiecker, P. M.; Gawrys, K. L.; Trail, C. B.; Kilpatrick, P. K. *Colloids Surf., A.* **2003**, *220*, 9–27.

(52) Hannisdal, A.; Ese, M.–H.; Hemmingsen, P. V.; Sjöblom, J. *Colloids Surf., A.* **2006**, *276*, 45–58.

(53) Abudu, A.; Goual, L. *Energy Fuels* **2009**, *23*, 1237–1248.

(54) Pernyeszi, T.; Dékány, I. *Colloids Surf., A.* **2001**, *194*, 25–39.

(55) de Gennes, P. G. *Adv. Colloid Interface Sci.* **1987**, *27*, 189–209.

(56) Butt, H. J.; Kappl, M.; Mueller, H.; Raiteri, R.; Meyer, W.; Ruhe, J. *Langmuir* **1999**, *15*, 2559–2565.

(57) Wang, H.; Xu, H.; Jia, W.; Liu, J.; Ren, S. *Energy Fuels* **2017**, *31*, 2488–2495.

(58) Goual, L.; Sedghi, M.; Wang, X.; Zhu, Z. *Langmuir* **2014**, *30*, 5394–5403.

(59) Gawrys, K. L.; Blankenship, G. A.; Kilpatrick, P. K. *Energy Fuels* **2006**, *20*, 705–714.

(60) Sodero, A. C. R.; Santos Silva, H.; Guevara Level, P.; Bouyssiere, B.; Korb, J. P.; Carrier, H.; Alfarra, A.; Bégué, D.; Baraille, I. *Energy Fuels* **2016**, *30*, 4758–4766.

(61) da Costa, L. M.; Stoyanov, S. R.; Gusarov, S.; Tan, X.; Gray, M. R.; Stryker, J. M.; Tykwinski, R.; De M. Carneiro, J. W.; Seidl, P. R.; Kovalenko, A. *Energy Fuels* **2012**, *26*, 2727–2735.

CHAPTER 6 CONCLUSION AND RECOMMENDATIONS FOR FUTURE WORK

6.1 CONCLUSIONS

Asphaltenes are the heaviest and least soluble fraction of crude oil, and they are recognized as the challenging species in petroleum production due to their strong adsorption at solid surfaces and oil−water interfaces. As the demand for oil continuously increases, asphaltene−rich sources such as oil sands and heavy oils are growing in significance as substitute oil sources (known as unconventionals). Despite their importance, asphaltenes remain as poorly understood materials. Asphaltenes are defined as a solubility class (typically soluble in toluene but insoluble in *n*−alkanes like *n*−heptane). The coarse definition of asphaltenes inherently indicates the presence of a wide range of molecules with distinct chemical compositions and structures in the asphaltene category. Some molecular species in asphaltenes are even insoluble in toluene since asphaltenes are present in the form of aggregates in the natural state, the solubility behavior of individual asphaltene molecules is not evident in such a complex mixture.

The fractionation of asphaltenes is thus recommended as a protocol to study and characterize asphaltenes. In this work, the extended−saturates, aromatics, resins, and asphaltenes (E−SARA) analysis was proposed and established as an effective asphaltene fractionation method to directly target the real problematic asphaltene subfractions depending upon asphaltene adsorption at oil−water interfaces and solid surfaces (Figure 6.1). By fractionating asphaltenes based on their adsorption onto calcium carbonate, the important role of carbonyl, carboxylic acid, or derivative groups in asphaltene adsorption at solid surfaces has been indicated. By fractionating asphaltenes based on their adsorption at oil−water interfaces, it was shown that less than 2 wt% of asphaltenes is responsible for stabilizing water−in−oil (W/O) emulsions. The asphaltenes irreversibly attached to water droplets after emulsification were extracted as “interfacially active asphaltenes” (IAA), while the asphaltenes remaining in the oil phase were named as “remaining asphaltenes” (RA). IAA were able to form rigid films at oil−water interfaces preventing water coalescence, in contrast to RA showing no stabilization potential for W/O emulsions.

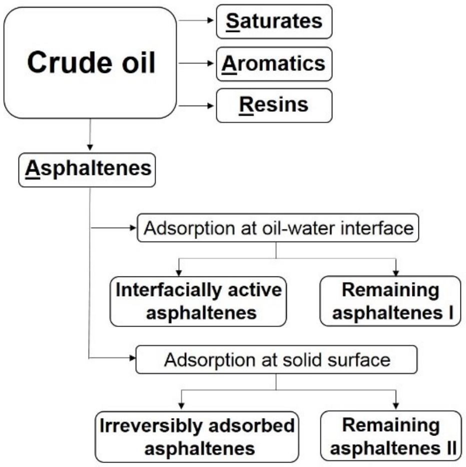

Figure 6.1 E−SARA analysis.

Solvent aromaticity had a profound effect on IAA compositions. Toluene−extracted IAA contained a higher amount of sulfur and oxygen than heptol 50/50−extracted IAA (HT−IAA). Heptol 50/50 is a mixture of *n*−heptane and toluene at a 1:1 volume ratio. Such sulfur and oxygen difference, which was manifested in the form of oxygenated functional groups, resulted in the higher interfacial activity and the greater stabilization potential of T−IAA than HT−IAA, in spite of the lower proportion of T−IAA in whole asphaltenes. In comparison with IAA subfractions, the more abundant RA subfractions (T−RA and HT−RA) showed much lower sulfur and oxygen content which were not changed significantly by varying solvent aromaticity. Sulfoxide groups among several oxygenated groups were believed to play an essential role in enhancing asphaltene adsorption at oil−water interfaces primarily though inducing hydrogen bonding interactions between asphaltene molecules and water.

As asphaltenes adsorb at oil−water interfaces in the form of aggregates, the aggregation kinetics of IAAs (T−IAA and HT−IAA) and RAs (T−RA and HT−RA) were studied using dynamic light scattering (DLS) in organic media of varying aromaticity. Decreasing solvent aromaticity promoted aggregation for all asphaltene subfractions, and their aggregation tendency in a given solvent followed in the same order of their interfacial activity and emulsion stabilization potential (T−IAA > HT−IAA > T−RA ≈ HT−RA). The DLS results were well−corroborated by the interaction force studies using an atomic force microscope (AFM). As solvent aromaticity decreased, the steric repulsion between asphaltenes reduced accompanied by increasing adhesion with asphaltenes adopting a more compressed conformation. IAAs, particularly T−IAA, exhibited higher adhesion forces than RAs when separating two asphaltene film in contact. The oxygenated polar groups, such as sulfoxides, were considered the predominant contributor to asphaltene aggregation by providing attractive π−π interactions between the asphaltene aromatic cores, as well as hydrogen bonding interactions between the polar groups of asphaltenes.

E−SARA analysis simplifies the compositional complexity of whole asphaltenes, and provides an effective approach to understand the underlying molecular mechanisms of asphaltene aggregation and adsorption. Rather than studying asphaltenes as a whole, it optimizes the asphaltene studies by selectively distinguishing the problematic asphaltene subfractions based on asphaltene adsorption at oil−water interfaces and solid surfaces, and consequently determines the key chemical functionalities of certain asphaltene properties. The problematic asphaltenes isolated by E−SARA analysis could undergo advanced chemical characterizations followed by appropriate computational modeling, providing an in−depth understating of their behaviors at the molecular level. This knowledge could guide the rational design of "smart additives" to selectively targeting problematic asphaltenes, thus mitigating or preventing asphaltene−related problems in oil industry. As a result, a large portion of remaining asphaltenes could be conserved instead of being rejected, greatly reducing asphaltene remediation costs.

6.2 RECOMMENDATIONS FOR FUTURE WORK

- It would be valuable to perform the compositional analysis of IAA and RA using Fourier transform ion cyclotron resonance mass spectrometry (FT−ICR MS). FT−ICR MS is a high−resolution analytical technique for crude oil characterization. It can simultaneously monitor thousands of heteroatom (oxygen, sulfur, and nitrogen)−containing molecular species. Using FT−ICR MS, it can greatly improve our understanding of the molecular compositions of IAA and RA, providing critical information about the chemistry involved in asphaltene adsorption at oil−water interfaces and asphaltene aggregation. We will collaborate with National High

Magnetic Field Laboratory in Tallahassee, Florida, U.S.A. to perform FT−ICR MS analysis of IAA and RA samples.

- Based on the compositional analysis results from FT−ICR MS, the representative molecular representations of asphaltene subfractions could be estimated. Such information is vital for simulating the systems containing asphaltenes through molecular dynamics (MD), which could expand our knowledge of interfacial and bulk behaviors of asphaltenes at the nanoscale or molecular level. For example, the energetics of asphaltene aggregation in the bulk oil phase, and the diffusion of interfacially active asphaltene molecules towards the oil−water interface could be modeled.
- The findings from this work combined with the future FT−ICR MS and MD experiments could facilitate the rational design of appropriate inhibitors for asphaltene aggregation and adsorption. Such inhibitors could specifically target the key chemical functionalities (e.g. sulfoxides) in the problematic asphaltene subfractions, providing an effective approach to resolve asphaltene−induced issues (W/O emulsion stabilization, deposition, etc.).
- The aggregation of fractionated asphaltenes at various solvent conditions could be further exploited using small−angle neutron scattering (SANS) and small−angle X-ray scattering (SAXS), giving the geometrical information such as shape, characteristic dimensions and polydispersity of asphaltene aggregates. The preliminary results of our SANS work (performed at Laue Langevin Institute, Grenoble, France) showed that IAA subfractions form larger nanoaggregates than RA subfractions, and the asphaltene nanoaggregate size is independent of asphaltene concentration. The SANS work is collaborated with Dr. David Harbottle's group from University of Leeds, U.K.
- The effect of water chemistry (such as pH, salts) on the chemical compositions of IAA and RA could be investigated. The packing and reorganization of asphaltene aggregates at oil−water interfaces is likely to be influenced by water chemistry.
- The demulsification mechanisms for asphaltene−stabilized W/O emulsions can be studied using IAA and a number of demulsifiers (such as ethylcellulose), as a good comparison with other studies using whole asphaltenes, providing valuable information for the optimization of demulsifier design.

- It has been observed that IAA exhibited a higher adsorption potential on glass surface than RA. It would be of interest to study the adsorption of IAA and RA onto different solid surfaces, and compare their adsorption behaviors with those asphaltene subfractions originally fractionated based on solid adsorption. It would be valuable to study if the certain chemical functionalities control asphaltene adsorption at both oil−water interfaces and solid surfaces.

BIBLIOGRAPHY

Abdallah, W. A.; Taylor, S. D. *J. Phys. Chem. C* **2008**, *112*, 18963–18972.

Abdallah, W. A.; Taylor, S. D. *Nucl. Instrum. Methods Phys. Res., Sect. B* **2007**, *258*, 213–217.

Abudu, A.; Goual, L. *Energy Fuels* **2009**, *23*, 1237–1248.

Acevedo, S.; Castillo, J.; Fernández, A.; Goncalves, S.; Ranaudo, M. A. *Energy Fuels* **1998**, *12*, 386–390.

Acevedo, S.; Castro, A.; Negrin, J. G.; Fernández, A.; Escobar, G.; Piscitelli, V.; Delolme, F.; Dessalces, G. *Energy Fuels* **2007**, *21*, 2165–2175.

Acevedo, S.; Méndez, B.; Rojas, A.; Layrisse, I.; Rivas, H. *Fuel* **1985**, *64*, 1741–1747.

Adams, J. J. *Energy Fuels* **2014**, *28*, 2831–2856.

Agrawala, M.; Yarranton, H. W. *Ind. Eng. Chem. Res.* **2001**, *40*, 4664–4672.

Akbarzadeh, K.; Bressler, D. C.; Wang, J.; Gawrys, K. L.; Gray, M. R.; Kilpatrick, P. K.; Yarranton, H. W. *Energy Fuels* **2005**, *19*, 1268–1271.

Akbarzadeh, K.; Hammami, A.; Kharrat, A.; Zhang, D.; Allenson, S.; Creek, J.; Kabir, S.; Jamaluddin, A. J.; Marshall, A. G.; Rodgers, R. P.; Mullins, O. C.; Solbakken, T. *Oilfield. Rev.* **2007**, *19*, 22–43.

Alboudwarej, H.; Pole, D.; Svrcek, W. Y.; Yarranton, H. W. *Ind. Eng. Chem. Res.* **2005**, *44*, 5585–5592.

Alshareef, A. H.; Scherer, A.; Stryker, J. M.; Tykwinski, R. R.; Gray, M. R. *Energy Fuels* **2012**, *26*, 3592–3603.

Alvarez, G.; Poteau, S.; Argillier, J.−F.; Langevin, D.; Salager, J.−L. *Energy Fuels* **2009**, *23*, 294–299.

Alvarez−Ramírez, F.; García−Cruz, I.; Tavizón, G.; Martínez−Magadán, J. M. *Pet. Sci. Technol.* **2004**, *22*, 915–926.

Andersen, S. I. *Energy Fuels* **1999**, *13*, 315–322.

Andreatta, G.; Bostrom, N.; Mullins, O. C. *Langmuir* **2005**, *21*, 2728–2736.

Angle, C. W.; Long, Y.; Hamza, H.; Lue, L. *Fuel* **2006**, *85*, 492–506.

Anisimov, M. A.; Ganeeva, Y. M.; Gorodetskii, E. E.; Deshabo, V. A.; Kosov, V. I.; Kuryakov, V. N.; Yudin, D. I.; Yudin, I. K. *Energy Fuels* **2014**, *28*, 6200–6209.

Anisimov, M. A.; Yudin, I. K.; Nikitin, V.; Nikolaenko, G.; Chernoutsan, A.; Toulhoat, H.; Frot, D.; Briolant, Y. *J. Phys. Chem.* **1995**, *99*, 9576–9580.

Araújo, R. S.; Azevedo, D. C. S.; Cavalcante, C. L.; Jiménez−López, A.; Rodríguez−Castellón, E. *Microporous Mesoporous Mater.* **2008**, *108*, 213–222.

Artok, L.; Su, Y.; Hirose, Y.; Hosokawa, M.; Murata, S.; Nomura, M. *Energy Fuels* **1999**, *13*, 287–296.

Badre, S.; Carla Goncalves, C.; Norinaga, K.; Gustavson, G.; Mullins, O. C. *Fuel* **2006**, *85*, 1–11.

Balabin, R. M.; Syunyaev, R. Z.; Schmid, T.; Stadler, J.; Lomakina, E. I.; Zenobi, R. *Energy Fuels* **2011**, *25*, 189–196.

Berkowitz, N. *Fossil Hydrocarbons: Chemistry and Technology*; Academic Press: San Diego, 1997.

Bi, J.; Yang, F.; Harbottle, D.; Pensini, E.; Tchoukov, P.; Simon, S.; Sjöblom, J.; Dabros, T.; Czarnecki, J.; Liu, Q.; Xu, Z. *Langmuir* **2015**, *31*, 10382−10391.

Bissada, K. K. A.; Tan, J.; Szymczyk, E.; Darnell, M.; Mei, M. *Org. Geochem.* **2016**, *95*, 21–28.

Borton, D.; Pinkston, D. S.; Hurt, M. R.; Tan, X.; Azyat, K.; Scherer, A.; Tykwinski, R.; Gray, M.; Qian, K.; Kenttämaa, H. I. *Energy Fuels* **2010**, *24*, 5548–5559.

Bouhadda, Y.; Bormann, D.; Sheu, E.; Bendedouch, D.; Krallafa, A.; Daaou, M. *Fuel* **2007**, *86*, 1855–1864.

Bouriat, P.; Kerri, N. El; Graciaa, A.; Lachaise, J. *Langmuir* **2004**, *20*, 7459–7464.

Buenrostro−Gonzalez, E.; Groenzin, H.; Lira−Galeana, C.; Mullins, O. C. *Energy Fuels* **2001**, *15*, 972–978.

Butt, H. J.; Kappl, M.; Mueller, H.; Raiteri, R.; Meyer, W.; Ruhe, J. *Langmuir* **1999**, *15*, 2559–2565.

Carbognani, L. *Pet. Sci. Technol.* **2000**, *18*, 335–360.

Castillo, J.; Goncalves, S.; Fernández, A.; Mujica, V. *Opt. Commun.* **1998**, *145*, 69–75.

Chacón−Patiño, M. L.; Blanco−Tirado, C.; Orrego−Ruiz, J. A.; Gómez−Escudero, A.; Combariza, M. Y. *Energy Fuels* **2015**, *29*, 6330–6341.

Chacón–Patiño, M. L.; Rowland, S. M.; Rodgers, R. P. *Energy Fuels* **2018**, *32*, 314–328.

Chang, C. L.; Fogler, H. S. *Langmuir* **1994**, *10*, 1749–1757.

Chang, C. L.; Fogler, H. S. *Langmuir* **1994**, *10*, 1758–1766.

Chapman, W. G.; Gubbins, K. E.; Jackson, G.; Radosz, M. *Fluid Phase Equilib.* **1989**, *52*, 31–38.

Chapman, W. G.; Jackson, G.; Gubbins, K. E. *Mol. Phys.* **1988**, *65*, 1057–1079.

Chen, T.; Lin, F.; Primkulov, B.; He, L.; Xu, Z. *Can. J. Chem. Eng.* **2017**, *95*, 281–289.

Cho, Y.; Kim, Y. H.; Kim, S. *Anal. Chem.* **2011**, *83*, 6068–6073.

Cho, Y.; Na, J.−G.; Nho, N.−S.; Kim, S.; Kim, S. *Energy Fuels* **2012**, *26*, 2558–2565.

Clementz, D. M. *Clays Clay Miner.* **1976**, *24*, 312–319.

Clingenpeel, A. C.; Rowland, S. M.; Corilo, Y. E.; Zito, P.; Rodgers, R. P. *Energy Fuels* **2017**, *31*, 5933–5939.

Cortés, F. B.; Mejía, J. M.; Ruiz, M. A.; Benjumea, P.; Riffel, D. B. *Energy Fuels* **2012**, *26*, 1725–1730.

Cunico, R. L.; Sheu, E. Y.; Mullins, O. C. *Pet. Sci. Technol.* **2004**, *22*, 787–798.

Czarnecka, E.; Gillott, J. E. *Clays Clay Miner.* **1980**, *28*, 197–203.

Czarnecki, J.; Tchoukov, P.; Dabros, T. *Energy Fuels* **2012**, *26*, 5782–5786.

Czarnecki, J.; Tchoukov, P.; Dabros, T.; Xu, Z. *Can. J. Chem. Eng.* **2013**, *91*, 1365–1371.

da Costa, L. M.; Stoyanov, S. R.; Gusarov, S.; Tan, X.; Gray, M. R.; Stryker, J. M.; Tykwinski, R.; De M. Carneiro, J. W.; Seidl, P. R.; Kovalenko, A. *Energy Fuels* **2012**, *26*, 2727–2735.

David Ting, P.; Hirasaki, G. J.; Chapman, W. G. *Pet. Sci. Technol.* **2003**, *21*, 647–661.

de Gennes, P. G. *Adv. Colloid Interface Sci.* **1987**, *27*, 189–209.

de la Cruz, J. L. M.; Argüelles−Vivas, F. J.; Matías−Pérez, V.; Durán−Valencia, C. d. l. A.; López−Ramirez, S. *Energy Fuels* **2009**, *23*, 5611–5625.

Dickie, J. P.; Yen, T. F. *Anal. Chem.* **1967**, *39*, 1847–1852.

Drummond, C.; Israelachvili, J. *J. Pet. Sci. Eng.* **2004**, *45*, 61–81.

Dudášová, D.; Silset, A.; Sjöblom, J. *J. Dispers. Sci. Technol.* **2008**, *29*, 139–146.

Dudášová, D.; Simon, S.; Hemmingsen, P. V.; Sjöblom, J. *Colloids Surf., A.* **2008**, *317*, 1–9.

Dutta Majumdar, R.; Gerken, M.; Mikula, R.; Hazendonk, P. *Energy Fuels* **2013**, *27*, 6528–6537.

Dutta Majumdar, R.; Montina, T.; Mullins, O. C.; Gerken, M.; Hazendonk, P. *Fuel* **2017**, *193*, 359–368.

Dutta, P. K.; Holland, R. J. *Fuel* **1984**, *63*, 197–201.

Ekholm, P.; Blomberg, E.; Claesson, P.; Auflem, I. H.; Sjöblom, J.; Kornfeldt, A. *J. Colloid Interface Sci.* **2002**, *247*, 342–350.

Eley, D. D.; Hey, M. J.; Symonds, J. D. *Colloids Surf.* **1988**, *32*, 87–101.

Eskin, D.; Mohammadzadeh, O.; Akbarzadeh, K.; Taylor, S. D.; Ratulowski, J. *Can. J. Chem. Eng.* **2016**, *94*, 1202–1217.

Exerowa, D.; Ivanov, I.; Scheludko, A. *Issledovaniya v Oblasti Poverkhnostnykh Sil*; Nauka: Moscow, Russia, 1964.

Eyssautier, J.; Frot, D.; Barré, L. *Langmuir* **2012**, *28*, 11997–12004.

Eyssautier, J.; Levitz, P.; Espinat, D.; Jestin, J.; Gummel, J.; Grillo, I.; Barré, L. *J. Phys. Chem. B* **2011**, *115*, 6827–6837.

Fan, T.; Buckley, J. S. *Energy Fuels* **2002**, *16*, 1571–1575.

Feng, X.; Wang, S.; Hou, J.; Wang, L.; Cepuch, C.; Masliyah, J.; Xu, Z. *Ind. Eng. Chem. Res.* **2011**, *50*, 6347–6354.

Fenistein, D.; Barré, L. *Fuel* **2001**, *80*, 283–287.

Flory, P. J. *J. Chem. Phys.* **1942**, *10*, 51–61.

Fossen, M.; Kallevik, H.; Knudsen, K. D.; Sjöblom, J. *Energy Fuels* **2007**, *21*, 1030–1037.

Franco, C. A.; Nassar, N. N.; Ruiz, M. A.; Pereira−Almao, P.; Cortés, F. B. *Energy Fuels* **2013**, *27*, 2899–2907.

Freer, E. M.; Radke, C. J. *J. Adhes.* **2004**, *80*, 481–496.

Fritschy, G.; Papirer, E. *Fuel* 1**978**, *57*, 701–704.

Gafonova, O. V.; Yarranton, H. W. *J. Colloid Interface Sci.* **2001**, *241*, 469–478.

Gao, F.; Xu, Z.; Liu, G.; Yuan, S. *Energy Fuels* **2014**, *28*, 7368–7376.

Gao, S.; Moran, K.; Xu, Z.; Masliyah, J. *Energy Fuels* **2009**, *23*, 2606–2612.

Gawel, I.; Bociarska, D.; Biskupski, P. *Appl. Catal., A* **2005**, *295*, 89–94.

Gawrys, K. L.; Blankenship, G. A.; Kilpatrick, P. K. *Energy Fuels* **2006**, *20*, 705–714.

Gawrys, K. L.; Blankenship, G. A.; Kilpatrick, P. K. *Langmuir* **2006**, *22*, 4487–4497.

Ghosh, A. K.; Chaudhuri, P.; Panja, S. S. *Fuel* **2016**, *185*, 164–170.

Ghosh, A. K.; Srivastava, S. K.; Bagchi, S. *Fuel* **2007**, *86*, 2528–2534.

Gonzalez, D. L.; Ting, P. D.; Hirasaki, G. J.; Chapman, W. G. *Energy Fuels* **2005**, *19*, 1230–1234.

González, M. F.; Stull, C. S.; López−Linares, F.; Pereira−Almao, P. *Energy Fuels* **2007**, *21*, 234–241.

Goual, L.; Abudu, A. *Energy Fuels* **2010**, *24*, 469–474.

Goual, L.; Horváth−Szabó, G.; Masliyah, J. H.; Xu, Z. *Langmuir* **2005**, *21*, 8278–8289.

Goual, L.; Sedghi, M. *J. Colloid Interface Sci.* **2015**, *440*, 23–31.

Goual, L.; Sedghi, M.; Wang, X.; Zhu, Z. *Langmuir* **2014**, *30*, 5394–5403.

Gray, M. R.; Tykwinski, R. R.; Stryker, M.; Tan, X. *Energy Fuels* **2011**, *25*, 3125–3134.

Groenzin, H.; Mullins, O. C. *Energy Fuels* **2000**, *14,* 677–684.

Groenzin, H.; Mullins, O. C. *J. Phys. Chem. A* **1999**, *103*, 11237–11245.

Gross, J.; Sadowski, G. *Ind. Eng. Chem. Res.* **2001**, *40*, 1244–1260.

Hannisdal, A.; Ese, M.−H.; Hemmingsen, P. V.; Sjöblom, J. *Colloids Surf., A.* **2006**, *276*, 45–58.

Harbottle, D.; Chen, Q.; Moorthy, K.; Wang, L.; Xu, S.; Liu, Q.; Sjoblom, J.; Xu, Z. *Langmuir* **2014**, *30*, 6730–6738.

Harbottle, D.; Liang, C.; El−thaher, N.; Liu, Q.; Masliyah, J.; Xu, Z. Particle−stabilized emulsions in heavy oil processing. In *Particle Stabilized Emulsions and Colloids:*

Formation and Application; Ngai, T.; Bon, S. A. F., Eds.; The Royal Society of Chemistry: London, UK, 2015.

Hassan, A.; Ahmed, S.; Ali, M. A.; Hamid, H.; Inui, T. *Appl. Catal., A* **2001**, *220*, 59–68.

Hassan, P. A.; Rana, S.; Verma, G. *Langmuir* **2015**, *31*, 3–12.

He, L.; Lin, F.; Li, X.; Sui, H.; Xu, Z. *Chem. Soc. Rev.* **2015**, *44*, 5446–5494.

Headen, T. F.; Boek, E. S.; Jackson, G.; Totton, T. S.; Müller, E. A. *Energy Fuels* **2017**, *31*, 1108–1125.

Hoepfner, M. P.; Fávero, C. V. B.; Haji−Akbari, N.; Fogler, H. S. *Langmuir* **2013**, *29*, 8799–8808.

Hosseini−Dastgerdi, Z.; Tabatabaei−Nejad, S. A. R.; Khodapanah, E.; Sahraei, E. *Asia−Pac. J. Chem. Eng.* **2015**, *10*, 1–14.

Hou, J.; Feng, X.; Masliyah, J.; Xu, Z. *Energy Fuels* **2012**, *26*, 1740–1745.

Huggins, M. L. *J. Chem. Phys.* **1941**, *9*, 440.

Jada, A.; Debih, H. *Compos. Interfaces* **2009**, *16*, 219–235.

Jada, A.; Debih, H.; Khodja, M. *J. Pet. Sci. Eng.* **2006**, *52*, 305–316.

Japanwala, S.; Chung, K. H.; Dettman, H. D.; Gray, M. R. *Energy Fuels* **2002**, *16*, 477–484.

Jarvis, J. M.; Robbins, W. K.; Corilo, Y. E.; Rodgers, R. P. *Energy Fuels* **2015**, *29*, 7058–7064.

Jeribi, M.; Almir−Assad, B.; Langevin, D.; Hénaut, I.; Argillier, J. F. *J. Colloid Interface Sci.* **2002**, *256*, 268–272.

Jewell, D. M.; Albaugh, E. W.; Davis, B. E.; Ruberto, R. G. *Ind. Eng. Chem. Fundam.* **1974**, *13*, 278–282.

Jewell, D. M.; Weber, J. H.; Bunger, J. W.; Plancher, H.; Latham, D. R. *Anal. Chem.* **1972**, *44*, 1391–1395.

Kharrat, A. M. *Energy Fuels* **2009**, *23*, 828–834.

Kharrat, A. M.; Zacharia, J.; Cherian, V. J.; Anyatonwu, A. *Energy Fuels* **2007**, *21*, 3618–3621.

Kilpatrick, P. K. *Energy Fuels* **2012**, *26*, 4017–4026.

Kiran, S. K.; Acosta, E. J.; Moran, K. *Energy Fuels* **2009**, *23*, 3139–3149.

Klein, G. C.; Kim, S.; Rodgers, R. P.; Marshall, A. G.; Yen, A. *Energy Fuels* **2006**, *20*, 1973–1979.

Klein, G. C.; Kim, S.; Rodgers, R. P.; Marshall, A. G.; Yen, A.; Asomaning, S. *Energy Fuels* **2006**, *20*, 1965–1972.

Kozłowski, M. *Fuel* **2004**, *83*, 259–265.

Kraiwattanawong, K.; Fogler, H. S.; Gharfeh, S. G.; Singh, P.; Thomason, W. H.; Chavadej, S. *Energy Fuels* **2007**, *21*, 1248–1255.

Labrador, H.; Fernández, Y.; Tovar, J.; Muñoz, R.; Pereira, J. C. *Energy Fuels* **2007**, *21*, 1226–1230.

Langevin, D.; Argillier, J.−F. *Adv. Colloid Interface Sci.* **2015**, *233*, 83–93.

Lisitza, N. V; Freed, D. E.; Sen, P. N.; Song, Y. Q. *Energy Fuels* **2009**, *23*, 1189–1193.

Liu, F.; Li, W.; Chen, H.; Li, B. *Fuel* **2007**, *86*, 360–366.

Liu, J.; Xu, Z.; Masliyah, J. *AIChE J.* **2004**, *50*, 1917–1927.

Liu, J.; Xu, Z.; Masliyah, J. *Colloids Surf., A.* **2005**, *260*, 217–228.

Liu, J.; Xu, Z.; Masliyah, J. *Langmuir* **2003**, *19*, 3911–3920.

Liu, J.; Zhao, Y.; Ren, S. *Energy Fuels* **2015**, *29*, 1233–1242.

Long, J.; Xu, Z.; Masliyah, J. H. *Langmuir* **2007**, *23*, 6182–6190.

Long, J.; Zhang, L.; Xu, Z.; Masliyah, J. H. *Langmuir* **2006**, *22*, 8831–8839.

Mannistu, K. D.; Yarranton, H. W.; Masliyah, J. H. *Energy Fuels* **1997**, *11*, 615–622.

Maqbool, T.; Balgoa, A. T.; Fogler, H. S. *Energy Fuels* **2009**, *23*, 3681–3686.

Marchal, C.; Abdessalem, E.; Tayakout−Fayolle, M.; Uzio, D. *Energy Fuels* **2010**, *24*, 4290–4300.

Martin, S. J.; Granstaff, V. E.; Frye, G. C. *Anal. Chem.* **1991**, *63*, 2272–2281.

Masliyah, J. H.; Czarnecki, J.; Xu, Z. *Handbook on Theory and Practice of Bitumen Recovery from Athabasca Oil Sands*; Kingsley Knowledge Publishing: Calgary, Alberta, Canada, 2011.

McLean, J. D.; Kilpatrick, P. K. *J. Colloid Interface Sci.* **1997**, *196*, 23–34.

Merino−Garcia, D.; Andersen, S. I. *Pet. Sci. Technol.* **2003**, *21*, 507–525.

Mikami, Y.; Liang, Y.; Matsuoka, T.; Boek, E. S. *Energy Fuels* **2013**, *27*, 1838–1845.

Mostowfi, F.; Indo, K.; Mullins, O. C.; McFarlane, R. *Energy Fuels* **2009**, *23*, 1194–1200.

Muller, H.; Pauchard, V. O.; Hajji, A. A. *Energy Fuels* **2009**, *23*, 1280–1288.

Mullins, O. C. *Annu. Rev. Anal. Chem.* **2011**, *4*, 393–418.

Mullins, O. C. *Energy Fuels* **2010**, *24*, 2179–2207.

Mullins, O. C.; Martínez−Haya, B.; Marshall, A. G. *Energy Fuels* **2008**, *22*, 1765–1773.

Mullins, O. C.; Sabbah, H.; Eyssautier, J.; Pomerantz, A. E.; Barré, L.; Andrews, A. B.; Ruiz−Morales, Y.; Mostowfi, F.; McFarlane, R.; Goual, L.; Lepkowicz, R.; Cooper, T.; Orbulescu, J.; Leblanc, R. M.; Edwards, J.; Zare, R. N. *Energy Fuels* **2012**, *26*, 3986–4003.

Nassar, N. N. *Energy Fuels* **2010**, *24*, 4116–4122.

Nassar, N. N.; Hassan, A.; Pereira−Almao, P. *Energy Fuels* **2011**, *25*, 1566–1570.

Nassar, N. N.; Hassan, A.; Pereira−Almao, P. *J. Colloid Interface Sci.* **2011**, *360*, 233–238.

Natarajan, A.; Xie, J.; Wang, S.; Liu, Q.; Masliyah, J.; Zeng, H.; Xu, Z. *J. Phys. Chem. C* **2011**, *115*, 16043–16051.

Nikookar, M.; Omidkhah, M. R.; Pazuki, G. R. *Pet. Sci. Technol.* **2008**, *26*, 1904–1912.

Nordgåd, E. L.; Landsem, E.; Sjöblom, J. *Langmuir* **2008**, *24*, 8742–8751.

Nordgård, E. L.; Sjoblom, J. *J Dispers. Sci.Technol.* **2008**, *29*, 1114–1122.

Nordgård, E. L.; Sørland, G.; Sjöblom, J. *Langmuir* **2010**, *26*, 2352–2360.

Oh, K.; Ring, T. A.; Deo, M. D. *J. Colloid Interface Sci.* **2004**, *271*, 212–219.

Östlund, J.−A.; Nydén, M.; Fogler, H. S.; Holmberg, K. *Colloids Surf., A.* **2004**, *234*, 95–102.

Painter, P.; Veytsman, B.; Youtcheff, J. *Energy Fuels* **2015**, *29*, 2120–2133.

Pauchard, V.; Rane, J. P.; Zarkar, S.; Couzis, A.; Banerjee, S. *Langmuir* **2014**, *30*, 8381–8390.

Pauchard, V.; Roy, T. *Colloids Surf., A.* **2014**, *443*, 410–417.

Peng, J.; Liu, Q.; Xu, Z.; Masliyah, J. *Adv. Funct. Mater.* **2012**, *22*, 1732–1740.

Peng, J.; Liu, Q.; Xu, Z.; Masliyah, J. *Energy Fuels* **2012**, *26*, 2705–2710.

Pensini, E.; Harbottle, D.; Yang, F.; Tchoukov, P.; Li, Z.; Kailey, I.; Behles, J.; Masliyah, J.; Xu, Z. *Energy Fuels* **2014**, *28*, 6760–6771.

Pernyeszi, T.; Dékány, I. *Colloids Surf., A.* **2001**, *194*, 25–39.

Pernyeszi, T.; Patzkó, Á.; Berkesi, O.; Dékány, I. *Colloids Surf., A.* **1998**, *137*, 373–384.

Pfeiffer, J. P.; Saal, R. N. J. *J. Phys. Chem.* **1940**, *44*, 139–149.

Pinkston, D. S.; Duan, P.; Gallardo, V. A.; Habicht, S. C.; Tan, X.; Qian, K.; Gray, M.; Mullen, K.; Kenttämaa, H. I. *Energy Fuels* **2009**, *23*, 5564–5570.

Pomerantz, A. E.; Hammond, M. R.; Morrow, A. L.; Mullins, O. C.; Zare, R. N. *J. Am. Chem. Soc.* **2008**, *130*, 7216–7217.

Qian, K.; Mennito, A. S.; Edwards, K. E.; Ferrughelli, D. T. *Rapid Commun. Mass Spectrom* **2008**, *22*, 2153–2160.

Qiao, P.; Harbottle, D.; Li, Z.; Tang, Y.; Xu, Z. *Energy Fuels* **2018**, *32*, 10478−10485.

Qiao, P.; Harbottle, D.; Tchoukov, P.; Masliyah, J. H.; Sjoblom, J.; Liu, Q.; Xu, Z. *Energy Fuels* **2017**, *31*, 3330−3337.

Qiao, P.; Harbottle, D.; Tchoukov, P.; Wang, X.; Xu, Z. *Energy Fuels* **2017**, *31*, 9179−9187.

Quintero, C. G.; Noïk, C.; Dalmazzone, C.; Grossiord, J. L. *Oil Gas Sci. Technol.* **2009**, *64*, 607–616.

Rane, J. P.; Pauchard, V.; Couzis, A.; Banerjee, S. *Langmuir* **2013**, *29*, 4750–4759.

Rane, J. P.; Zarkar, S.; Pauchard, V.; Mullins, O. C.; Christie, D.; Andrews, A. B.; Pomerantz, A. E.; Banerjee, S. *Energy Fuels* **2015**, *29*, 3584–3590.

Rodgers, R. P.; Marshall, A. G. In *Asphaltenes, Heavy Oils and Petroleomics*; Mullins, O. C., Sheu, E. Y., Hammami, A., Marshall, A. G., Eds.; Springer: New York, 2007.

Rogel, E.; Miao, T.; Vien, J.; Roye, M. *Fuel* **2015**, *147*, 155–160.

Rudrake, A.; Karan, K.; Horton, J. H. *J. Colloid Interface Sci.* **2009**, *332*, 22–31.

Ruiz−Morales, Y.; Wu, X.; Mullins, O. C. *Energy Fuels* **2007**, *21*, 944–952.

Saada, A.; Siffert, B.; Papirer, E. *J. Colloid Interface Sci.* **1995**, *174*, 185–190.

Sabbah, H.; Morrow, A. L.; Pomerantz, A. E.; Zare, R. N. *Energy Fuels* **2011**, *25*, 1597–1604.

Santos, R. G.; Loh, W.; Bannwart, A. C.; Trevisan, O. V. *Braz. J. Chem. Eng.* **2014**, *31*, 571–590.

Scheludko, A. *Adv. Colloid Interface Sci.* **1967**, *1*, 391–464.

Scheludko, A.; Platikanov, D. *Kolloid−Z.* **1961**, *175*, 150–158.

Schneider, M. H.; Andrews, A. B.; Mitra−Kirtley, S.; Mullins, O. C. *Energy Fuels* **2007**, *21*, 2875–2882.

Schuler, B.; Fatayer, S.; Meyer, G.; Rogel, E.; Moir, M.; Zhang, Y.; Harper, M. R.; Pomerantz, A. E.; Bake, K. D.; Witt, M.; Peña, D.; Kushnerick, J. D.; Mullins, O. C.; Ovalles, C.; Van Den Berg, F. G. A.; Gross, L. *Energy Fuels* **2017**, *31*, 6856–6861.

Schuler, B.; Meyer, G.; Peña, D.; Mullins, O. C.; Gross, L. *J. Am. Chem. Soc.* **2015**, *137*, 9870–9876.

Sedghi, M.; Goual, L.; Welch, W.; Kubelka, J. *J. Phys. Chem. B* **2013**, *117*, 5765–5776.

Sharma, A.; Groenzin, H.; Tomita, A.; Mullins, O. C. *Energy Fuels* **2002**, *16*, 490–496.

Sheu, E. Y. *Energy Fuels* **2002**, *16*, 74–82.

Shojaati, F.; Riazi, M.; Mousavi, S. H.; Derikvand, Z. *Colloids Surf., A.* **2017**, *531*, 99–110.

Sirota, E. B.; Lin, M. Y. *Energy Fuels* **2007**, *21*, 2809–2815.

Siskin, M.; Kelemen, S. R.; Eppig, C. P.; Brown, L. D.; Afeworki, M. *Energy Fuels* **2006**, *20*, 1227–1234.

Sjöblom, J.; Aske, N.; Auflem, I. H.; Brandal, Ø.; Havre, T. E.; Sæther, Ø.; Westvik, A.; Johnsen, E. E.; Kallevik, H. *Adv. Colloid Interface Sci.* **2003**, *100*, 399–473.

Sodero, A. C. R.; Santos Silva, H.; Guevara Level, P.; Bouyssiere, B.; Korb, J. P.; Carrier, H.; Alfarra, A.; Bégué, D.; Baraille, I. *Energy Fuels* **2016**, *30*, 4758–4766.

Speight, J. G. *Handbook of Petroleum Analysis*; Wiley−Interscience: New York, 2001.

Spiecker, P. M.; Gawrys, K. L.; Kilpatrick, P. K. *J. Colloid Interface Sci.* **2003**, *267*, 178–193.

Spiecker, P. M.; Gawrys, K. L.; Trail, C. B.; Kilpatrick, P. K. *Colloids Surf., A.* **2003**, *220*, 9–27.

Spiecker, P. M.; Kilpatrick, P. K. *Langmuir* **2004**, *20*, 4022–4032.

Stanford, L. A.; Rodgers, R. P.; Marshall, A. G.; Czarnecki, J.; Wu, X. A.; Taylor, S. *Energy Fuels* **2007**, *21*, 973–981.

Stanford, L. A.; Rodgers, R. P.; Marshall, A. G.; Czarnecki, J.; Wu, X. A. *Energy Fuels* **2007**, *21*, 963–972.

Stockbridge, C. D. *Vacuum Microbalance Techniques*; Plenum Press: New York, 1966.

Strausz, O. P.; Lown, E. M. *The Chemistry of Alberta Oil Sands, Bitumens and Heavy Oils*; Alberta Energy Research Institute: Calgary, Alberta, Canada, 2003.

Strausz, O. P.; Torres, M.; Lown, E. M.; Safarik, I.; Murgich, J. *Energy Fuels* **2006**, *20*, 2013–2021.

Subramanian, S.; Humborstad, G.; Simon, S.; Xu, Z.; Sjöblom, J. *Colloids Surf., A.* **2017**, *514*, 79–90.

Subramanian, S.; Simon, S.; Gao, B.; Sjöblom, J. *Colloids Surf., A.* **2016**, *495*, 136–148.

Subramanian, S.; Simon, S.; Sjoblom, J. *J. Dispers. Sci. Technol.* **2016**, *37*, 1027–1049.

Syunyaev, R. Z.; Balabin, R. M.; Akhatov, I. S.; Safieva, J. O. *Energy Fuels* **2009**, *23*, 1230–1236.

Sztukowski, D. M.; Jafari, M.; Alboudwarej, H.; Yarranton, H. W. *J. Colloid Interface Sci.* **2003**, *265*, 179–186.

Sztukowski, D. M.; Yarranton, H. W. *Langmuir* **2005**, *21*, 11651–11658.

Tchoukov, P.; Czarnecki, J.; Dabros, T. *Colloids Surf., A.* **2010**, *372*, 15–21.

Tchoukov, P.; Yang, F.; Xu, Z.; Dabros, T.; Czarnecki, J.; Sjöblom, J. *Langmuir* **2014**, *30*, 3024–3033.

Teklebrhan, R. B.; Ge, L.; Bhattacharjee, S.; Xu, Z.; Sjöblom, J. *J. Phys. Chem. B* **2014**, *118*, 1040–1051.

Torkaman, M.; Bahrami, M.; Dehghani, M. *Energy Fuels* **2017**, *31*, 11169–11180.

Torres, C. A.; Treint, F.; Alonso, C.; Milne, A.; Lecomte, A. *Proceedings of the SPE/ICoTA Coiled Tubing Conference and Exhibition*; The Woodlands, TX, April 12−13, 2005; SPE−93272−MS, DOI: 10.2118/93272−MS.

Tu, Y.; Kung, J.; McCracken, T.; Kotlyar, L.; Kingston, D.; Sparks, B. *Clay Sci.* **2006**, *12*, 194–198.

Tu, Y.; Woods, J.; Kung, J.; McCracken, T.; Kotlyar, L.; Sparks, B.; Dong, M. *Clay Sci.* **2006**, *12*, 183–187.

Tu, Y.; Woods, J.; McCracken, T.; Kotlyar, L.; Sparks, B.; Chung, K. *Clay Sci.* **2006**, *12*, 188–193.

Turgman−Cohen, S.; Smith, M. B.; Fischer, D. A.; Kilpatrick, P. K.; Genzer, J. *Langmuir* **2009**, *25*, 6260–6269.

Vafaie−Sefti, M.; Mousavi−Dehghani, S. A. *Fluid Phase Equilib.* **2006**, *247*, 182–189.

Verruto, V. J.; Le, R. K.; Kilpatrick, P. K. *J. Phys. Chem. B* **2009**, *113*, 13788–13799.

Vilas Bôas Fávero, C.; Maqbool, T.; Hoepfner, M.; Haji−Akbari, N.; Fogler, H. S. *Adv. Colloid Interface Sci.* **2016**, *244*, 267–280.

Wang, H.; Xu, H.; Jia, W.; Liu, J.; Ren, S. *Energy Fuels* **2017**, *31*, 2488–2495.

Wang, J. X.; Buckley, J. S. *Energy Fuels* **2001**, *15*, 1004–1012.

Wang, J.; Ferguson, A. L. *J. Phys. Chem. B* **2016**, *120*, 8016–8035.

Wang, S.; Liu, J.; Zhang, L.; Masliyah, J.; Xu, Z. *Langmuir* **2010**, *26*, 183–190.

Wang, S.; Liu, J.; Zhang, L.; Xu, Z.; Masliyah, J. *Energy Fuels* **2009**, *23*, 862–869.

Wang, S.; Xu, J.; Wen, H. *Comput. Phys. Commun.* **2014**, *185*, 3069–3078.

Wang, X.; Zhang, R.; Liu, L.; Qiao, P.; Simon, S.; Sjöblom, J.; Xu, Z.; Jiang, B. *Energy Fuels* **2017**, *31*, 9201−9212.

Wattana, P.; Fogler, H. S.; Yen, A.; Carmen Garcia, M. D. Carbognani, L. *Energy Fuels* **2005**, *19*, 101–110.

Wattana, P.; Wojciechowski, D. J.; Bolaños, G.; Fogler, H. S. *Pet. Sci. Technol.* **2003**, *21*, 591–613.

Wertheim, M. S. *J. Stat. Phys.* **1984**, *35*, 19–34.

Wertheim, M. S. *J. Stat. Phys.* **1984**, *35*, 35–47.

Wertheim, M. S. *J. Stat. Phys.* **1986**, *42*, 459–476.

Wertheim, M. S. *J. Stat. Phys.* **1986**, *42*, 477–492.

Wong, S. F.; Lim, J. S.; Dol, S. S. *J. Pet. Sci. Eng.* **2015**, *135*, 498–504.

Wu, Q.; Pomerantz, A. E.; Mullins, O. C.; Zare, R. N. *Energy Fuels* **2014**, *28*, 475–482.

Wu, X. *Energy Fuels* **2003**, *17*, 179–190.

Xie, K.; Karan, K. *Energy Fuels* **2005**, *19*, 1252–1260.

Xiong, Y.; Cao, T.; Chen, Q.; Li, Z.; Yang, Y.; Xu, S.; Yuan, S.; Sjöblom, J.; Xu, Z. *J. Phys. Chem. C* **2017**, *121*, 5020–5028.

Xu, Y.; Dabros, T.; Hamza, H.; Shefantook, W. *Pet. Sci. Technol.* **1999**, *17*, 1051–1070.

Yan, Z.; Elliott, J. A. W.; Masliyah, J. H. *J. Colloid Interface Sci.* **1999**, *220*, 329–337.

Yang, F.; Tchoukov, P.; Dettman, H.; Teklebrhan, R. B.; Liu, L.; Dabros, T.; Czarnecki, J.; Masliyah, J.; Xu, Z. *Energy Fuels* **2015**, *29*, 4783−4794.

Yang, F.; Tchoukov, P.; Pensini, E.; Dabros, T.; Czarnecki, J.; Masliyah, J.; Xu, Z. *Energy Fuels* **2014**, *28*, 6897–6904.

Yang, F.; Tchoukov, P.; Qiao, P.; Ma, X.; Pensini, E.; Dabros, T.; Czarnecki, J.; Xu, Z. *Colloids Surf., A.* **2018**, *540*, 215–223.

Yarranton, H. W. *J. Dispers. Sci. Technol.* **2005**, *26*, 5–8.

Yarranton, H. W.; Hussein, H.; Masliyah, J. H. *J. Colloid Interface Sci.* **2000**, *228*, 52–63.

Yarranton, H. W.; Ortiz, D. P.; Barrera, D. M.; Baydak, E. N.; Barré, L.; Frot, D.; Eyssautier, J.; Zeng, H.; Xu, Z.; Dechaine, G.; Becerra, M.; Shaw, J. M.; McKenna, A. M.; Mapolelo, M. M.; Bohne, C.; Yang, Z.; Oake, J. *Energy Fuels* **2013**, *27*, 5083–5106.

Yarranton, H. W.; Sztukowski, D. M.; Urrutia, P. *J. Colloid Interface Sci.* **2007**, *310*, 246–252.

Yeung, A.; Dabros, T.; Masliyah, J.; Czarnecki, J. *Colloids Surf., A.* **2000**, *174*, 169–181.

Yudin, I. K.; Anisimov, M. A. Dynamic light scattering monitoring of asphaltene aggregation in crude oils and hydrocarbon solutions. In *Asphaltenes, Heavy Oils and Petroleomics*; Mullins, O. C.; Sheu, E. Y.; Hammami, A.; Marshall, A. G.; Eds. Springer: New York, 2007.

Zahabi, A.; Gray, M. R.; Dabros, T. *Energy Fuels* **2012**, *26*, 1009–1018.

Zeng, H.; Song, Y. Q.; Johnson, D. L.; Mullins, O. C. *Energy Fuels* **2009**, *23*, 1201–1208.

Zhang, L. Y.; Lopetinsky, R.; Xu, Z.; Masliyah, J. H. *Energy Fuels* **2005**, *19*, 1330–1336.

Zhang, L.; Shi, C.; Lu, Q.; Liu, Q.; Zeng, H. *Langmuir* **2016**, *32*, 4886–4895.

APPENDIX A

Additional information for Chapter 4 regarding the precipitation of whole asphaltenes from bitumen.

The vacuum distillation feed bitumen was mixed with certified *n*−pentane (Fisher Scientific, Canada) at a 40:1 (mL/g) *n*–pentane/bitumen ratio in a glass container wrapped in aluminum foil. The diluted bitumen was shaken gently for 2 h on a mechanical shaker, and then left undisturbed overnight to allow the precipitated asphaltenes to settle. Once settled, the supernatant was carefully removed from the container followed by the addition of fresh *n*−pentane at an equivalent volume to that removed into the container for continuous asphaltene washing. The washing procedure was repeated until the supernatant appeared colorless. After the final wash, the supernatant was removed and the asphaltenes were dissolved in Optima^{TM}−grade toluene at a 20:1 (mL/g) toluene/asphaltene ratio. The fine solids remained in collected asphaltenes were removed through the centrifugation of asphaltene−in−toluene solution at 20000 g for 20 min. The toluene was then removed under reduced pressure to obtain dry asphaltenes. The yield of whole asphaltenes accounted for approximately 16 wt% of the original bitumen.

APPENDIX B

Additional information for Chapter 5 regarding the use of an AFM for topographical imaging and colloidal force measurements.

The silica wafer (NanoFab, University of Alberta, Canada) was cleaned by being soaked in a freshly prepared piranha solution [3:1 (v/v) H_2SO_4/H_2O_2] for 1 h followed by a thorough rinsing with DI water prior to use. The clean silica wafer was hydrophilic with a water contact angle less than 10°. The AFM colloidal probe was made by attaching a silica microsphere ($D \approx 9$ μm, Whitehouse Scientific, U.K.) onto the apex of an AFM tipless silicon nitride cantilever (NP–O10, Bruker Scientific, U.S.A.) using a two–component epoxy glue (EP2LV, Master Bound, U.S.A.). The colloidal probe was kept under vacuum overnight and then exposed to an ultraviolet light for 30 min to remove residual organic contaminants. To coat the asphaltenes onto clean colloidal probes and silica wafers, the probes and wafers were immersed in 0.1 g/L fractionated asphaltene–in–toluene solutions for 1 h followed by a thorough washing using pure toluene, and then dried with gentle nitrogen gas blow.

The clean and fractionated asphaltene–deposited silica wafers were imaged in air with a silicon tip (NCHV, Bruker Scientific, U.S.A.) at a scan rate of 1 Hz and a scan size of 500 nm at a constant temperature (22 ± 1 °C) using a Dimension Icon AFM (Bruker Scientific, U.S.A.) in tapping mode. The amplitude setpoint was determined automatically during the engage process. The integral gain and proportional gain were initially set to 0.5 and 5, respectively, and then adjusted in the measurements to bring the trace and retrace lines in to coincidence to get the optimized imaging results. For each sample, images were obtained at several locations and a representative image was presented.

Interaction forces between fractionated asphaltenes immobilized on silica wafers and colloidal probes were measured using the same Dimension Icon AFM. Force profiles were collected in toluene, heptol 50/50 and heptol 70/30 using a custom–made liquid cell at a constant temperature of 22 ± 1 °C. After the solvent was injected into the cell, the system was allowed to equilibrate for 15 min before initiating force measurements. The approach and retract velocity of the colloidal probe to the silica wafer was fixed at 1 μm/s to minimize the hydrodynamic force and highlight the effects of surface interactions. The spring constants of AFM cantilevers (NP–O10, Bruker Scientific, U.S.A.) were ~0.24 N/m and did not change significantly during the force measurements (<10%). The deflection setpoint was set to 0.3 V. The integral gain and proportional gain were initially set to 2 and 5, respectively, and then adjusted in the measurements to obtain the optimized force curves. The raw force curves were treated by NanoScope Analysis (Bruker Scientific, U.S.A.) to conduct the baseline corrections and obtain the force–separation distance curves. All interaction forces were normalized by the radius of the colloidal probe coated with the fractionated asphaltenes. A number of different surface locations on at least two independent samples for each asphaltene–asphaltene pair were chosen to ensure that representative interaction forces were captured.